Shahid Bahonar University of Kerman

Faculty of Engineering

Department of Mechanical Engineering

Vibration Reduction on Beams Subjected to Traveling Loads Using Linear and Nonlinear Dynamic Absorbers

Supervisor:

Prof. Francesco Pellicano

Prepared by:

Farhad Sheykh Samani

Dissertation Submitted as a Partial Fulfillment of the Requirements for the Degree of Doctor of Philosophy in Mechanical Engineering (Ph.D.)

July 2010

Acknowledgments

I wish to express my deep appreciation to my ex-supervisor, Dr. Farzad Ariana, he is one of the best persons I have meet in my life; God bless his soul.

It is great pleasure for me to express my highest gratitude to Prof. Francesco Pellicano for his intensive supervision, advices and encouragements to forming and ripening this research work and his important positive effects on my life. Moreover, I would like to thank the Lab SIMECH/INTERMECH (HIMECH District, Emilia Romagna Region) for supporting the present research.

I am extremely grateful to Prof. S.H. Mansouri and Prof. M. Ameri, head of mechanical department, for their supervision and supports to form this research work and also for all of scientific life of mine in Bahonar university of Kerman.

I would like to thank: Prof. E. Esmailzadeh, Faculty of Engineering and Applied Science, University of Ontario Institute of Technology, for his major constructive comments.

I am indebted and thanks to Prof. M. Rahnama, Dr. M. Fooladi, Dr. M.A. Hajabbasi, Dr. A.R. Saidi and Dr. G. Baradaran for their influence, they have had on my professional growth.

Finally, I owe my special gratitude to my wife, dear Asma, for her help and encouragement; specially, for her endurance for traveling with me when we are waiting for our baby.

Special thanks to my mother and my father, God bless his soul.

Abstract

Flexible structures (such as long-span suspension bridges which undergo moving load, wind or earthquake excitations) exhibit complex dynamic behavior. Due to high cost of strengthening such structures, as well as the technological advances in recent years, much attention has been given to using innovative means of enhancing structural functionality and safety against dynamic excitations. Among the methods used to mitigate the excessive vibration of structures, the energy absorber systems are more promising.

This dissertation presents a comprehensive assessment for nonlinear passive vibration absorbers applied on the beams subjected to traveling loads. It begins with explanation and formulation of moving loads excitations and continues by the basic concept and features of nonlinear isolators and inherent nonlinear phenomena. For three types of excitations: transient moving load, transient moving vehicle and steady state successive moving loads the dynamics of the system has been studied and for each type of excitation different types of nonlinear passive dynamic dampers are examined. By optimizing each type of absorber the best optimal parameter set is defined. Comparisons among the performances of different types of dampers, linear and nonlinear, are carried out.

Simply supported beams are analyzed using the Euler-Bernoulli theory, the partial differential equation governing the beam dynamics is reduced to an ordinary differential equation set by means of the Galerkin-Bubnov method, a multimode expansion of the displacement field allows to analyze the problem with good accuracy. Under transient excitation, the performance of the dynamic dampers in reducing vibrations is estimated through two indicators: i) the maximum amplitude of vibration; ii) the portion of energy dissipated by the dynamic damper; the same indicators are used as objective functions for developing optimization approachs. Under transient excitation, two conservation laws are found in term of optimal parameters and beam geometry for cubic nonlinear dynamic dampers.

The study shows that the types of suitable nonlinear dynamic damper for the transient excitations: traveling load and traveling vehicle are similar. Under transient excitation the most effective type of dynamic damper in reducing the maximum amplitude of vibration is the one characterized by a piecewise linear restoring force. Classical linear TMD presents the best performance in order to dissipate maximum input energy.

Under successive traveling loads, dynamic dampers characterized by nonlinear restoring forces does not present pure periodic responses; while depends on nonlinear absorber parameters quasi periodic response, super harmonics and chaotic responses appear. The behavior of dynamics system is illustrated by different nonlinear dynamic tools such as Poincare maps and bifurcation diagrams. Periodic response is desired for successive moving load excitation. Unlike nonlinear restoring force, with nonlinear damping force the response remain always periodic. Note that, this result is valid for the types of nonlinearities investigated in this study. Finally, the dynamic damper possessing linear stiffness and linear-quadratic nonlinear damping, presents the most effective behavior in order to minimize beam deflections under successive traveling loads.

Table of contents

CHAPTER 1

Traveling Loads and Traveling Vehicles

1.1. Introduction

Transportation infrastructure is an important factor affecting the development of a national economy. Because of space and terrain limitations, more transportation structures, such as highways and railways, have been constructed as bridges in urban areas. With the rapid advances in the field of high performance materials and construction techniques, these bridges have a trend towards long and flexible as those of the high-rise buildings. When excessive external loads occur, these bridges may suffer large deflections and even cause damages that will endanger human life and property. In order to understand the dynamic behavior of bridges under natural loads such as wind or earthquake excitations, considerable numerical and experimental efforts have been made over the past two decades.

In Europe, particularly in the near past, the operating high-speed railway network has suffered a remarkable expansion, which can be partially explained by the advantages of this large capacity means of transportation when compared with other means of transportation. Among these advantages, one can refer the high levels of safety, low energy consumption and near absence of environmental pollution.

The first high-speed railway line was built in Japan and had called Tokaido Shinkansen. It was opened in 1964 and trains moved at the running speed of 210 km/h. In the 1960s, after the Shinkansen construction began, the idea of the TGV was proposed. However, only a few years later, the French government start the construction of the first French high-speed line, which called South-East TGV line, and was the first European high-speed railway line. Its construction elapsed between 1981 and 1983 linking Paris to Lyon in an extension of 410 km; in the case that it designed for a running speed of 270 km/h. Since then, the development of the European high speed framework has never stopped, expanding to countries like Belgium, Germany, Italy, Netherlands, Spain and United Kingdom, Fig. 1-1.

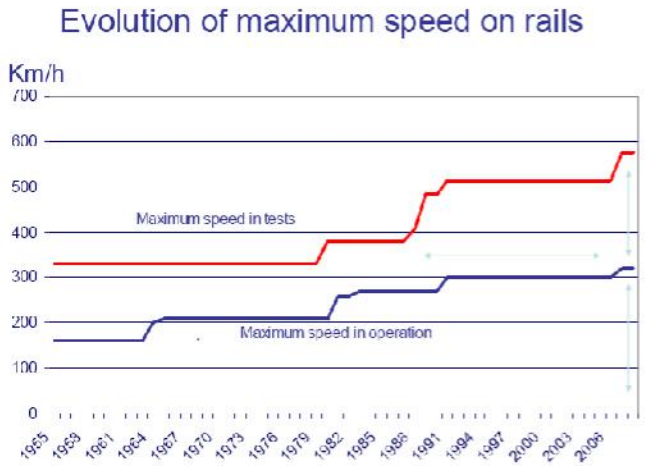

Fig. 1-1, Evolution of Maximum speed on rails during 1955 till 2006.

From the structural point of view, the design of high-speed railway bridges has to account for the special requirements of structures subjected to actions different from those that are accounted for in conventional railways. Thus, the dynamic effects associated to the moving loads from train traffic are one of the major issues that bridge designers have to considerer.

The speed of circulation of trains in high-speed lines is in the origin of an important phenomenon that can occur on bridges - the Resonance - which tends to appear for speeds above 200 km/h. Recently two new speed records were reached. The first, 554.3 km/h, was measured in February of 2007 in TGV East line and the second on the third day of April of the same year, also in the TGV East line, where the current speed record of 574.8 km/h was reached. These and other events are an excellent indicator of the "need for speed" and point out the speeds range that will be commercially practicable in a future not too far away.

In comparison with buildings subjected to wind or earthquake excitations, the location of train (traveling load) on bridges (beam) is time–variant. Further, because of the interaction effect between the train and bridge, the magnitude of the train load is dependent upon the response of the bridge. Therefore, it would be difficult to establish a clear correlation between the governing parameters and bridge responses if precise train models were used in the analytical studies. To clearly identify the dominant parameters and to obtain the analytical solutions, simplified models were usually employed initially, after that the importance of considering inertial effect and internal stiffness of the load is studied. Once the basic parameters have been identified, it is possible to refine the model to include other variables for advanced work. In this study, several assumptions were made to make the problem easier, as follows: (1) The bridge is regarded as a

straight beam made of homogeneous, elastic, isotropic material. The supports of the bridge are rigid and the shape of the bridge's cross-section is unchanged during vibration. The rail irregularity is negligible. (2) In order to understand the dynamic responses of the cars, the load is modeled as a periodic series of moving forces or moving suspension masses. In the last chapter, the infinite sequence of train loads is applied at the centerline of the beam and move along the longitudinal direction with a constant speed.

The basic assumptions made by all models are as follows.

1. One dimension (axial direction) is considerably larger than the other two.
2. The material is linear elastic (Hookean).
3. The Poisson effect is neglected.
4. The cross-sectional area is symmetric so that the neutral and centroidal axes coincide.
5. Planes perpendicular to the neutral axis remain perpendicular after deformation.
6. The angle of rotation is small so that the small angle assumption can be used.

The analysis of the dynamic response of bridges under moving loads is a problem that has been investigated by several researchers in the past. The first known study in history about this subject was performed in the early 19th century, when the collapse of the Chester rail bridge over the river Dee, in England, 1847, led the Queen to establish a commission with the aim of investigating its causes.

Studies on oscillations of bridges under travelling loads date back to the middle of the nineteenth century, when the early railways were developed; such applications are the most important examples of travelling loads. Readers interested to a comprehensive treatment of the problem of structures excited by moving loads are suggested to read Ref. [1], where several applications are reported.

1.2. Bibliographical survey

One of the first modern studies on the subject of moving loads is due to Timoshenko et al [2], which found an analytical solution and presented an expression for the critical velocity. Considering moving masses instead of purely moving loads seems more realistic; however, in Ref. [3] it was shown that the behavior of beams under moving loads and moving masses is almost the same when the moving mass is assumed small with respect to the beam mass.

In recent years and the development of the high-speed framework in Japan and Europe, the interest about the dynamic effects induced by trains on bridges has increased. Theoretical, numerical and experimental studies have been carried on several bridges in order to extend the knowledge about this subject, identifying the aspects that govern the behavior of bridges under high-speed trains and developing new approaches to be used by bridge engineers.

Within the larger research field of dynamic behavior of high-speed railway bridges under moving loads, the issue of vibration control to conform with safety and serviceability limit states of bridges, especially under resonant conditions, has increased over the last years. This can be explained by the growing interest in the construction of new high-speed lines and in the retrofitting of some conventional railway lines for operation under higher speeds, as happens in some European and Asiatic countries.

Among the earliest remarkable works on this subject, those by Timoshenko [2] should be stressed. This author studied the case of a moving load or pulsating force passing over a simple beam, neglecting the inertia of the vehicle. Later, the same author established a solution for the case of a concentrated force traveling with constant speed along a prismatic bar, disregarding the contribution of damping forces. An expression for the critical speed was also presented.

A substantial contribute to the awareness of dynamic behavior of structures under moving loads has been given by Frýba [1], with his comprehensive text “Vibration of Solids and Structures under Moving Loads”. Detailed results for a large number of cases were here included, considering from one-dimensional structures to three-dimensional solids. Train excitations were assumed as moving constant forces, harmonic forces, or continuous loads. Moving forces arbitrarily varying on time and moving multi-axle system were also considered, as well as a complete number of special problems, including load motion at variable speed, random loads and forces moving at high-speed.

More recently, Fryba [4] investigated a theoretical model of a bridge aiming to study the resonance vibrations that may occur at critical speeds. Two different reasons for resonance vibration on railway bridges are described:

i) Repeated action of train axle loads;

ii) High speed of moving loads by itself.

Fryba stresses that resonant behavior due to the high speed of moving loads by itself cannot appear currently in high-speed lines with today's trains. Nevertheless, under the repeated action of train axle loads resonant behavior may occur, leading to unacceptable values of bridge deck acceleration, which is pointed out as the main cause for ballast destabilization on small and medium span bridges, as observed on some French bridges [5].

1.3. Background of moving force models

1.3.1. Models of bridge–vehicle system

In practice, the bridge–vehicle system is a very complicated system. The interaction between the bridge and the vehicle is a complex phenomenon governed by a large number of different parameters. The use of simplified models is more effective to establish a clear connection between the governing parameters and the bridge response than a complex model. Normally, the bridge decks are modeled as beams (Euler-Bernoulli beam or Timoshenko beam) or plates (isotropic plates or orthotropic plates) and vehicles are modeled as a moving force, a moving mass or a moving oscillator for simple analysis of vehicle interaction, Ref. [6].

1.3.2. Models of bridges

There are two kinds of models of bridges in the moving force identification systems. One is the *Beam-Element Model* [7] in which a bridge can be modeled as an assembly of lumped masses interconnected by massless elastic beam elements. The total modal responses, $[R]_{total}$, on the bridge equal to the equivalent static responses, $[R]_{static}$, caused by the external loads less the responses caused by the inertia forces, $[R]_{inertia}$, and the damping forces, $[R]_{damping}$, or equivalently as: $[R]_{total}=[R]_{static}-[R]_{inertia}-[R]_{damping}$.

The other model is the *Continuous Beam Model* [8] ,assuming an Euler-Bernoulli or Timoshenko beam [9] of constant cross-section with constant mass per unit length, having linear, viscous proportional damping and with small deflections. From there follow three special cases:

If the effect of rotatory inertia is neglected and only the effect of shear on the dynamic deflection of the beam is considered, it is called a shear beam. If the effect of shear is neglected and only the effect of rotatory inertia is considered, the so-called Rayleigh beam model results. If both the effect of shear and the effect of rotatory inertia are neglected, the classical Euler-Bernoulli beam model is obtained. In most problems encountered in practice the effects of rotatory inertia and shear can safely be neglected with little error (Euler-Bernoulli beam); however, for short, deep beams with height-span ratios larger than about 1/10 or beams made of materials sensitive to shear stresses, it is desirable to give consideration to the effect of shear and rotatory inertia.

Considering the linear Euler-Bernoulli theory for the beam modeling, the equations of motion of the system are given by,

$$EIy_{,xxxx}(x,t) + Cy_{,t}(x,t) + \rho Ay_{,tt}(x,t) = F_0\delta(x-Vt)\left[H\left(\frac{L}{V}-t\right)\right], x \in (0,L), t > 0 \qquad (1\text{-}1a)$$

$$y(0,t) = 0, y(L,t) = 0, y_{,xx}(0,t) = 0, y_{,xx}(L,t) = 0 \qquad (1\text{-}1b)$$

$$y(x,0) = 0, y_{,t}(x,0) = 0 \qquad (1\text{-}1c)$$

The beam dynamics is governed by the PDE represented by equation (1-1*a*) with simply supported boundary conditions (1-1*b*) and initial conditions (1-1*c*); *F*(*x*,*t*) is the external force which can be time dependent in terms of position along the beam (moving load). *y*(*x*,*t*) is the transverse displacement field of the beam (down is positive), $y_{,x} = \partial y/\partial x$ (similar meaning for the other derivatives), *E* is the Young's modulus, *I* is the moment of inertia of the cross section area, $m=\rho A$ is the mass per unit length, ρ is the material density, *A* is the cross section area, *C* is the viscous proportional damping. δ is the Dirac function and *H*(t) is the Heaviside function; find the explanations in appendix A.

Based on modal superposition, the solution of Eq. (1) can be expressed as follows:

$$\phi_r(x) = (2/mL)^{1/2}\sin(r\pi x/L), \quad \omega_r = (r\pi)^2(EI/mL^4)^{1/2}, \quad r = 1,2,\ldots \qquad (1\text{-}2)$$

Where ω_r is the natural frequency of the rth mode.

The eigenfunctions satisfy the following orthonormality conditions,

$$\int_0^L m\phi_i(x)\phi_j(x)dx = \delta_{ij}; \quad \int_0^L \phi_i(x)\left(EI\phi_j''(x)\right)''dx = \omega_j^2\delta_{ij}, \quad i,j = 1,2,\ldots \qquad (1\text{-}3)$$

Where δ_{ij} is Kronecker's delta and $(\cdot)' = d(\cdot)/dx$.

It can be assumed that the transverse vibration of the beam is expressed in the form

$$y(x,t) = \sum_{r=1}^{\infty} a_r(t)\,\phi_r(x) \tag{1-4}$$

Where $a_r(t)$ are unknown functions of time (modal coordinates) and $\phi_r(x)$ are the normalized eigenfunctions.

By substituting equation (1-4) into equation (1-1), projecting on the p^{th} eigenfunction and using the orthonormality conditions, one obtains:

$$\ddot{a}_p(t) + 2\xi_p\omega_p\dot{a}_p(t) + \omega_p^2 a_p(t) = F_0\phi_p(Vt)\left[H\left(\frac{L}{V}-t\right)\right],\quad p = 1,2,\ldots \tag{1-5}$$

1.3.3. Models of vehicles

For the case of low moving speed or low mass ratio, the simple moving force model can be a good approximation to the complex moving mass problem [1]. For the case of a high mass ratio and a high moving speed, the moving force model cannot be applied, and the complicated time-variant system analysis for the moving mass problem must be conducted to ensure an accurate investigation [10, 11]. If a softly sprung vehicle traverses a flexible structure, the interaction effects become very important, and the moving oscillator model should be adopted as it is more realistic in some engineering applications [12]. Usually, a quarter-truck model, a half-single-unit two-axle truck model, and a half five-axle semi-trailer truck model developed by Todd and Kulakowski [13] are adopted.

CHAPTER 2

Dynamic Vibration Absorbers

2.1. Principal

The dynamic damper is a classical device for avoiding large amplitude vibrations of a mechanical system subject to a sinusoidally varying excitation when the forcing frequency coincides or is near one of the natural frequencies of the system. Obviously, severe vibrations of a given structure or mechanical system may cause considerable disturbance, which is inconvenient from a human factors viewpoint, it may conduce to failure due to fatigue, etc.

A tuned mass damper, also known as an active mass damper (AMD) or harmonic absorber, is a device mounted in structures to prevent discomfort, damage, or outright structural failure caused by vibration. They are frequently used in power transmission, automobiles, and buildings.

A linear dynamic vibration absorber (DVA) called tuned mass damper (TMD) is a vibration absorber system composed usually by a secondary mass suspended by a viscous damper and a spring from a point on the primary structure, tuned to a particular structural frequency of the bridge in order to, when excited, the damper will resonate out of phase with the bridge motion, i.e., the TMD mass oscillates in the opposite direction of the primary structure. Therefore, considering this property, it provides the opportunity to dissipate energy by the damper inertia force acting on the structure. A TMD is one of the simplest and most used passive control devices for several types of structures, including, obviously, bridges. It carries out two major functions: firstly, it reduces the resonant response of the main structure, and secondly, increases the overall damping of the structure through the attached dashpot, providing a supplementary source of energy dissipation.

Usually, the mass and stiffness of the TMD are chosen in order to tune its natural frequency to values near the resonant frequency of the structure to be damped. The current dashpots used in TMDs to provide damping are frequently linear or nonlinear viscous dampers.

TMDs stabilize against violent motion caused by harmonic vibration. A tuned damper reduces the vibration of a system with a comparatively lightweight component so that the worst-case vibrations are less intense. Roughly speaking practical systems are tuned to either move the main mode away from a troubling excitation frequency, or to add damping to a resonance that is difficult or expensive to damp directly. An example of the latter is a crankshaft torsional damper. Mass dampers are frequently implemented with a frictional or hydraulic component that turns mechanical kinetic energy into heat, like an automotive shock absorber. Figure 2-1 presents a

schematic of a simple spring–mass–damper system used to demonstrate the tuned mass damper system.

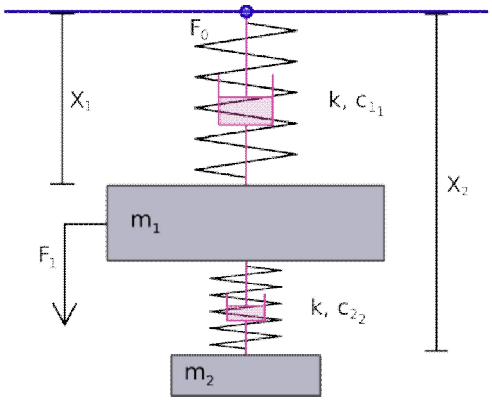

Fig. 2-1. A schematic of a simple TMD.

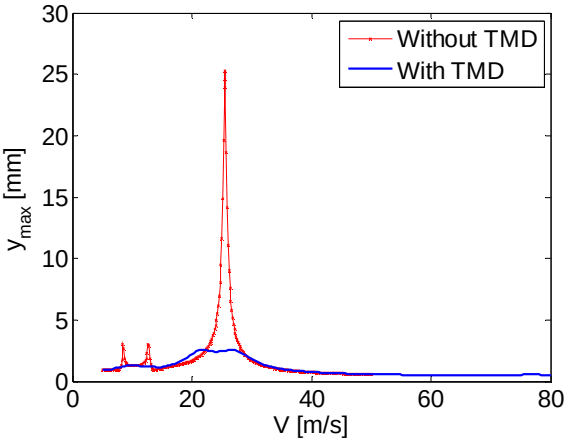

Fig. 2-2. The performance of TMD in order to reduce beam vibration subjected to infinite sequence of the traveling loads.

Consider a motor with mass m_1 attached via motor mounts to the ground. The motor vibrates as it operates and the soft motor mounts act as a parallel spring and damper, k_1 and c_1. The force on the motor mounts is F_0; suppose we wish to reduce the maximum force on the motor mounts as the motor operates over a range of speeds.

Let F_1 be the effective force on the motor due to its operation. A small mass, m_2, is connected to m_1 by a spring and a damper, k_2 and c_2. The graph shows the effect of a tuned mass damper on a simple spring–mass–damper system, excited by vibrations with amplitude of one unit of force applied to the main mass, m_1. An important measure of performance is the ratio of the force on the motor mounts to the force vibrating the motor, F_0 / F_1. (It is assumed that the system is linear, so if the force on the motor were to double, so would the force on the motor mounts.) The blue

line represents the baseline system, with a maximum response of 9 units of force at around 9 units of frequency. The red line shows the effect of adding a tuned mass of 10% of the baseline mass. It has a maximum response of 5.5, at a frequency of 7. As a side effect, it also has a second normal mode and will vibrate somewhat more than the baseline system at frequencies below about 6 and above about 10.

The heights of the two peaks can be adjusted by changing the stiffness of the spring in the tuned mass damper. Changing the damping also changes the height of the peaks, in a complex fashion. The split between the two peaks can be changed by altering the mass of the damper (m_2). Figure 2-2 shows the performance of TMD in order to reduce beam vibration subjected to infinite sequence of the traveling loads. The TMD is able to reduce vibration up to 90%.

The first recorded use of a dynamic vibration absorber was described in a paper by Watts [14] in 1883, followed by Frahm patent [15] in 1909. Ormondroyd and Den Hartog [16] published the first mathematical treatment of the passive dynamic vibration absorbers.

2.2. Mass dampers in automobiles

2.2.1. Motorsport

The tuned mass damper was introduced as part of the suspension system by Renault, on its 2005 F1 car (the R25), at the 2005 Brazilian Grand Prix. It was deemed to be legal at first, and it was in use up to the 2006 German Grand Prix. At Hockenheim, the mass damper was deemed illegal by the FIA (Fédération Internationale de l'Automobile French term for International Automobile Federation), since the mass wasn't rigidly attached to the chassis and, due to the influence it had on the pitch attitude of the car, which in turn significantly effected the gap under the car and hence the ground effects of the car, to be a movable aerodynamic device and hence as a consequence, to be illegally influencing the performance of the aerodynamics. The Stewards of the meeting deemed it legal, but the FIA appealed against that decision. Two weeks later, the FIA International Court of Appeal deemed the mass damper illegal [17].

2.2.2. Production cars

Tuned mass dampers are widely used in production cars, typically on the crankshaft pulley to control torsional vibration and bending modes of the crankshaft, on the driveline for gear whine, and other noises. They are also used on the exhaust, on the body and on the suspension. Almost all cars will have at least one dynamic absorber; in some cases it may have 10 or more.

2.3. Mass dampers in spacecraft

One proposal to reduce vibration on NASA's Ares solid fuel booster is to use 16 tuned mass dampers as part of a design strategy to reduce peak loads from 6g to 0.25g, the TMDs being responsible for the reduction from 1g to 0.25g, the rest being done by conventional vibration isolators between the upper stages and the booster [18].

2.4. Dampers in power transmission lines

High-tension lines often have small barbell-shaped Stockbridge dampers hanging from the wires to reduce the high-frequency, low-amplitude oscillation termed flutter, see figure 2-3.

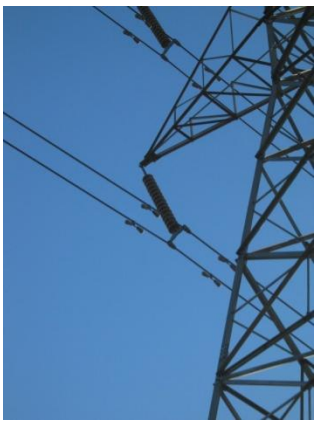

Fig. 2-3. Stockbridge dampers on power lines

2.5. Dampers in buildings and related structures

Typically, the dampers are huge concrete blocks or steel bodies mounted in skyscrapers or other structures, and moved in opposition to the resonance frequency oscillations of the structure by means of springs, fluid or pendulums.

Examples of buildings and structures with tuned mass dampers:

- Bally's to Bellagio, Bally's to Caesars Palace, and Treasure Island to The Venetian Pedestrian Bridges in Las Vegas.
- Berlin Television Tower (Fernsehturm) — tuned mass damper located in the spire.
- Bloomberg Tower/731 Lexington in New York.
- Burj al-Arab in Dubai — 11 tuned mass dampers.
- Citigroup Center in New York City — Designed by William Le Messurier and completed in 1977, it was one of the first skyscrapers to use a tuned mass damper to reduce sway. Uses a concrete version.
- London Millennium Bridge — 'The Wobbly Bridge'.
- Taipei 101 skyscraper — Contains one of the world's largest tuned mass damper at 730-tons.

2.6. Damper applications for bridges

Studies on oscillations of bridges under travelling loads date back to the middle of the nineteenth century, when the early railways were developed; such applications are the most important examples of travelling loads. Readers interested in a comprehensive treatment of structures excited by moving loads are advised to read Ref. [1], which reports several applications.

With the progress in design technology and in construction techniques, as well as the development of new high-performance materials over the last years, bridges became more flexible and span lengths increased, leading to lighter and slender structures, which can be observed more often on recent footbridges, but also in road and railway bridges. Consequently, these structures started to become more susceptible to the dynamic actions of moving loads.

On the field of vibration control, several systems have been used to reduce the dynamic responses of structures to desired values. These systems are frequently classified by their type of structural control in active, passive, semi-active and hybrid systems. Passive systems are those

that do not need an external power source in order to carry out its control function since its behavior depends only on the device characteristics. Among the devices classified as passive systems it can be included viscoelastic dampers and tuned mass dampers, which are well understood and widely accepted by the engineering community as a means to suppress the effects of dynamic loads in structures.

The importance of bridge vibrations induced by moving vehicles, which act as oscillators on a bridge as well as time variant forces, has long been recognized by engineers. Bridge vibrations can amplify the propagation of existing cracks, resulting in further damage to the bridge. Though major bridge failures are not usually caused directly by moving vehicles, vehicle-induced vibrations have become one of the causes of reduction in long-term serviceability of the bridge and a critical factor to a bridge's structure fatigue and rapid deterioration [19]. Millennium Bridge in London/UK, figure 2-5, and Okutama/Tokyo, figure 2-4, Cable-Stayed Bridge are two examples for application of TMDs on Bridges. A cable-stayed bridge is a bridge that consists of one or more columns (normally referred to as towers or pylons), with cables supporting the bridge deck.

One of the majors' examples of excessive vibrations occurs in the London Millennium footbridge. The London Millennium Footbridge is a pedestrian-only steel suspension bridge crossing the River Thames. On the first day, this bridge experienced horizontal vibrations induced by a synchronized horizontal pedestrian load, with central span displacements of about 70 mm. Thus, only two days after the opening, the bridge was closed in order to investigate the cause of vibrations and to find out mechanics for its reduction. In this way, after an extensive analysis, it was decided to adopt a passive damping solution by the use of 37 fluid-viscous dampers and 52 tuned mass dampers to control the bridge behavior.

Millennium Bridge, London

Vertical TMD installed below the bridge

Vertical TMD installed below the bridge

Horizontal TMD during installation and adjustment

Horizontal TMD during installation and adjustment

Vertical TMD installation

Fig. 2-4. TMD application on the London Millennium Footbridge.

Fig. 2-5. Okutama Cable-Stayed Bridge: TMD for suppression of Vortex-Induced Vibration

Regarding the major interest area of research related to dynamic behavior of beams under moving load, the effects on railway bridges induced by high-speed traffic are one of the most

specific and important areas of recent studies. This can be explained by the growing interest in the construction of new high speed lines and on the retrofitting of some conventional railway lines for operation under higher speeds, as can be seen in some European countries. Therefore, it is of the major interest to study not only the vibration problems in high-speed railway bridges but also different ways of controlling it, with regard to safety and serviceability of bridges, preventing the increase of maximum bridge displacements, accelerations and internal stresses, as well as train carriages' accelerations, especially important to measure the comfort of passengers.

When vibration problems occur, especially in resonant situations, two different solutions can be studied in order to improve the dynamic behavior of bridges. The first, perhaps those more conventional, is to increase the stiffness of the structure, while the other is to increase damping. It is not the aim of the current thesis to study possible solutions related with the increase of stiffness on a bridge, thus only a reference to this procedure is made.

Figure 2-6 shows the transient response of the beam without attachment, bare beam, as well as the beam with linear dynamic damper optimized in Ref. [20], V=21.5m/s. This graph illustrate the performance of a linear TMD for reducing the undesired beam vibration. The vertical green line shows the time instant for which the moving load leaves the beam (x_F=L); the maximum deflection occurs at the first peak, which happens before the load leaves the beam.

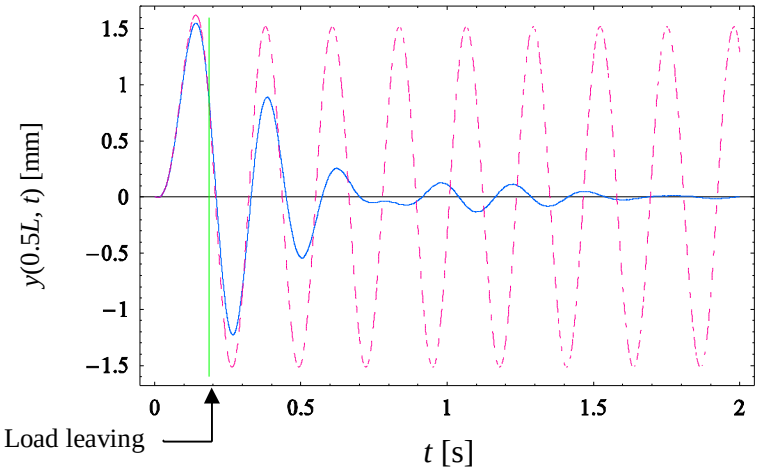

Fig. 2-6. Transient responses for the bare beam: '---' and the beam with linear dynamic damper: '——'.

2.7. Applicable research project in Iran

Tale Zang railway bridge is an example of current applicable research for using TMDs on bridges. Tale Zang railway bridge is located in the 587th km. of Lorestan Railway route, between Dorood and Andimeshk [21]. In order to improve the train and vehicle velocities with optimal structural weight the dynamic absorbers is required.

2.8. Complex forms of the vibration absorbers

2.8.1. Multiple tuned mass dampers

One of the main drawbacks of passive DVA is its sensitiveness to tuning frequency ratio, even when optimally designed [22], leading to a significant performance deterioration if the dynamic characteristics of the structure are different from those used to achieve its optimum design. This limitation could be overcome by the use of multiple tuned mass dampers (MTMDs), which allows the control of more than one mode of a multi degree of freedom (MDOF), Ref. [23]; structure by tuning each one of the TMDs to the corresponding interest vibration mode of the primary structure, or to tune the TMDs to frequencies in the vicinity of a mode of the system, see figure 2-7 as an example of MTMD. The explicit formulae for the optimum parameters and the effectiveness of a TMD to control structural oscillations caused by different types of external excitations is now well established [24-31].

Nevertheless, in spite of their greater effectiveness and robustness with compare to single TMDs, MTMDs suffer from the lack of real time retuning capabilities, thus they are unable to adapt to frequency varying excitation.

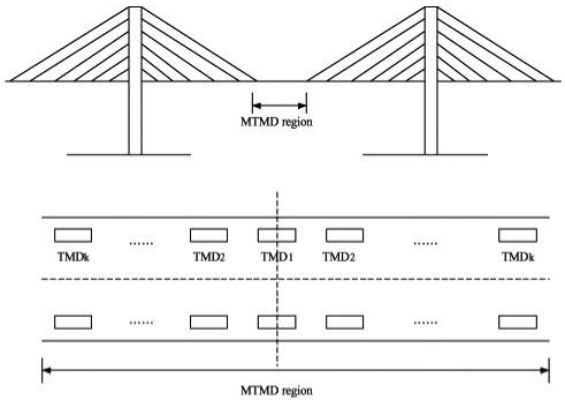

Fig. 2-7. Layout of the MTMDs on a bridge, Ref. [32].

2.8.2. Fluid viscous dampers

Other types of passive devices are the fluid viscous dampers (FVDs), Ref. [33], classified as velocity dependent dissipation devices. FVDs consist in a closer cylinder containing a viscous fluid, being the energy dissipated by forcing the fluid through orifices around and through the piston head, causing a damping pressure which creates a force, see figure 2-8.

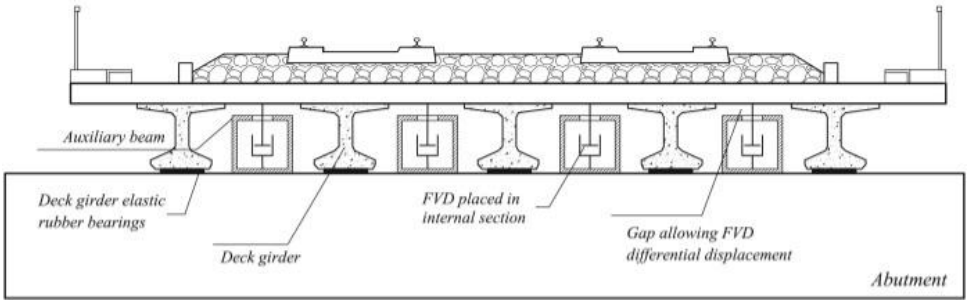

Fig. 2-8. Application of FVD on high-speed railway bridge.

When comparing FVDs with other passive energy dissipation devices, the former do not present tuning and detuning problems, which is one of the main drawback of TMDs. In relation to replacement operations and maintenance costs, some FVDs are equipped with labyrinth seals that eliminate mechanical friction, allowing them to be submitted to a huge number of cycles without the need of replacement.

2.8.3. Active, semi-active and hybrid TMDs

On the other hand, active systems are those that need an external power source that allows the reading of the input transmitted by detectors sending the motion of the structure and through an actuator affects its behavior and the way the device will act to control those motions. Previously, it was only referred the existence of passive tuned mass dampers. However, depending on the adopted control strategy and on the use of a supplementary active controlled device, these tuned mass devices could also be active, semi-active or hybrid.

Active tuned mass dampers eliminate some of the drawbacks of passive TMDs systems through the use of an actuator, which is installed between the primary and the auxiliary systems. Therefore, the force produced by the actuator and acting on the primary structure can enhance the auxiliary system damping effect if properly controlled. One of the most popular control strategies is to use the linear quadratic regulator (LQR) method, or, as an alternative, an active tuned mass damper with linear displacement, velocity and acceleration feedback could also be considered. On opposition to what happens when a single passive TMD is used, the aforementioned control strategy can lead to high damping levels in the controlled structure; moreover, damping can be introduced in several structural vibration modes.

By definition, a semi-active control device is one device that cannot supply mechanical energy into the controlled structural system, which includes the structure and the control device, but presents properties that can be controlled to optimally reduce the dynamic responses of the system, see Ref. [22]. Thus, in semi-active control systems the conventional damper is replaced by an adjustable damper which, in its turn, needs an external power source, however of limited power. According to Spencer et al. [22], semi-active control systems appear to be a particularly interesting and promising system since it offers the reliability of passive devices and the versatility and adaptability of fully active systems, without the need of large power sources since they can operate under battery power supply. Variable-orifice fluid dampers, variable-stiffness devices, smart tuned mass dampers, tuned liquid dampers and controllable fluid dampers are some examples of semi-active control systems.

Smart tuned mass dampers (STMDs) are a type of semi-active control device that offers additional advantages when compared with conventional passive TMDs, because of the possibility of continuously retuning its frequency due to real time control, [22].

Magneto rheological dampers are another kind of semi-active control device similar to fluid viscous dampers; however, the fluid inside the damper presents special properties. This fluid, denominated as magneto rheological, consists on suspensions of micron-sized magnet able particles in a suitable carrier liquid like synthetic oil, water or silicone oil. When exposed to a magnetic field, the particles acquire a dipole moment aligned with the external field, which causes particles to form linear chains parallel to the field, leading to the ability of reversibly change from free flowing linear viscous liquids to semi-solids having controllable yield strength in milliseconds.

Finally, there are the so-called hybrid TMDs systems, when assembling active and passive TMD systems in series. These systems can reduce some of the restrictions and limitations inherent to each of the active or passive systems when acting alone, in order to obtain higher performance levels. In addition, when comparing a fully active control system with a hybrid one, the latter can be more reliable; although it is often more complicated, see Ref. [22].

By attaching an auxiliary mass and an actuator to a TMD, if the response be out of phase with the response of the tuned mass, the effectiveness of a TMD can be increased. When the structure is vibrating, this auxiliary mass will produce a force that complements those produced by the tuned mass, increasing the equivalent damping of the TMD.

2.9. Nonlinear vibration absorbers

Linear vibration isolators are only useful if their natural frequencies are well below the excitation frequency, [34]. Thus, they are limited to such applications as moderate environmental disturbances. However, under severe environmental disturbances such as shocks, impact loads, or random ground motion, their spectrum will definitely contain dangerous low-frequency components. The isolator under these conditions experiences excessive deflections that can cause over-stress and even damage to the system. For this reason, it is imperative to consider effective nonlinear isolators, which can serve several applications, such as:

1. Reducing line spectra in the radiated acoustical signature of marine vessels.

2. Isolating equipment mounted in ships navigating in extreme sea waves.

3. Reducing the magnitude of the high launch loads across all frequency bands acting on spacecraft.

4. Reducing severe vibrations due to impact loads.

5. Protecting buildings, bridges, liquid storage tanks, oil pipelines, and nuclear reactor plants against the damaging effects of earthquakes.

6. Isolating laser interferometers of gravitational wave detectors.

7. Isolating electronic equipment, automotive vehicle front-end-cooling systems, and passengers from road roughness excitation.

8. Isolating automotive power-train system, engine through proper design of rubber and hydraulic mounting systems.

9. Protecting operators of hand-held machines.

The influence of isolator nonlinearity on transmissibility depends on whether its stiffness is hard or soft. It is known that soft nonlinearity causes a reduction in the resonant frequency and the isolation may be improved. Nonlinearity becomes important in the study of an isolator when large deflections occur due to the effects of equipment weight and sustained acceleration. These effects are encountered in the behavior of suspensions of high-speed vehicles and mounts for sensitive instruments [35].

Many researchers have conducted studies considering various combinations of restoring and damping forces. Earlier activities include the work of Den Hartog [36] who developed an exact solution for the vibratory response of a symmetric system with both coulomb and viscous damping when subjected to a harmonic forcing function. Ruzicka and Derby [37] presented extensive results for isolation systems with linear stiffness and nonlinear p^{th} power damping. The magnitude of stiffness nonlinearity required in the design of nonlinear isolators with reference to resonant amplitudes and force transmissibility was predicted using the analogue computer and finite element method. Metwalli [38] proposed a model to optimize nonlinear suspension systems which were found to outperform their linear counterparts. Nayfeh et al. [39] and Yu et al. [40] considered a passive nonlinear mechanical vibration isolator consisting of discrete mass, stiffness, and damping elements. They showed that by suitably designing the stiffness nonlinearities, localized nonlinear normal modes could be induced in the system. It was found that when the isolator with localized nonlinear normal modes is subjected to a harmonic excitation in certain frequency ranges, the resulting resonances become similarly localized and the level of the transmitted undesirable vibrations is greatly reduced.

The influence of nonlinearity on the performance of these isolators is manifested in shifting the resonance frequency and possibility of chaotic motion. Other factors include the type of excitation and its frequency spectrum, which are addressed in the next sections.

CHAPTER 3

Transient Traveling Load Excitation

3.1. Introduction

Studies on oscillations of bridges under traveling loads date back to the middle of the nineteenth century, when the early railways were developed; such applications are the most important examples of travelling loads. Readers interested to a comprehensive treatment of the problem of structures excited by moving loads are suggested to read Ref. [1], where several applications are reported.

One of the first modern studies on the subject of moving loads is due to Timoshenko et al [41], which found an analytical solution and presented an expression for the critical velocity. Considering moving masses instead of purely moving loads seems more realistic; however, in Ref. [3] it was shown that the behavior of beams under moving loads and moving masses is almost the same when the moving mass is assumed small with respect to the beam mass.

Controlling the vibration of structures can be achieved by means of a suitable structural design or using active/passive devices, which are particularly interesting when no modifications can be made to the structure. Passive devices have a primary quality in the extreme reduction of maintenance, no need of power supply; moreover, the service time is of the same order of the structure life.

A short analysis of the literature strictly related to the present work is now presented. Wu [40] proposed the application of a linear dynamic absorber to the problem of beams subjected to moving loads; the damper position was in the middle of the beam span. A finite element method (FEM) was used to model the beam, and the dynamics was analyzed after reducing the governing equations to the first modal coordinate; i.e. the N-dof problem arising from the FEM was reduced to a 1-dof model; such a simplified model was used to obtain optimal values for the stiffness and damping ratio of the absorber, following the Den Hartog's approach [42]. It should be mention that in the Wu model the absorber equation was modified to take into account the spring mass.

Greco and Santini [43] analyzed a beam under moving loads connected with two rotational viscous dampers attached at its ends; they proved numerically that the damper effectiveness is strongly dependent on the loading speed. Lee et al. [44] analyzed the dynamics of a 2-dof system consisting of a grounded linear oscillator coupled to a light mass by means of an essentially nonlinear spring; they found that the periodic orbits of the undamped system greatly influence

the damped dynamics; complicated transitions between modes in the damped transient motion was evidenced.

Kwon et al. [45] proved that when a TGV train (Train a Grande Vitesse, French “high-speed train”) passes a bridge, the maximum vertical displacement induced by TGV is decreased by 21% and the free vibration dies more quickly using a Tuned Mass Damper (TMD) at the middle of the bridge. In Ref. [46] a new approach for reducing the resonant vibration of simply supported beams under moving loads was presented: viscous dampers were used to connect the main beam, which carries the loads, to an auxiliary beam placed underneath the main one. The results show that the resonant response of the main beam can be drastically reduced with this type of device.

The application of passive TMDs to suppress the train-induced vibration on bridges was studied in [47]; it was shown that, if the maximum dynamic response of the bridge and train are dominated by the resonant response, within the design train speed, the passive TMD has a good vibration control performance.

Yau and Yang [48] studied the vibration reduction of cable-stayed bridges subjected to the passage of high-speed trains. The train was modeled as a series of spring masses, the bridge deck and towers by nonlinear beam-column elements, and the stay cables by truss elements with Ernst’s equivalent modulus. The numerical examples demonstrated that the proposed hybrid TMD system (that consists of several dynamic dampers, each one is tuned to a different dominant frequency of the main structure) is effective for suppressing the multiple resonant peaks encountered in the vibration of cable-stayed bridge due to high-speed trains.

In Ref. [49] it was proved that TMDs, tuned to a particular mode, have a negligible effect on the other modes. The effectiveness of TMDs in reducing the vibration of primary structures subjected to random loads greatly depends on the nature of the eigenfrequencies distribution.

An elastic beam subjected to a moving vehicle was studied by Lin et al. in Ref. [50]. They used a linear TMD as an energy-absorbing system and presented results regarding several absorbers parameters. The road roughness was considered, assuming that the road profile could be modeled by a stationary random process. Lin [51] studied the vibration reduction of an elastic continuum carrying a moving mass-spring-damper oscillator using a multi-time scale fuzzy controller. This method works very well for the maximum deflection reduction.

Recently, it was shown in Refs.[52-54] that, under certain conditions, essentially non-linear dynamic dampers can passively absorb energy from a linear non-conservative (damped) structure, acting as essentially nonlinear energy sink (NES). Georgiades and Vakakis [52] provided numerical evidence of passive and broadband targeted energy transfer from a linear flexible beam under shock excitation to a local NES. They have shown numerically that an appropriately designed and placed NES can passively absorb and locally dissipate a major portion of the shock energy of the beam, up to an optimal value of 87%. The essential non-linearity (non-linearizable) of the attachment enables it to resonate with any of the linearized modes of the substructure, leading to the energy pumping phenomenon, i.e. passive, one-way, irreversible transfer of energy from the substructure to the attachment [53].

In the present work the dynamics of an Euler-Bernoulli beam subjected to a moving load and coupled with a linear or essentially nonlinear (cubic) dynamic damper is studied. The goal is to find the optimal damper parameters (location, stiffness and damping) and to compare the effectiveness of linear and nonlinear dampers. The optimization was based on two kinds of goal functions: i) minimizing the absolute maximum deflection; ii) maximizing the amount of energy transferred from the beam to the damper. Both time and space positions of the maximum beam deflection are unknown (optimization case i)); therefore, a suitable search must be carried out. When the portion of the input energy dissipated by the dynamic damper is evaluated (optimization case ii)), it is crucial to estimate correctly the phenomenon duration.

The governing equations of the beam dynamics (partial differential equations) have been reduced to a set of ordinary differential equations (ODEs) by means of the Galerkin-Bubnov approach, which leads to a linear or nonlinear system of ODEs depending on the type of damper connected to the beam; eigenfunctions of the beam problem without dampers are considered in the displacement expansion. Both linear and nonlinear models have been tested by comparisons with the literature and convergence tests have been performed in order to truncate the series without loss of accuracy.

The evaluation of the objective functions needs an accurate solution of the ODE system during the transient vibration; in order to use a general approach, the dynamics is studied by integrating numerically the ODEs using the Gauss Kronrod method (Mathematica [55]); which is based on an adaptive Gaussian quadrature with error estimation through the evaluation at Kronrod points.

Two optimization strategies are used in this chapter: the first one is a brute force approach (see section 3.2.2) that consists of spanning the parameter space, such approach suffers of a huge computational cost and give coarse results when the parameter space is large; the second approach is a random search (see section 3.2.5), which consists of randomly moving all parameters of interest; it is slightly more efficient than the brute force approach and more suitable for large parameters space.

3.2. Formulation of the problem

Consider the system represented in Fig. 3-1: a simply supported beam is connected to a small mass through a linear or nonlinear spring and a linear viscous damper; the beam is loaded with a point load that can be either moving or time varying. In this dissertation, "bare beam" means the beam without any attachment, Ref. [40].

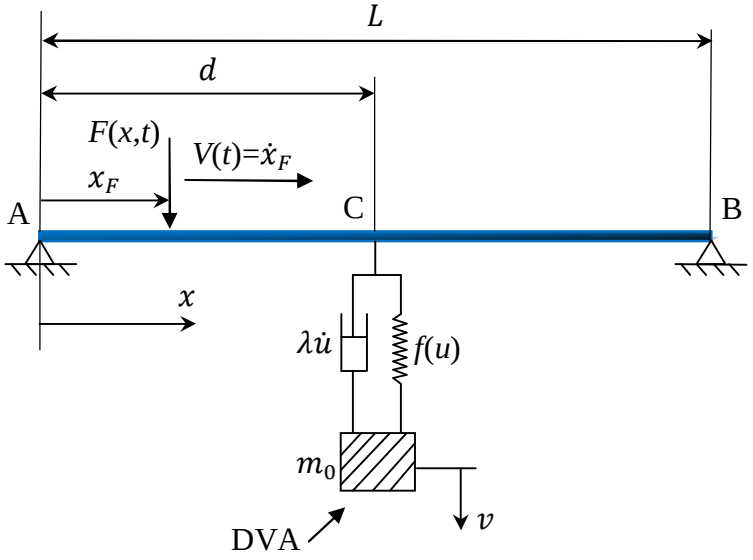

Fig. 3-1. The beam model.

Considering the linear Euler-Bernoulli theory for the beam modeling, the equations of motion of the system are given by,

$$EIy_{,xxxx}(x,t) + \rho A y_{,tt}(x,t) + [f(u) + \lambda u_{,t}(t)]\delta(x-d) = F(x,t), \qquad x \in (0,L), \ t > 0 \qquad (3\text{-}1a)$$

$$y(0,t) = 0, y(L,t) = 0, y_{,xx}(0,t) = 0, y_{,xx}(L,t) = 0 \quad (3\text{-}1b)$$

$$y(x,0) = 0, y_{,t}(x,0) = 0 \quad (3\text{-}1c)$$

$$m_0 v_{,tt}(t) - f(u) - \lambda u_{,t}(t) = 0\,, \;\; v(0) = 0, \;\; v_{,t}(0) = 0\,, \;\; t > 0 \quad (3\text{-}2a)$$

$$u(t) = y(d,t) - v(t), \qquad f(u) = ku \; or \; Cu^3 \quad (3\text{-}2b)$$

The beam dynamics is governed by the PDE represented by equation (3-1*a*) with simply supported boundary conditions (3-1b) and initial conditions (3-1c); the term $[f(u) + \lambda u_{,t}(t)]\delta(x-d)$ represents the force exerted by the dynamic damper, $f(u)$ is stiffness force, see equation (3-2b) for definition, $\lambda u_{,t}(t)$ is viscous damping force and $\delta(x-d)$ defines the location of dynamic damper; $F(x,t)$ is the external force which can be time dependent in terms of amplitude (transient excitation) or in terms of position along the beam (moving load). Equation (3-2*a*) governs the dynamics of the dynamic damper. $y(x,t)$ is the transverse displacement field of the beam (down is positive), $y_{,x} = \partial y/\partial x$ (similar meaning for the other derivatives), E is the Young's modulus, I is the moment of inertia of the cross section area, $m=\rho A$ is the mass per unit length, ρ is the material density, A is the cross section area, $v(t)$ is the absolute position of the mass m_0, $x=d$ represents the location of the damper on the beam, λ is the damping coefficient of the viscous damper, m_0 is the mass of the dynamic damper.

The attached mass is lightweight compared to the beam mass; indeed, using weighty masses for the dynamic damper causes a more effective vibration–reduction on the beam; however, the static deflection of the beam increases as well. Therefore, the mass of the absorber cannot be too large; in this work, the lumped mass of the absorber is taken to be 5% of total mass of the beam [40].

The dynamics of the system (3-1) and (3-2) is analyzed after projecting the partial differential equation (3-1*a*) into a complete and orthonormal basis; for the present problem the eigenfunctions of the linear operator representing the simply supported beam with no attachments can be used,

$$\phi_r(x) = (2/mL)^{1/2} \sin(r\pi x/L), \qquad \omega_r = (r\pi)^2 (EI/mL^4)^{1/2}, \quad r = 1,2,\ldots \quad (3\text{-}3a)$$

Where ω_r is the natural frequency of the rth mode.

The eigenfunctions satisfy the following orthonormality conditions,

$$\int_0^L m\phi_i(x)\phi_j(x)dx = \delta_{ij};\ \int_0^L \phi_i(x)\left(EI\phi_j{}''(x)\right)''dx = \omega_j^2\delta_{ij}, \qquad i,j = 1,2,\dots \tag{3-3b}$$

Where δ_{ij} is Kronecker's delta and $(\cdot)' = d(\cdot)/dx$.

It can be assumed that the transverse vibration of the beam is expressed in the form

$$y(x,t) = \sum_{r=1}^{\infty} a_r(t)\,\phi_r(x) \tag{3-4}$$

Where $a_r(t)$ are unknown functions of time (modal coordinates) and $\phi_r(x)$ are the normalized eigenfunctions.

By substituting equation (3-4) into equation (3-1) and (3-2), projecting on the p^{th} eigenfunction and using the orthonormality conditions, one obtains

$$\ddot{a}_p(t) + 2\xi_p\omega_p\dot{a}_p(t) + \omega_p^2 a_p(t) + \left\{D(t) + \lambda\left[\sum_{r=1}^{\infty}\dot{a}_r(t)\,\phi_r(d) - \dot{v}(t)\right]\right\}\phi_p(d) = \bar{F}(t),\ \ p = 1,2,\dots \tag{3-5a}$$

$$m_0\ddot{v}(t) - D(t) + \lambda\left[\dot{v}(t) - \sum_{r=1}^{\infty}\dot{a}_r(t)\,\phi_r(d)\right] = 0 \tag{3-5b}$$

Where $\dot{a}_p(t) = da_p/dt$ and

$$D(t) = k\left[\sum_{r=1}^{\infty} a_r(t)\,\phi_r(d) - v(t)\right] \qquad \text{For linear dynamic damper} \tag{3-5c}$$

$$D(t) = C\left[\sum_{r=1}^{\infty} a_r(t)\,\phi_r(d) - v(t)\right]^3 \qquad \text{For nonlinear dynamic damper} \tag{3-5d}$$

$$\bar{F}(t) = F_0\phi_p(Vt)\left[H\left(\frac{L}{V} - t\right)\right] \qquad \text{For moving load} \tag{3-5e}$$

$$\bar{F}(t) = F_1(t)\phi_p(x_F) \qquad \text{For transient constant load} \tag{3-5f}$$

which are obtained by considering the following forcing in Eq. (3-1*a*)

$$F(x,t) = F_0\delta(x - Vt)\left[H\left(\frac{L}{V} - t\right)\right] \quad \text{For moving load} \tag{3-6a}$$

$$F(x,t) = F_1(t)\delta(x - x_F) \quad \text{For transient constant load} \tag{3-6b}$$

where δ is the Dirac function and $H(t)$ is the Heaviside function:

$$H(t) = \begin{Bmatrix} 0, & t < 0 \\ 1, & t > 0 \end{Bmatrix} \tag{3-7}$$

A viscous damping term is added to the generic modal equation (3-5*a*) after projection.

The attachment couples all modes through the infinite summation terms; in the case of linear dynamic damper one can transform system (3-5) by finding the new vibration mode; conversely, in the case of nonlinear spring the system cannot be uncoupled.

The transient dynamics is studied by numerically integrating the dynamical system represented by equations (3-5*a*,*b*), after truncating the series (3-4); the truncation is suitably chosen by checking the convergence of the expansion.

3.3. Validation

3.3.1. Nonlinear dynamic damper and fixed transient load

In order to check the accuracy of the present model, the case of a beam connected with a nonlinear dynamic damper, loaded with a transient force, having a fixed position on the beam, is now investigated; comparisons with Ref. [52] are performed.

Consider the system of Fig. 3-1 with $V = 0$, x_F =*constant,* $f(u) = Cu^3$; an impulsive force (a half sine pulse, see Fig. 3-2) excites the beam

$$F_1(t) = \begin{cases} F_a sin\left(\frac{2\pi t}{T}\right), & 0 \le t < T/2 \\ 0, & t < 0 \text{ and } t \ge T/2 \end{cases} \tag{3-8}$$

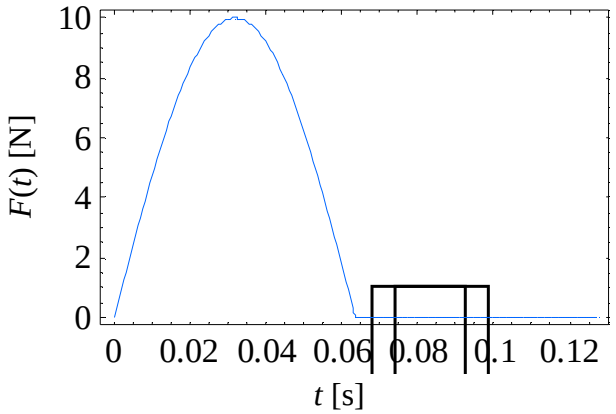

Fig. 3-2. Half sine pulse excitation force, Ref. [52].

For such comparisons the following parameters are considered: $F_a = 10.0\text{N}, T = 0.4/\pi\,\text{s}$, $EI = 1.0\text{Pa m}^4$, $\rho A = 1.0\,\text{kg/m}$, $2\xi_p\omega_p = 0.05\text{s}^{-1}$, $L = 1.0\text{m}$, $m_0 = 0.1\text{kg}$, $x_F = 0.3m$, $\lambda = 0.05\text{Ns/m}$, $d = 0.65\text{m}$ and $C = 1.322 \times 10^3\text{N/m}^3$, 5 mode shapes are considered. Note that in this model the modal damping ratio is not constant for the beam, for example $\xi_1 = 0.00253, \xi_2 = 0.000633, \ldots$

The portion of input energy dissipated by the viscous damper of the NES (the dynamic damper is also called Nonlinear Energy Sink, see Ref. [52]) at time t_1 is computed by the expression,

$$\eta = \frac{E_{NES}}{E_{in}} = \frac{\int_0^{t_1} \lambda[\dot{v}(t) - \sum_{r=1}^{n} \dot{a}_r(t)\phi_r(d)]^2 dt}{\int_0^{t_0} F_i[\sum_{r=1}^{n} \dot{a}_r(t)\phi_r(x_F)]dt} \tag{3-9}$$

Where, in the case of moving load $F_i = F_0$ (see equations 3-6*a*) and $x_F = Vt$ and in the case of impulse load (present section) $F_i = F_1$ (see equations 3-6*b* and 3-8) and $x_F = constant$.

E_{NES} is the energy passively absorbed and locally dissipated by the NES, t_1 is assumed large enough in order to assure that the transient dynamics is nearly damped; E_{in} represents the total portion of the input energy of the beam due to the load and $t_0 = T/2$ is the impulse duration.

The comparison between the present model and results of Ref. [52] is shown in Figs 3-3 till 3-10; the series (3-4) is truncated at the fifth term, t_1 is set equal to 150s. Figs. 3-3 and 3-4 show $y(0.8, t)$ and $v(t)$, i.e. the response of the beam at x=0.8m and NES deflection. Figs. 3-5 and 3-6 are those overall schematic comparisons. Figs. 3-7 and 3-8 show the portion of energy dissipated by the viscous damper, η, for different positions and different stiffness coefficients of the NES, respectively. Again, Figs. 3-9 and 3-10 are those overall schematic comparisons. Black dots are

reproduced from Ref. [52] and the continuous line represents the present results; a good agreement among Ref. [52] and the present model is found.

Figure 3-7 shows that, for the present problem (fixed location and impulsive excitation) the best position of the dynamic damper is not in the middle, due to the broadband excitation and to the location of the force.

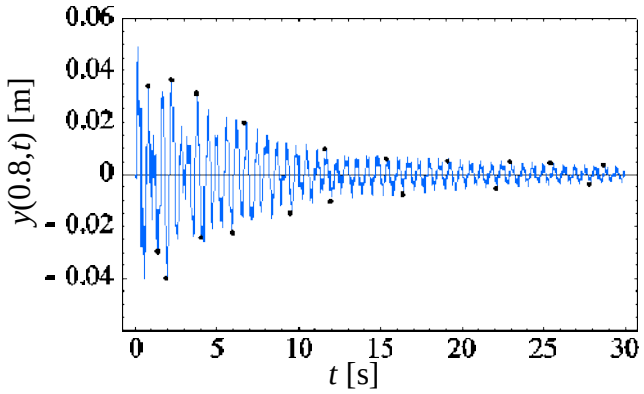

Fig. 3-3. Comparisons: transient response of beam at the location $x = 0.8$ m. '—' present results, '•' Ref.[52].

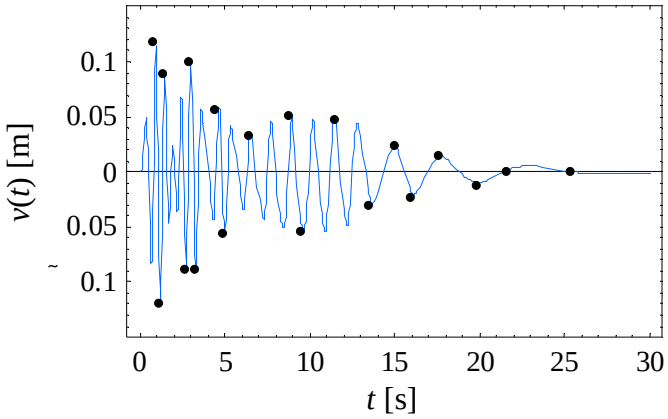

Fig. 3-4. Comparisons: transient response of NES deflection. '—' present results, '•' Ref.[52].

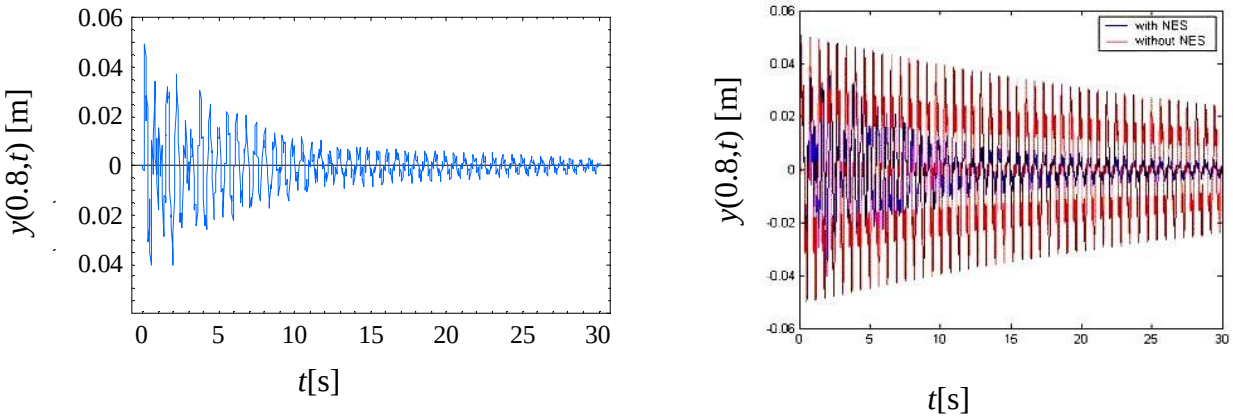

a:Present Result (5modes, with NES) *b:Ref. [52]*

Fig. 3-5. Schematic comparison: time history response, mid-span beam deflection.

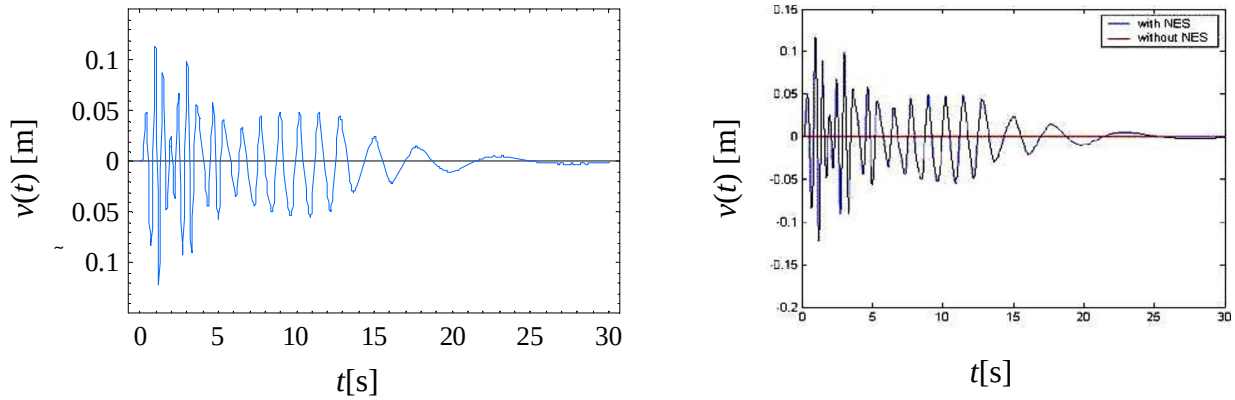

a:Present Result (5modes, with NES) *b:Ref. [52]*

Fig. 3-6. Schematic comparison: time history response, NES deflection.

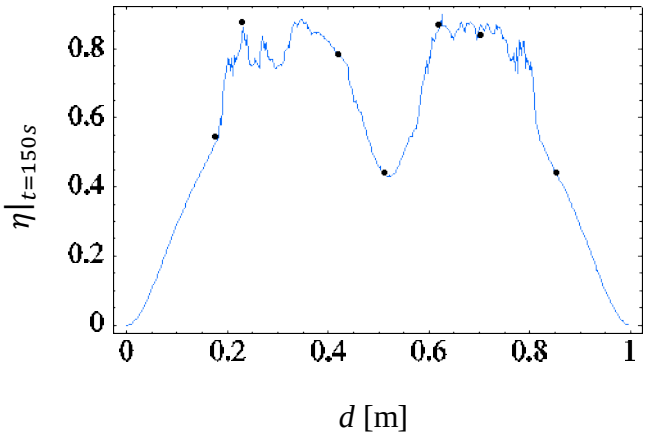

Fig. 3-7. Comparisons: portion of input energy dissipated by the NES (η) vs. the NES position *d*. '——' present results, '•' Ref. [52].

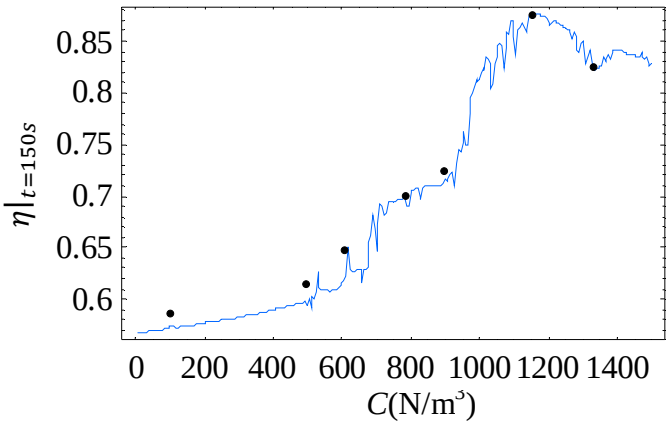

Fig. 3-8. Comparisons: transient response of NES stiffness.
'—' present results, '•' Ref.[52].

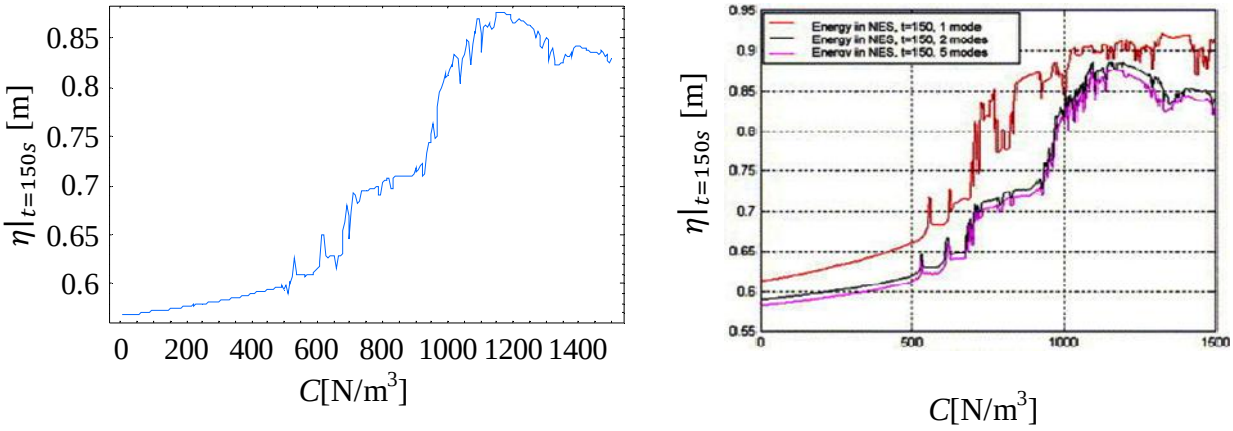

a:Present Result (5modes, 300samples) *b:Ref. [52]*

Fig. 3-9. Schematic comparison: the portion of input energy absorbed and dissipated by the NES as function of NES stiffness (*C*).

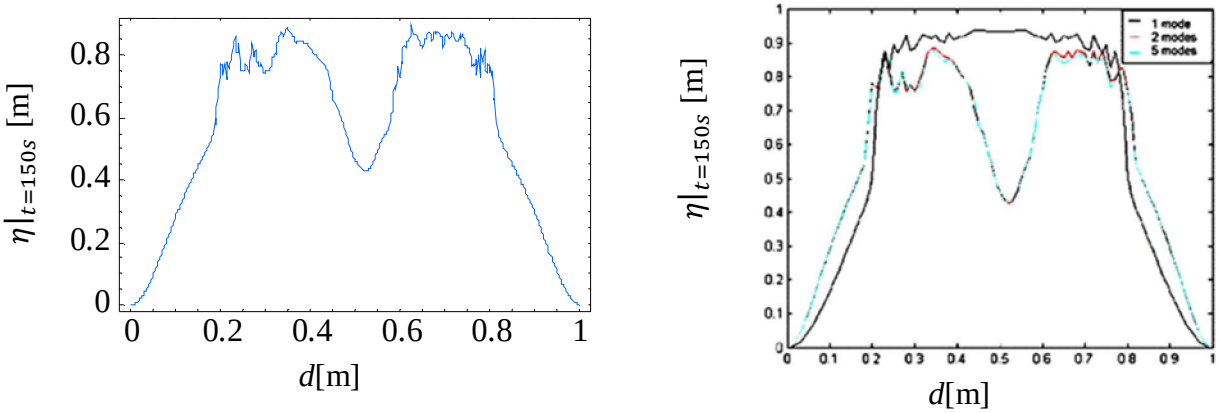

a:Present Result (5modes, 300samples) *b:Ref. [52]*

Fig. 3-10. Schematic comparison: the portion of input energy absorbed and dissipated by the NES as function of the NES position *d*.

3.3.2. Linear dynamic damper and moving load

A further verification of the present model is now carried out in order to check the accuracy of the approach in the case of moving loads; data from Ref. [40] are used for this purpose.

Consider the system of Fig. 3-1 with $V(t)$=*constant*≠0 and $f(u) = ku$: the external force is constant in terms of amplitude but moving along the beam, the dynamic absorber is linear. The external force is given by equation (3-6*a*).

For this simulation the system parameters are: E=206800MPa, ρ=7820kg/m^3, A=0.03m×0.03m, L=4m, F_0=9.8N, ξ_p=0 (p=1, 2, ...) and m_0=1.4076kg.

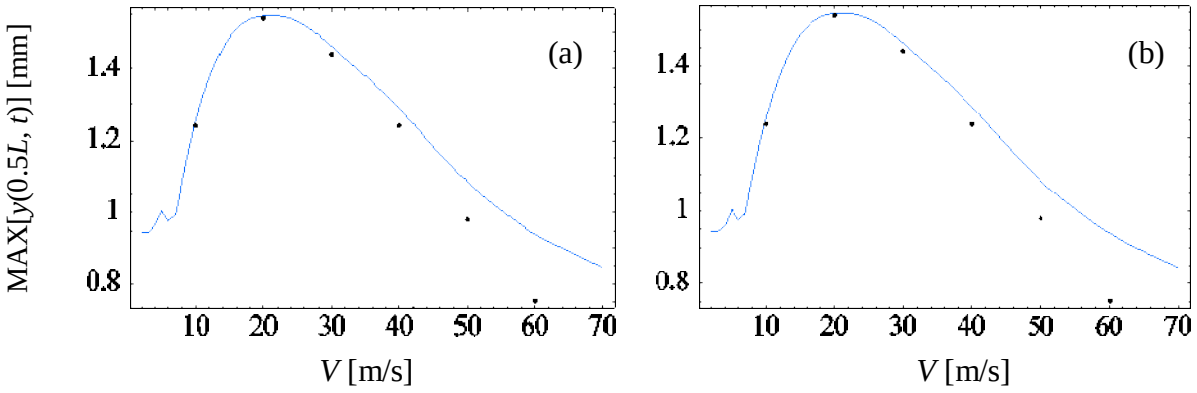

Fig. 3-11. Comparison beam subjected to moving load and connected to linear dynamic damper; '——' present results, '•' Ref. [40]; (a) 1-mode expansion, (b) 5-modes expansion

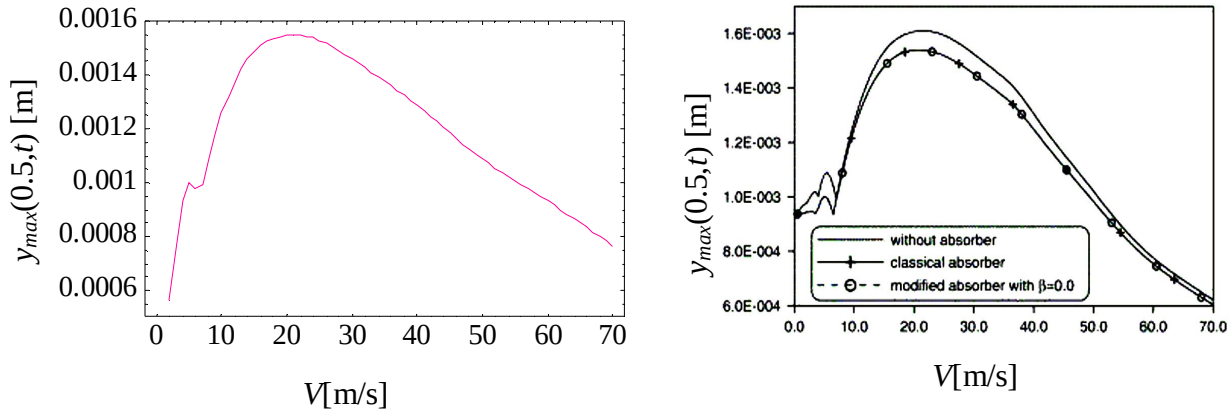

a:Present Result (classical absorber) *b:Ref. [40]*

Fig. 3-12. Schematic comparison: maximum beam dynamic response vs. load velocity.

Figures 3-11a and b show the maximum deflection of the mid span of the beam vs. the velocity of the moving load. Figure 3-12 shows the overall schematic comparison considering 5

modes. There is a maximum close to V=21.5m/s that is 61% the critical velocity as defined in Ref. [1] for moving loads without absorbers. The dynamics is mainly governed by the first mode of the beam, as proved by comparing Figs. 3-11a and b where one and five mode expansions are used respectively. Moreover, a good agreement with Ref. [40] is found; slight differences for the high speed range are probably due to the beam modeling: Wu [40] used a finite element method and reduced numerically the governing equations to the first beam mode; here exact eigenfunctions are used and the reduction of the PDE to ODEs is made analytically; moreover, different time integration approaches are used.

3.4. On the convergence of Galerkin method

3.4.1. Galerkin method and nonlinear dynamic problems

The mathematical basis of the Galerkin method for discretization is on the functional analysis. The spectral theorem proves that the eigenfunctions of an associated symmetric linear operator are a complete set of the Hilbert space.

Galerkin methods are a class of methods for converting a continuous operator problem (such as a differential equation) to a discrete problem. In principle, it is the equivalent of applying the method of variation to a function space, by converting the equation to a weak formulation. Typically one then applies some constraints on the function space to characterize the space with a finite set of basis functions.

The mathematical concept of a Hilbert space, generalizes the notion of Euclidean space. It extends the methods of vector algebra and calculus from the two-dimensional Euclidean plane and three-dimensional space to spaces with any finite or infinite number of dimensions. A Hilbert space is an abstract vector space possessing the structure of an inner product that allows length and angle to be measured. Hilbert spaces are in addition required to be complete, a property that stipulates the existence of enough limits in the space to allow the techniques of calculus to be used.

Galerkin method widely has been used for nonlinear dynamic models. Christie and Sanz-Serna [56] investigated the performance of Galerkin method for the numerical solution of a nonlinear model of a string; the increase in tension due to extension is taken into account. They proved the convergence of the Galerkin method for the present nonlinear model. Research of

Yoshimura and Hino [57] presents the analysis of dynamic deflections of a beam, including the effects of geometric nonlinearity, subjected to moving vehicle loads. The dynamic reflections of the beam and vehicles are computed by using the Galerkin method. Convergence of the Galerkin method applied to a nonlinear parabolic partial differential equation and nonlinear problems involving chemical reaction has been proved by Ladyzhenskaja [58] and Finlayson [59], respectively. References [60-62] present some other usage of Galerkin method for nonlinear dynamic problems.

3.4.2. Series truncation

In order to evaluate the convergence of the present Galerkin method, appropriate series truncation is investigated. Fig. 3-13 presents the comparison of transient response of the beam model connected to nonlinear dynamic damper possessing linear damping and cubic stiffness. The excitation is transient moving load. Fig. 3-13a presents the response for V=40m/s, and Fig. 3-13b presents the response for V=21.5m/s, the velocity that presents maximum beam deflection. When V=40m/s the maximum deflection with 1-mode, 3-modes and 15-modes are 1.272mm, 1.269mm and 1.269, respectively. For V=21.5m/s the maximum deflection with 1-mode, 3-modes and 15-modes are 1.569mm, 1.564mm and 1.563, respectively. Several comparisons illustrate maximum less than 1% error between the results of 3-modes and 15-modes.

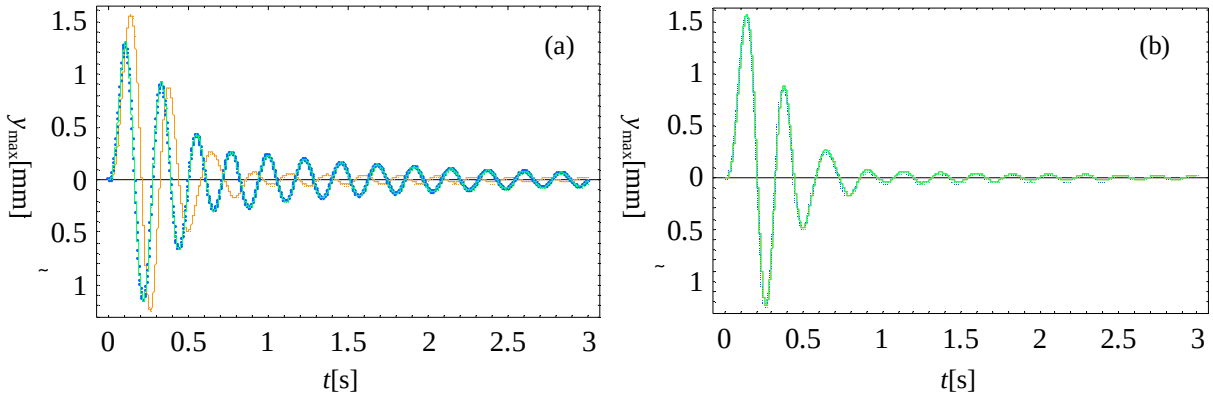

Fig. 3-13. Series truncation comparison; a: V=40m/s, b: V=21.5m/s; '——' 1 mode shape, '.....' 3 mode shape, '——' 15 mode shape.

3.5. Optimization methods

In mathematics and computer science, optimization refers to choosing the best element from some set of available alternatives.

In the simplest case, this means solving problems in which one seeks to minimize or maximize a real function by systematically choosing the values of real or integer variables from within an allowed set. This formulation, using a scalar, real-valued objective function, is probably the simplest example; the generalization of optimization theory and techniques to other formulations comprises a large area of applied mathematics. More generally, it means finding "best available" values of some objective function given a defined domain, including a variety of different types of objective functions and different types of domains.

Optimization problems are arising in nearly all fields of science and technology. Therefore the range of problems is huge and a large number of possible approaches for solutions are available. Following sections are some short survey on optimization methods.

3.5.1. Closed-form mathematical solutions

Closed-form mathematical solutions are only available if the function to be optimized is well-known in a mathematical sense. Maxima or minima can then be calculated by differentiating the function and setting the first derivative to zero.

3.5.2. Brute Force Approach

Brute-force search or exhaustive search, also known as generate and test, is a trivial but very general problem-solving technique that consists of systematically enumerating all possible candidates for the solution and checking whether each candidate satisfies the problem's statement.

Brute-force approach in optimization is straightforward and requires considerable computation power. This method try to calculate all possible solutions and decide afterwards which one is the best. These methods are feasible only for small problems (in terms of the dimensionality of the phase space), since the number of possible states of the system increases exponentially with the number of dimensions. In the case of continuous predictor variables, the numbers of states are infinite. Despite these drawbacks, brute force method has some benefits: they are simple to implement, and in the case of discrete systems, all possible states are checked.

However, its cost is proportional to the number of candidate solutions, which, in many practical problems, tends to grow very quickly as the size of the problem increases. Therefore, brute-force search is typically used when the problem size is limited, or when there are problem-specific heuristics that can be used to reduce the set of candidate solutions to a manageable size.

As a consequence, brute force methods are often seen as reference methods for calculating the number of states, or the number of calculations necessary to find the optimum with a probability of 100%. Hence, it can be used for the estimation of the effort to solve a problem. The implementation of brute force algorithms is rather simple. In fact, one only has to try out all possible states of a system. If this is not possible, because the system is described by continuous variables, one has to try all possibilities according to a certain definition of precision for each continuous variable.

3.5.2.1. Basic algorithm

In order to apply brute-force search to a specific class of problems, one must implement four procedures, first, next, valid, and output. These procedures should take as a parameter the data P for the particular instance of the problem that is to be solved, and should do the following:

1. First (*P*): generate a first candidate solution for *P*.
2. Next (*P*, *c*): generate the next candidate for *P* after the current one *c*.
3. Valid (*P*, *c*): check whether candidate c is a solution for *P*.
4. Output (*P*, *c*): use the solution *c* of *P* as appropriate to the application.

The next procedure must also tell when there are no more candidates for the instance *P*, after the current one *c*. A convenient way to do that is to return a "null candidate", some conventional data value Λ that is distinct from any real candidate. Likewise the first procedure should return Λ if there are no candidates at all for the instance *P*. The brute-force method is then expressed by the algorithm.

3.5.3. Gradient Descent

Gradient descent is a first-order optimization algorithm. To find a local minimum of a function using gradient descent, one takes steps proportional to the negative of the gradient (or of the approximate gradient) of the function at the current point, see Fig. 3-14 for illustration. If

instead one takes steps proportional to the gradient, one approaches a local maximum of that function; the procedure is then known as gradient ascent.

The idea behind gradient descent, or "hill climbing", methods is to find the maximum or minimum of a response surface by following the gradient, either up or down. One of the big advantages of such a method is that the nearest optimum can be found by only comparatively few calculations. However, gradient descent methods show several drawbacks. One of the most important points is that gradient descent methods do not necessarily find the global optimum. As can be seen from the figure below, whether or not the global optimum is found depends on the starting point.

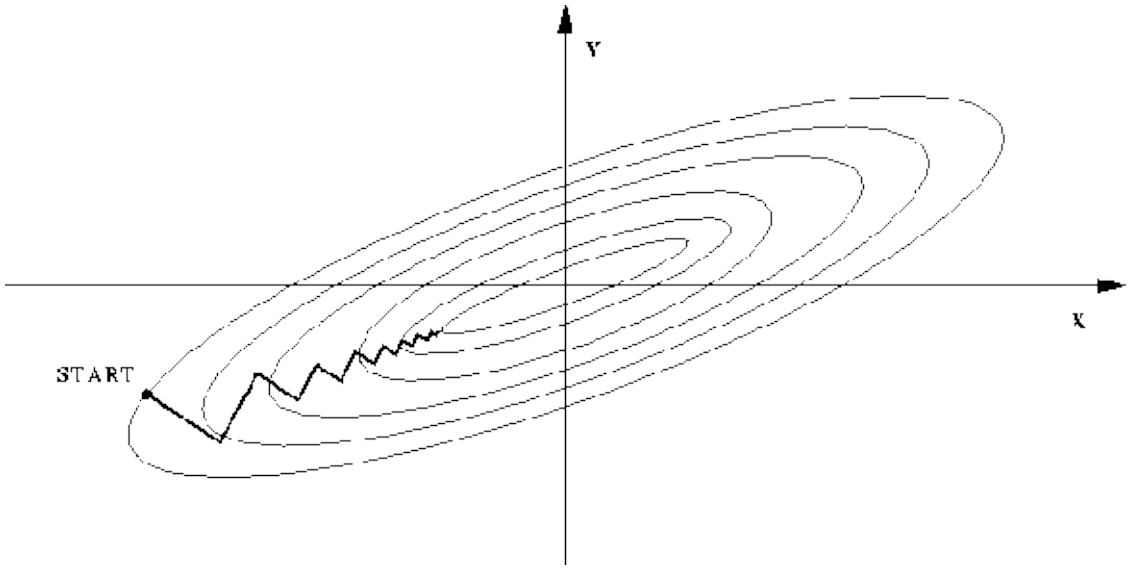

Fig. 3-14. Illustration of gradient descent.

Another problem with gradient descent methods is that finding the gradient at a particular point of a high-dimensional response surface may require a considerable amount of experiments (in fact one has to test an n-dimensional sphere around the current location, in order to find the direction of the next step). In terms of practical usage, it is recommended to perform a set of independent hill-climbing approaches with different starting conditions. There are several methods available which are based on some kind of gradient design. One of the more important methods is the simplex optimization.

3.5.4. Simplex Algorithm

The simplex algorithm is a gradient search procedure and is quite popular, since it is based on simple principles and is therefore easy to understand and implement. The journal Computing in

Science and Engineering listed simplex algorithm as one of the top 10 algorithms of the century. The idea is as follows: if the parameter to be optimized depends on k variables, then select k+1 points. These points must not form collinear vectors. Now, find the points with the worst response, the best response, and the next-to-worst response. Next, mirror the worst point about the centroid of the face spanned by the other k points. This procedure is repeated until the best response is reached. An additional rule has to be introduced in order to prevent the simplex from oscillating about a ridge: if the mirrored point remains the worst point, then use the next-to-worst point for reflection across the centroid.

Fig. 3-15. Illustrate a system of linear inequalities defines a polytope as a feasible region. The simplex algorithm begins at a starting vertex and moves along the edges of the polytope until it reaches the vertex of the optimum solution.

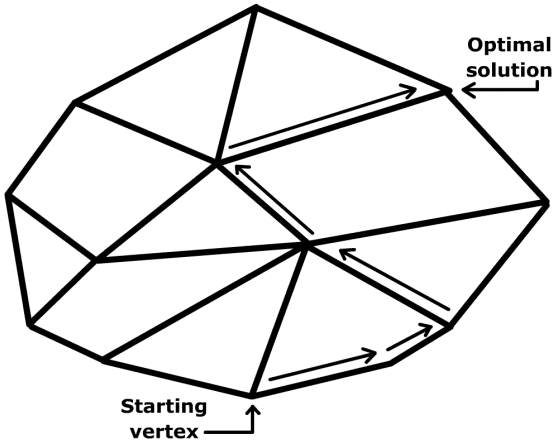

Fig. 3-15. Illustration of simplex algorithm of linear inequalities.

3.5.5. Monte Carlo Simulations

Monte Carlo methods or random search methods are a class of computational algorithms that rely on repeated random sampling to compute their results. Monte Carlo methods are often used in simulating physical and mathematical systems. Because of their reliance on repeated computation of random or pseudo-random numbers, these methods are most suited to calculation by a computer and tend to be used when it is unfeasible or impossible to compute an exact result with a deterministic algorithm, Ref. [63].

The goal of Monte Carlo method is to obtain a frequency distribution of the interesting phase space which allows the obtaining an overview of the search space. Locations which are of interest for the optimization (i.e. the maxima and the minima of the response variable) can be

sampled with higher precision to obtain more accurate information on those particular areas. Monte Carlo simulation methods are especially useful in studying systems with a large number of coupled degrees of freedom.

3.5.6. Genetic Algorithms

The genetic algorithm (GA) is a search heuristic that mimics the process of natural evolution. This heuristic is routinely used to generate useful solutions to optimization and search problems. GA is one particular approach, has been made to combine the advantages of deterministic and random-search methods.

The idea behind these methods is to exploit the principles of genetics for the optimization theory. First of all, a population of "explorers" is created. These explorers are positioned at random within the search (phase) space. Each "explorer" detects the value of the response function at its own location and feeds it to a fitness function. The fitness is designed in a way that it maximizes when the search goal is reached. Depending on the value of the fitness function, several basic operations are performed as follow.

Selection: Select the k "fittest" explorers from the population. These selected explorers are further processed.

Mating: The selected explorers are allowed to mate with other individuals of the population. The strategy for selecting the mating partners may vary from implementation to implementation. The offspring of the pairs replace the individuals of the population which perform worst (in terms of the fitness function).

Crossover: Crossover means the exchange of genetic information between two mating individuals. The idea is to create a "child" which has better properties (in terms of the fitness function) than the two parents. If both parents are located close to an optimum, this strategy tends to perform a hill-climbing strategy.

Mutation: Mutation means adding some random fluctuations to the location of the explorers in the phase space. The consequence is that random jumps to other locations become possible with a certain low probability.

These steps are repeated, until some termination criterion is fulfilled; e.g. the best explorer reached some defined threshold of fitness, or a defined number of generations have been

calculated. The second strategy is often applied if no information about the global optimum is available.

The most important advantage of genetic algorithms is their ability to find an optimum in huge search spaces. In fact, genetic algorithms are efficient only in systems with very large search spaces. Among the disadvantages of genetic algorithms is their high demand for computational power. As a consequence of the high number of necessary evaluations of the fitness function, each single evaluation has to be cheap in terms of efforts to obtain the response value.

3.6. Optimization of the dynamic dampers

In the present section linear and nonlinear dynamic dampers acting on the beam defined in the previous section (Wu model [40]) are analyzed and different optimization approaches are applied to find the optimal absorber parameters; if other kind of beams will be analyzed, then specific data will be given. Two indicators are considered for the evaluation of the absorber performance and for optimization purposes: the maximum vibration amplitude or the factor η (see eq. 3-9). 3 mode shapes considered for truncating Galerkin series.

3.6.1. Optimization of the linear dynamic damper

3.6.1.1. Maximum deflection approach

Consider the system of Fig. 3-1, with ξ_p=0.01 (p=1,2,…), V=21.5m/s, and $f(u) = ku$. Now the optimization of the dynamic damper is focused on the minimization of the maximum beam deflection. Stiffness, viscous damping and location of the dynamic absorber can vary to find optimum. It can be proven that the optimal absorber has zero dissipation; in order to avoid numerical problems and improve the time integration efficiency, a very small dissipation is considered: λ = 0.1 (this means that, for example, in the case of optimal stiffness, the damping ratio of the absorber will be ξ=0.001). The maximum deflection for the undamped bare beam (without dynamic absorber and ξ_p=0, p=1,2,…) is 1.6279mm and for the damped bare beam is 1.6042mm. In Figures 3-16a and 3-16b the effect of the dynamic damper location and the effect of the stiffness on the maximum deflection are presented; Figure 3-16a is obtained using k=1795N/m and Figure 3-16b using d=0.55L (such stiffness and location are the optimal

absorber parameters), the maximum deflection occurs at x_{top}=0.53L. It is to note that the optimal damper location is not sensitive to the variation of the other parameters. The maximum transverse deflection (which occurs at x_{top}=0.53L) is 1.5054mm (6.15% reduction with respect to bare beam), the maximum deflection of the middle of the beam is 1.4989mm.

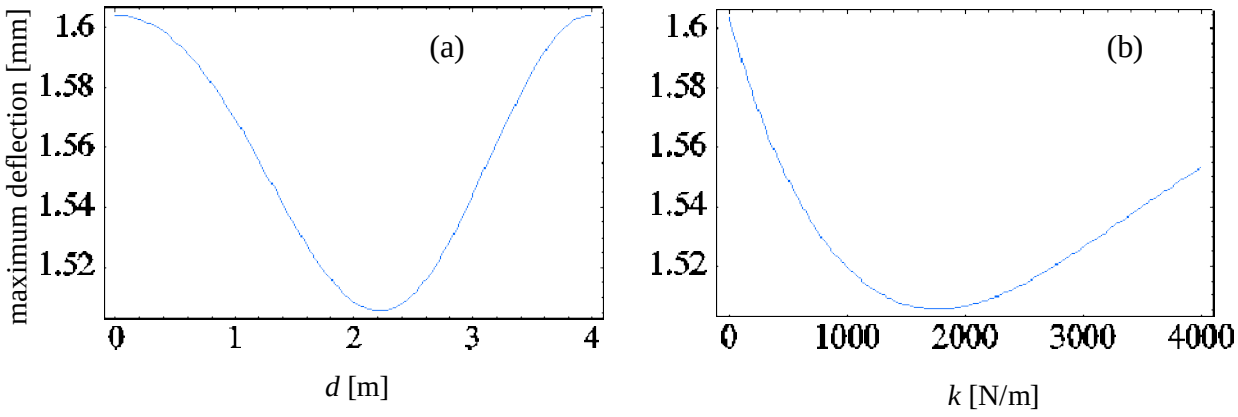

Fig. 3-16. Optimal location and stiffness of linear dynamic damper for deflection approch: (a) maximum beam deflection vs. damper location (k=1795N/m), (b) maximum beam deflection vs. stiffness (d=0.55L).

3.6.1.2. Energy approach

The second approach is focused to the maximization of the energy dissipated by the dynamic absorber, i.e. the indicator η (see Equation (3-9) with F_i=F_0 and x_F=Vt). Viscous damping and stiffness have been regularly sampled (a 100×100 grid is considered; it means that the resolution in terms of damping is 0.4Ns/m and 20N/m for the stiffness, the total number of cases analyzed is 10000); the damper location is d=0.55L, several numerical tests proved that such parameter does not change sensibly around the middle of the beam. The portion of input energy absorbed by the dynamic damper η is represented in Fig. 3-17 when λ and k are varied. The maximum η=88.9% is obtained for λ=10.5Ns/m and k=900N/m; the behavior of η is quite regular, there is only a maximum located on a flat region, which assures the robustness of the optimum. Fig. 3-18 illustrate the 3D variation of the maximum dissipated energy by linear DVA versus stiffness and damping coefficients.

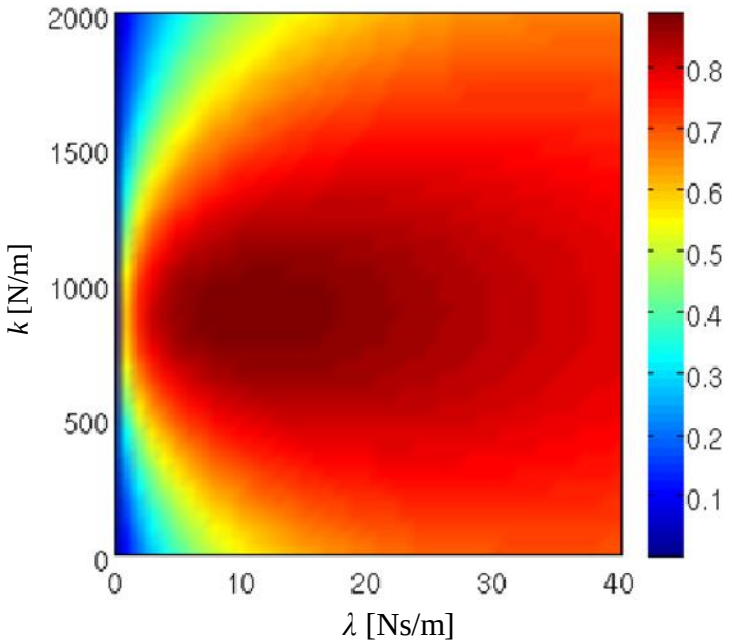

Fig. 3-17. Linear damper optimization: energy approach: map of the energy absorbed η.

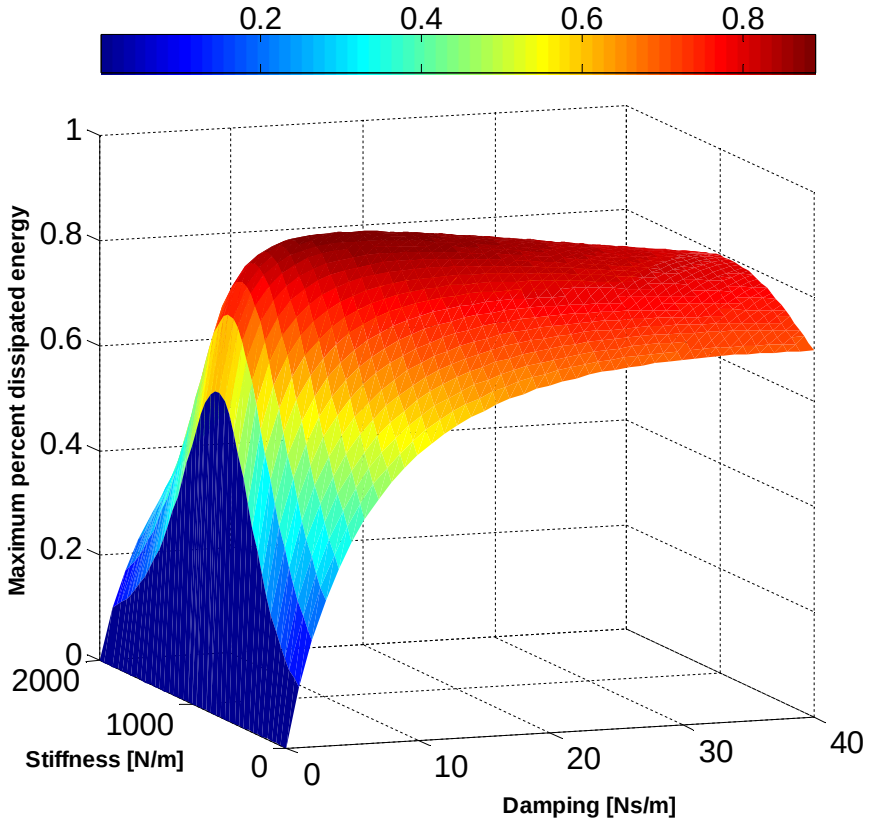

Fig. 3-18. Optimum maximum dissipated energy vs. damping and stiffness coefficients.

3.6.2. Optimization of the nonlinear dynamic damper

3.6.2.1. Maximum deflection approach

Consider the system of Fig. 3-1 with: ξ_p=0.01 (p=1,2,…), V=21.5m/s, and $f(u) = Cu^3$. Similarly to the previous section Figs. 3-19a and b show the maximum deflection vs. the damper location and the stiffness respectively; in Fig. 3-19a C=6.7×10^{9}N/m^3 and in Fig. 3-19b d=0.53L. The pair (C=6.7×10^{9}N/m^3, d=0.53L) is the optimal point of the parameter space; the maximum deflection occurs at x_{top}=0.53L. For the optimal case in such point the maximum transverse deflection is 1.4852mm (7.56% reduction with respect to bare beam). Values of linear and nonlinear stiffnesses are not comparable as they have different units.

Note that the maximum beam deflection with linear and nonlinear absorbers occurs at x_{top}=0.53L; but the optimal absorber location for nonlinear case is closer to middle, (d=0.53L), with respect to the linear case, (d=0.55L). The nonlinear absorber location has almost the same effect on transverse deflection reduction when it is moved from d=0.51L up to d=0.53L; for the sake of brevity details are omitted. Figure 3-20 shows the 2D plot of maximum mid-span beam deflection versus location and stiffness coefficients of the NES. Figure 3-21 presents 3D illustration of the absolute maximum deflection versus these parameters. These two present graphs are not symmetry respect to NES location and it depends on the velocity direction.

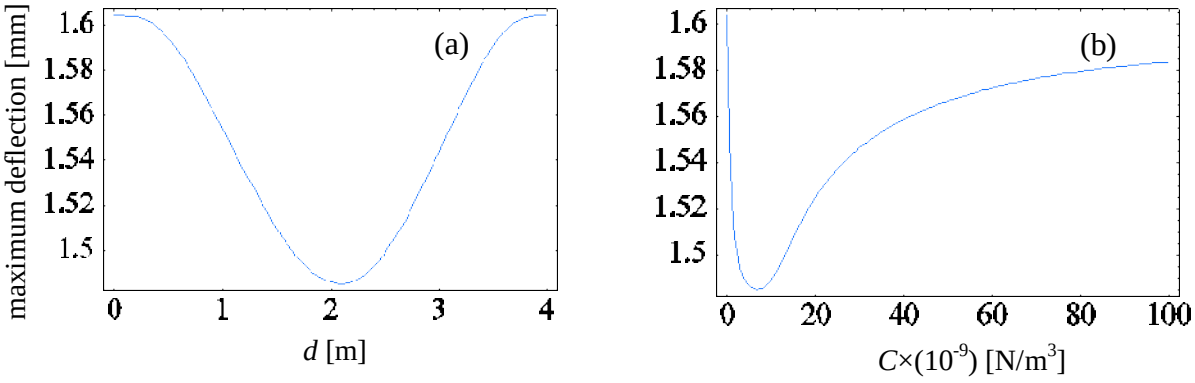

Fig. 3-19. Optimum location and stiffness of nonlinear absorber for deflection approch, (a)deflection amplitude vs. damper location (C=6.7×10^{9}N/m^3), (b) deflection amplitude vs. stiffness (d=0.53L).

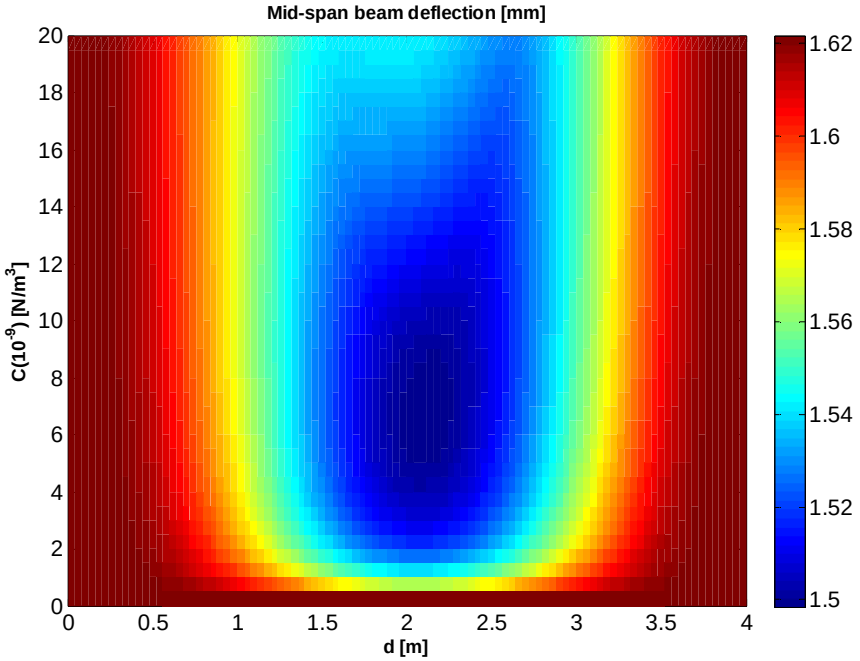

Fig. 3-20. 2D contour plot of maximum mid-span beam deflection vs. NES location and stiffness coefficients.

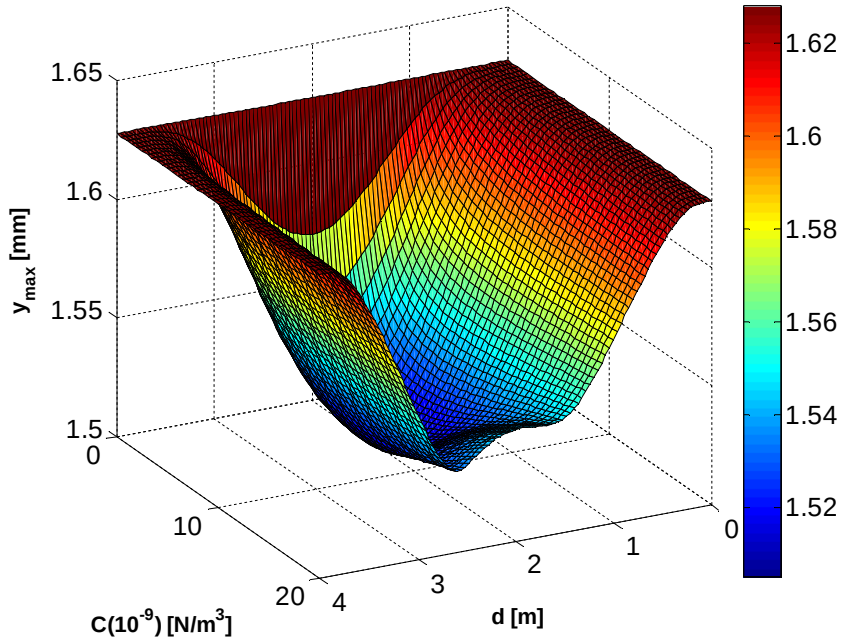

Fig. 3-21. 3D surface of the absolute maximum beam deflection vs. NES location and stiffness coefficients.

3.6.2.2. Energy approach

For the Energy approach, d=0.53L is considered, see considerations of the previous section. The portion of input energy absorbed by the dynamic damper η is represented in Fig. 3-22 when λ and C are varied; Fig. 3-23 is the 3D representation for Fig. 3-22. The maximum η=87.4% is obtained for λ=11Ns/m and C=0.30×10^9 N/m^3. It is interesting to note that, for the case of fixed shock load, the optimal nonlinear dynamic damper absorbs 87% of the shock energy of the beam, see Ref. [52]. The parameters are regularly sampled similarly to the Section 3.4.1.2. The behavior of η is regular, similarly to the linear case, and a unique maximum is found; however, the optimal point is close to non small gradients, i.e. it seems less robust with respect to the linear one.

Figures 3-24(a, b) show the transient response of the system without or with the dynamic absorber; these figures show the deflection vs. time at the point close to the middle of the beam, x=0.53L; this point undergoes to the largest oscillation along the beam. Fig. 3-24(a) shows the time history for the damped beam without attachment and Fig. 3-24(b) shows the deflection of the same point with the nonlinear dynamic damper, optimized for energy approach (λ=11Ns/m and C=0.30×10^9 N/m^3). The effectiveness of the dynamic damper is evident. The number of vibrating cycles is strongly reduced by using the damper; this greatly improves the fatigue life.

Table 3-1 summarizes results for: undamped and damped beam, without and with dynamic damper (linear or nonlinear). For the cases 1 and 2 of Table 3-1 there are not dynamic dampers and the energy cannot be pumped out from the beam, i.e. η must be zero. For the cases 3 and 4 there is no beam damping and the viscous dynamic damper absorbs all of the energy produced by the external moving load; therefore, if the time tends to infinite η must be 100%; accordingly, η equal 99.9% or 99.6% is found in the cases 3 and 4 respectively. For the cases 5 and 7 an extremely low viscous damping is considered, λ=0.1; it absorbs a small portion of energy, 3.4% and 2.3%. For the case 6 (linear) and 8 (nonlinear) η=88.9% and 87.4% is the maximum absorbed energy respectively.

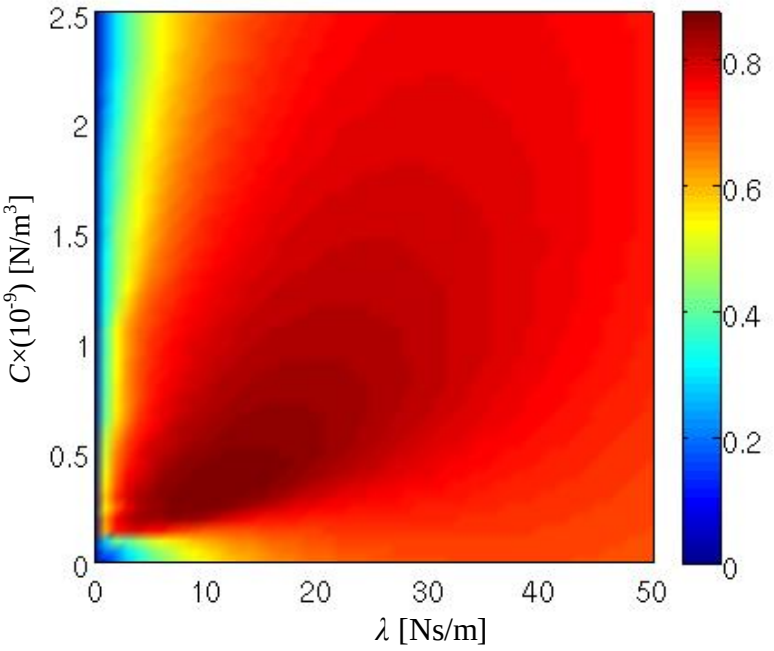

Fig. 3-22. Optimum η, for nonlinear dynamic damper and energy approach.

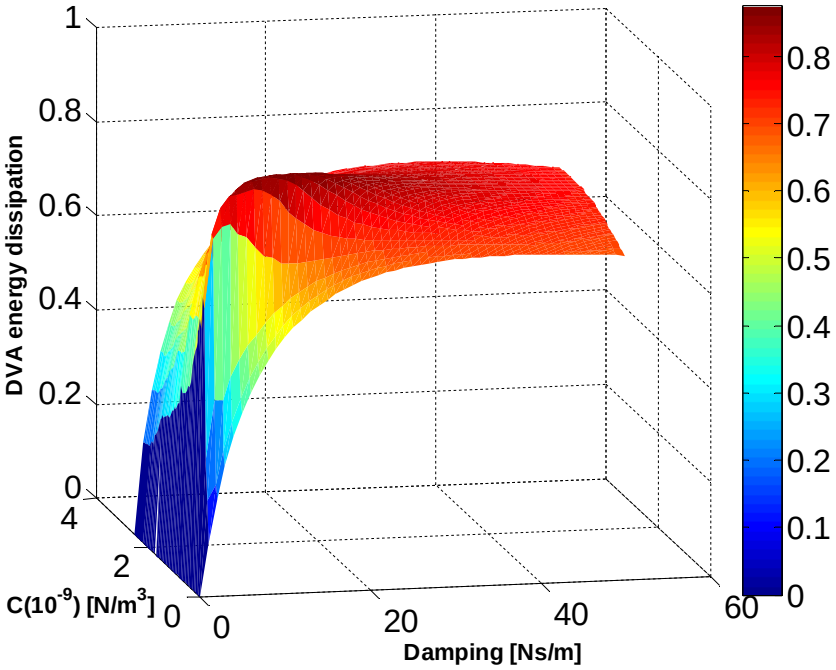

Fig. 3-23. 3D representation of Fig. 3-22.

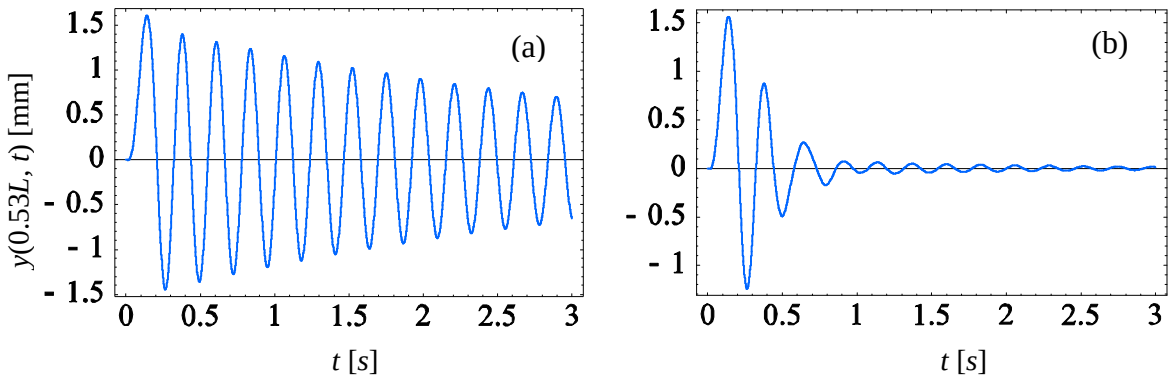

Fig. 3-24. Transient response of the system, (a) damped beam without dynamic damper, (b) damped beam with nonlinear dynamic damper

For the case 3, undamped beam with linear dynamic damper, using optimal values from Ref. [40], only 1.62% deflection reduction with respect to the bare beam (case 1) is found; while the case 4 (present optimal parameters) shows 6.26% deflection reduction. Moreover, the case 5, damped beam and present optimal parameters, shows 6.16% deflection reduction with respect to the case 2 (damped bare beam). The best deflection reduction is obtained by using the nonlinear dynamic damper (case 7), 7.42% deflection reduction is found with respect to the case 2.

Table 3-1. Comparison between various optimization results: moving load excitation

Case	Beam and dynamic damper condition	Stiffness	Viscous damping λ [Ns/m]	Dynamic damper location d [m]	Maximum deflection [mm]	Position of maximum deflection [m]	Time of maximum deflection [s]	η
1	Undamped beam without dynamic damper	0	0	-----	1.6279	2.11	0.1398	0%
2	Damped beam ($\xi_p = 0.01$) without dynamic damper	0	0	-----	1.6042	2.11	0.1401	0%
3	Undamped beam with linear dynamic damper, optimal values in Ref. [40]	877.8N/m	12.98	2	1.6016	2.11	0.1402	99.9%
4	Undamped beam with linear dynamic damper, deflection optimization approach	1795N/m	0.1	2.2	1.5260	2.12	0.1403	99.6%
5	Damped beam with linear dynamic damper, deflection optimization approach	1795N/m	0.1	2.2	1.5054	2.12	0.1407	3.4%
6	Damped beam with linear dynamic damper, energy optimization approach	900N/m	10.5	2.2	1.5306	2.12	0.1401	88.9%
7	Damped beam with nonlinear dynamic damper, deflection optimization approach	6.7×10^9N/m^3	0.1	2.12	1.4852	2.12	0.1402	2.3%
8	Damped beam with nonlinear dynamic damper, energy optimization approach	0.3×10^9N/m^3	11	2.12	1.5640	2.12	0.1398	87.4%

3.7. Optimal NES: beam length effect

In order to understand the effect of the beam length on the nonlinear dynamic damper optimization, the following beam lengths are considered: L=1m, L=4m and L=10m; the other beam parameters are the same of section 3.3.2, Wu [40] case. The optimal location for the nonlinear dynamic damper remains close to the middle, d=0.53L; a small viscous damping is considered (λ=0.1) when the optimization is carried out by considering the maximum beam deflection. The dynamic damper mass remains 5% of the total mass structure; it means that the damper mass varies accordingly with the beam length. Results have been reported in Table 3-2.

It is known in the literature that $V_{crit}L = constant$, this result is confirmed; moreover, it is found that for both the maximum deflection and the energy approaches $C_{opt}L^9$ = constant (for

example, for the max deflection: $C_{opt}L^9 = 1.7(10^{15}) \times 1^9 = 6.7(10^9) \times 4^9 = 1.7(10^6) \times 10^9 = 1.7(10^{15})\text{Nm}^6$; for the energy approach: $C_{opt}L^9 = 80(10^{12}) \times 1^9 = 0.30(10^9) \times 4^9 = 80(10^3) \times 10^9 = 80(10^{12})\text{Nm}^6$); in each case η_{max}=87.4% and $\lambda_{opt}L = constant$ ($\lambda_{opt}L = 44 \times 1 = 11 \times 4 = 4.4 \times 10 = 44$Ns). Such conservation laws can be extremely useful for practical designers; indeed, they define classes of structures having similar behavior. It means that when we find optimal location and stiffness for a particular length, they can be straightforwardly extended to other lengths.

Table 3-2. results for optimization of nonlinear dynamic damper with various length

Beam length L [m]	1	4	10
Velocity for which the max deflection occurs [m/s]	86	21.5	8.6
Dynamic damper mass [kg]	0.3519	1.4076	3.519
Optimized stiffness using the deflection approach C_{opt} [N/m^3]	1.7(1015)	6.7(109)	1.7(106)
Optimized maximum deflection [mm]	0.0235	1.4852	23.53
Optimized stiffness using the energy approach, C_{opt} [N/m^3]	80(1012)	0.30(109)	80(103)
Optimized viscous damping, λ_{opt} [Ns/m]	44	11	4.4
η	87.4%	87.4%	87.4%

3.8. Load velocity effect on the DVA performances

Now the behavior of optimal dynamic dampers is considered on a wide range of the moving load velocity. For the deflection approach, optimal linear and nonlinear stiffness for each case are used (Table 3-1) and λ=0.1Ns/m. For the linear dynamic damper d=0.55L and k=1795N/m, for the nonlinear dynamic damper d=0.53L and C=6.7×10^{9}N/m^3. The maximum deflection vs. the travelling load speed is shown in Fig. 3-25. Both linear and nonlinear dynamic dampers allow to improve the beam behavior over a wide speed range; the nonlinear dynamic damper is slightly more effective than the linear one, in the vicinity of the maximum amplitude (V=21.5m/s), see Figure 3-25. For higher speeds, linear and nonlinear dampers behave similarly; in any case the behavior with dampers is better than the bare beam.

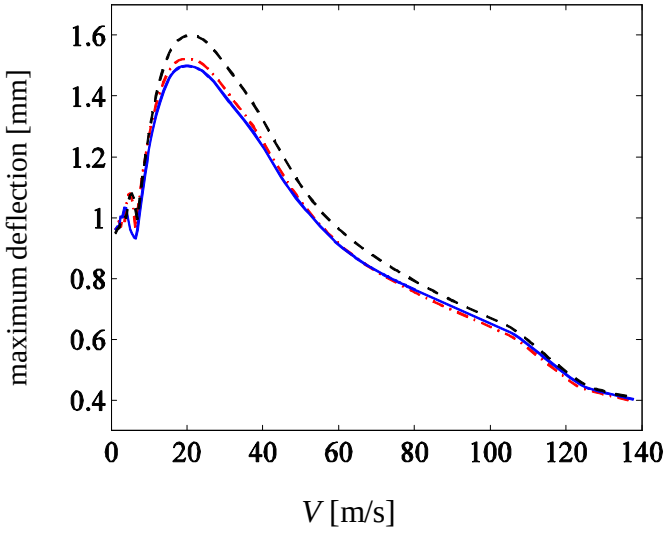

Fig. 3-25. Maximum deflection vs. the traveling load velocity, effect of dynamic dampers optimized for V=21.5 m/s: '- - -' bare beam, '-·-·-' Linear damper, '——' Nonlinear damper

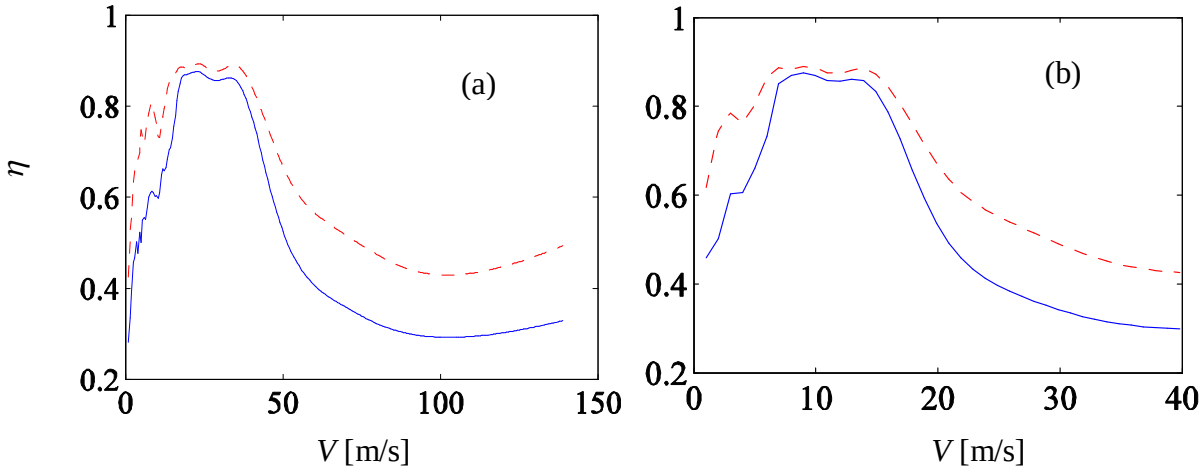

Fig. 3-26. Portion of input energy absorbed and dissipated by the dynamic damper versus velocity; (a) L=4m, (b) L=10m, '- - -' Linear dynamic damper, '——' Nonlinear dynamic damper

For energy approach the following damper parameters are considered, λ=10.5Ns/m and k=900N/m for linear dynamic damper and λ=11Ns/m and C=0.3×10^9 N/m^3 for the nonlinear one. The damper location is d=0.55L (linear case), d=0.53L (nonlinear case). The portion of the input energy dissipated by the damper, η, vs. load velocity is shown in Fig. 3-26 for two beam lengths. It is clear that linear dynamic damper is more effective than the nonlinear one in absorbing

energy; such behavior seems independent on the beam length. These dynamic dampers are more effective around the first critical load velocity; it is rational because parameters are optimized at this velocity.

3.9. Random Optimization

In this section the optimal parameter set is searched by randomly sampling the parameter space with uniform distribution. The location of the dynamic damper has a small effect on the two present goal functions, maximum deflection and η; therefore, only stiffness and viscous damping are considered in the optimization process. The total number cases for the random optimization is 8000, i.e. the same order of the uniform sampling approach.

For the linear dynamic damper the optimization is carried out considering the following parameter set ($k \in$[0, 2000 N/m], $\lambda \in$[0, 20Ns/m]).

Figures 3-27(*a, b*) show the effect of the viscous damping and stiffness on maximum deflection and Figures 3-27(*c,d*) show the effect of the same parameters on η.

Figures 3-27 is obtained from the two dimensional random search, the surface representing the results cannot be easily represented because of the random distribution of data; therefore, a lateral view of such surface is represented. This figure gives a general information about the damper performances; for example, let us consider Figure 3-27a and λ=10Ns/m, it shows the variation of the maximum deflection as the stiffness *k* is varied. Even though *k* cannot be identified from Figure 3-27a only, using Figures 12 a and b one can easily read the optimal values of λ and *k*. In Figs. 3-27(*a,b*) point *A* indicates the optimum (k=1682N/m, λ=0.0749 Ns/m) and the maximum amplitude of oscillation is 1.5055mm (the regular sampling gave 1.5054mm for k=1795N/m and λ=0.1 Ns/m). Point *B* shows the maximum deflection of the bare damped beam, y_{max}=1.6042mm. In Fig. 3-27(*c,d*) point *C* is the optimum for the energy approach (k=899N/m, λ=10.51Ns/m) and the energy absorption is 88.9% of input energy (the regular sampling gave η=88.9% for k=900N/m and λ=10.5Ns/m). By observing Fig. 3-27(c) close to the origin, it is clear that with λ=0 dynamic damper cannot absorb energy (η=0).

The random optimization obtains results quite close to the regular sampling. By using this method the effect of each parameter is clearer in some special situations. For example Fig. 3-27(a) shows that high values of the stiffness tend to decrease the effect of viscous damping on

the maximum deflection; Fig. 3-27(b) shows clearly that for k≈500N/m the viscous damping has a small effect on maximum deflection.

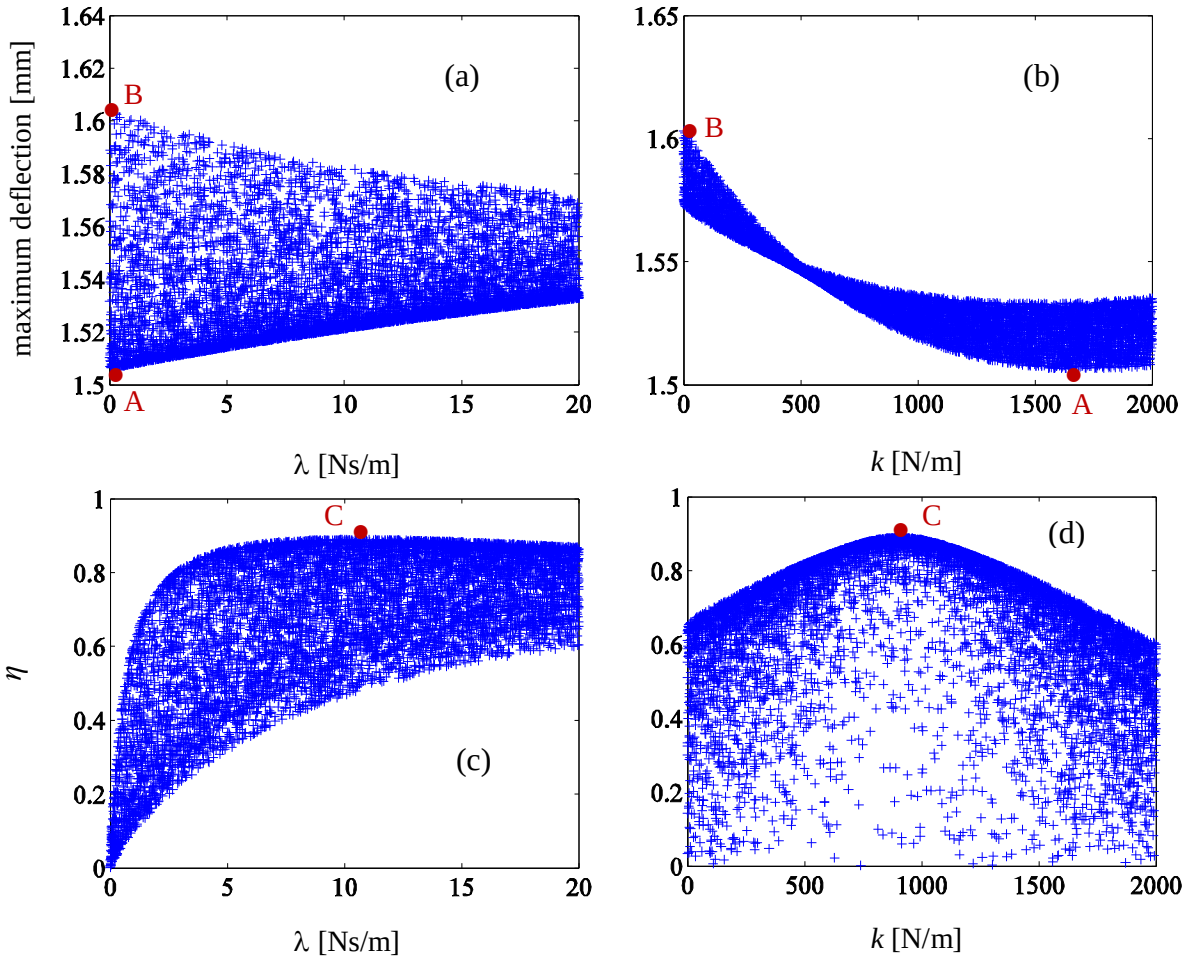

Fig. 3-27. Random optimization for linear dynamic damper.

For the case of the nonlinear dynamic damper, the optimization is carried out considering the following set (C∈[0, 15×10^{9}N/m^3], λ∈[0, 40Ns/m]). Point A of Figs. 3-28(a,b) indicates the optimum for the deflection approach (C=6.73×10^{9}N/m^3 and λ=0.0347Ns/m), the deflection is y_{max}=1.4850mm (for the uniform sampling y_{max}=1.4852mm, C=6.7×10^{9}N/m^3 and λ=0.1Ns/m). Point *B* of Figs. 3-28(*a*,*b*) shows the deflection of the bare damped beam, y_{max}=1.6042mm. Point

C of Figs. 3-28(c,d) shows the optimum for the energy approach, the dynamic damper can absorb up to 87.3% of input energy; the stiffness is $C=0.298\times10^{9}$N/m^3 and $\lambda=10.60$Ns/m (the uniform sampling gives $\eta_{max}=87.4\%$ for $C=0.3\times10^{9}$N/m^3 and $\lambda=11$Ns/m).

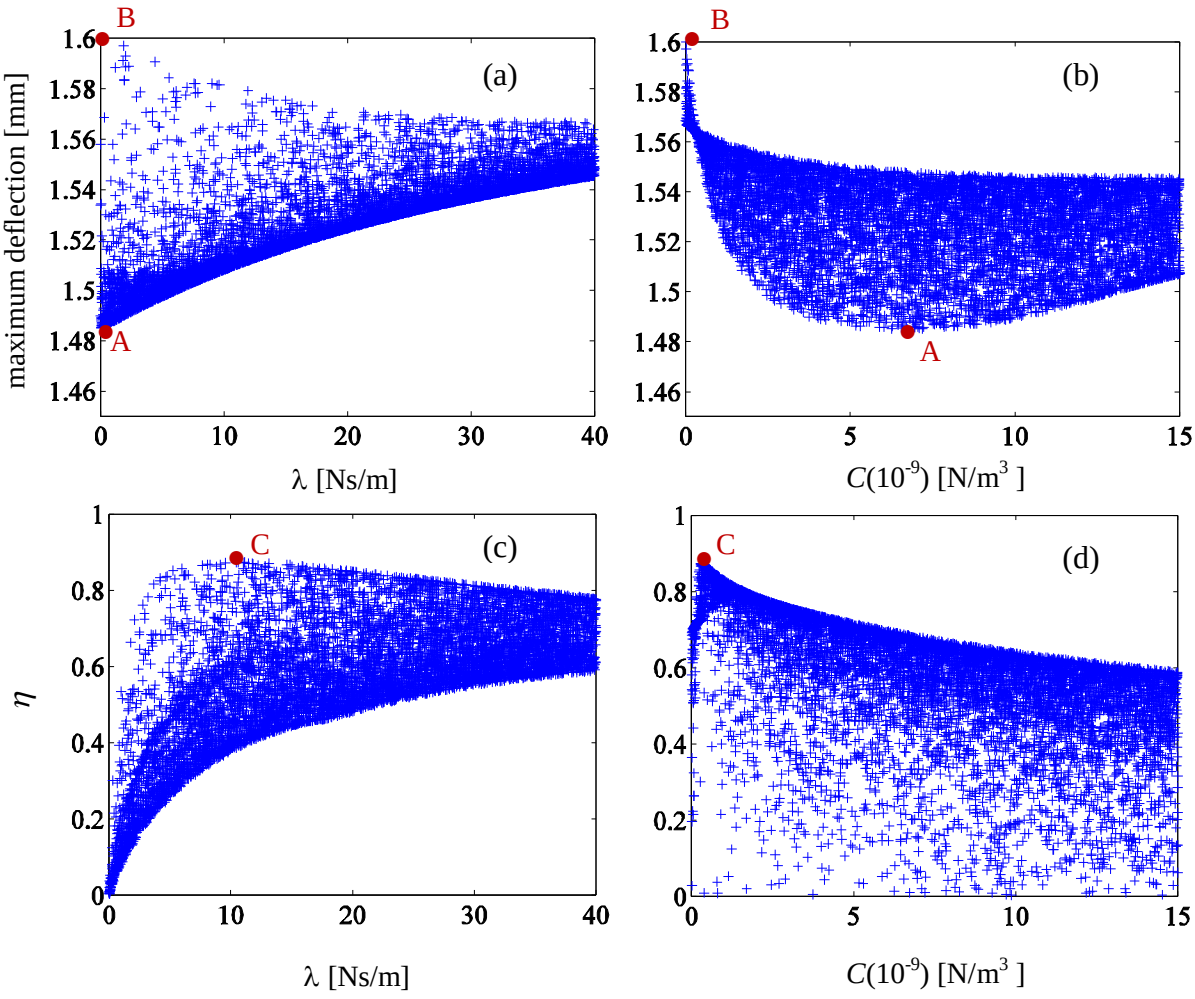

Fig. 3-28. Random optimization for nonlinear dynamic damper.

CHAPTER 4

Multifarious Nonlinear Vibration Absorbers

4.1. Introduction

Successful manufactured products rely on the best possible design and performance. They are usually produced using the tools of engineering design optimization in order to meet design targets. However, conventional design optimization may not always satisfy the desired targets. Ruzicka and Derby [36] have studied the effects on vibration isolation of a single degree of freedom system owing to various types of damping elements: for example, viscous, Coulomb, quadratic, nth power and hysteretic.

Snowdon [65] has studied the performance characteristics of isolators in which non-linear hardening and softening springs are used in parallel with a linear viscous damper. Snowdon [66] also proposed a dual phase viscous damper and studied its performance characteristics when its base is excited by rounded step or rounded pulse or oscillatory step displacements. Cornelius [67] has studied the performance characteristics of a dual acting type of isolator. The dual acting isolator has a damper whose characteristics are similar to those of a linear viscous damper if the velocity is below a certain predetermined value. However, if the velocity is above this predetermined value, the damping force is constant. The performance of different kinds of Dual phase damping shock mounts has studied by Guntura and Sankar [68]. They stated that conclusions of that study are of interest to engineers concerned with the design of shock mounts.

Recently Lee et al. [69] studied the performance of vibro-impact dynamic dampers in systems of coupled oscillators, consisting of single-degree-of-freedom primary linear oscillators (LOs) with vibro-impact attachments, acting as vibro-impact nonlinear energy sinks (VI NESs). They found that, the most efficient mechanism for vibro-impact targeted energy transfers (VI TET) is through the excitation of highly energetic VI impulsive orbits (IOs), i.e., periodic or quasi periodic orbits corresponding to zero initial conditions, except for the initial velocities of the linear oscillators. Deshpande et al. [70] developed a numerical analysis approach to optimize the performance of a piecewise linear vibration isolation system; they found that the optimal solution depends on damping coefficients, stiffness ratio, and clearance.

Rüdinger [71] studied the performance of nonlinear viscous damping for tuned mass dampers. The tuned mass damper was assumed to be attached to a single-degree-of-freedom system excited by white noise. They found that, the structural damping has very little influence on the

optimal parameters for a linear tuned mass damper; moreover, they revealed that the optimal linear and nonlinear tuned mass dampers have practically the same effect in terms of reducing the structural displacement.

The goal of the present chapter is to analyze the performances of different passive nonlinear dynamic dampers in reducing the deflection of an Euler Bernoulli beam under moving loads; local non-linear attachments having monomial, polynomial or piecewise linear stiffness are considered. From applicable point of view, the use of piecewise linear dynamic absorbers is less expensive with respect to other kinds of nonlinear dampers; therefore, they are more likely suitable for actual applications.

4.2. Dynamical model

Consider the system represented in Fig. 4-1: (almost similar to Fig. 3-1) a simply supported beam is connected to a small mass through a essential nonlinear spring and a linear viscous damper; the beam is loaded with a point moving load.

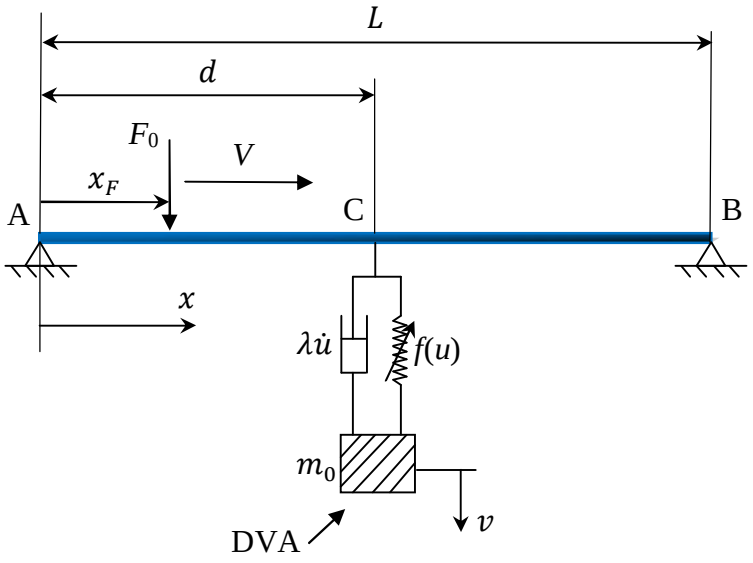

Fig. 4-1. The beam model.

Considering the linear Euler-Bernoulli theory for the beam modeling, the equations of motion of the system are given by,

$$EIy_{,xxxx}(x,t) + \rho A y_{,tt}(x,t) + [f(u) + \lambda u_{,t}(t)]\delta(x-d) = F_0\delta(x-Vt)\left[H\left(\frac{L}{V}-t\right)\right] \quad (4\text{-}1a)$$

$$y(0,t) = 0, y(L,t) = 0, y_{,xx}(0,t) = 0, y_{,xx}(L,t) = 0 \quad (4\text{-}1b)$$

$$y(x,0) = 0, y_{,t}(x,0) = 0 \quad (4\text{-}1c)$$

$$m_0 v_{,tt}(t) - f(u) - \lambda u_{,t}(t) = 0\,,\ \ v(0) = 0,\ \ v_{,t}(0) = 0\,,\ \ \ t > 0 \quad (4\text{-}2a)$$

$$u(t) = y(d,t) - v(t) \quad (4\text{-}2b)$$

$$f(u) = c_i u^i,\ i=1,3,5,7,9 \qquad \text{For monomial stiffness} \quad (4\text{-}3a)$$

$$f(u) = c_1 u + c_3 u^3 + c_5 u^5 + c_7 u^7 \qquad \text{For polynomial stiffness} \quad (4\text{-}3b)$$

$$f(u) = \begin{cases} k(u+\Delta) & u < -\Delta \\ 0 & -\Delta \le u \le \Delta \\ k(u+\Delta) & u > \Delta \end{cases} \qquad \text{For piecewise linear stiffness} \quad (4\text{-}3c)$$

The beam dynamics is governed by the PDE represented by equation (4-1*a*) with simply supported boundary conditions (3-1b) and initial conditions (3-1c); $f(u)$ is stiffness force, equation (4-3) is the definition of stiffness force for multifarious nonlinear stiffness DVAs; Δ is the piecewise linear stiffness tolerance. For details see the chapter 3-2.

Using Galerkin method and projecting on the p^{th} eigenfunction and taking advantage of the orthonormality conditions, one obtains

$$\ddot{a}_p(t) + 2\xi_p\omega_p\dot{a}_p(t) + \omega_p^2 a_p(t) + \left\{D(t) + \lambda\left[\sum_{r=1}^{\infty}\dot{a}_r(t)\,\phi_r(d) - \dot{v}(t)\right]\right\}\phi_p(d) = F_0\phi_p(Vt)\left[H\left(\frac{L}{V}-t\right)\right],\ \ p = 1,2,\ldots \quad (4\text{-}4a)$$

$$m_0\ddot{v}(t) - D(t) + \lambda\left[\dot{v}(t) - \sum_{r=1}^{\infty}\dot{a}_r(t)\,\phi_r(d)\right] = 0 \quad (4\text{-}4b)$$

Where $\dot{a}_p(t) = da_p/dt$ and a viscous damping term is added to the generic modal equation (4-4*a*) after projection. *D*(*t*) represent the restoring force acting on the beam due to the damper spring:

$$\begin{cases} D(t) = c_i \left[\sum_{r=1}^{\infty} a_r(t)\,\phi_r(d) - v(t)\right]^i, i = 1,3,5,7,9 \end{cases} \quad (4\text{-}5a)$$

$$\begin{cases} D(t) = c_1 \left[\sum_{r=1}^{\infty} a_r(t)\,\phi_r(d) - v(t)\right] + c_3 \left[\sum_{r=1}^{\infty} a_r(t)\,\phi_r(d) - v(t)\right]^3 \\ \quad + c_5 \left[\sum_{r=1}^{\infty} a_r(t)\,\phi_r(d) - v(t)\right]^5 + c_7 \left[\sum_{r=1}^{\infty} a_r(t)\,\phi_r(d) - v(t)\right]^7 \end{cases} \quad (4\text{-}5b)$$

$$\begin{cases} D(t) = k \times \left[\left(\sum_{r=1}^{\infty} a_r(t)\,\phi_r(d) - v(t)\right) - \Delta\right] \times H\left[\left(\sum_{r=1}^{\infty} a_r(t)\,\phi_r(d) - v(t)\right) - \Delta\right] \\ \quad + k \times \left[\left(\sum_{r=1}^{\infty} a_r(t)\,\phi_r(d) - v(t)\right) + \Delta\right] \times H\left[-\left(\sum_{r=1}^{\infty} a_r(t)\,\phi_r(d) - v(t)\right) - \Delta\right] \end{cases} \quad (4\text{-}5c)$$

Eq. (4-5*a*) presents the restoring force for the five different kinds of the monomial function; Eq. (4-5*b*) presents polynomial stiffness function and Eq. (4-5*c*) is the restoring force when damper stiffness has piecewise linear behavior.

The nonlinear attachment couples all modes through the series (4-5); in the case of linear dynamic damper, one can transform the system (4-4), after finding the new vibration modes, into a system of uncoupled linear equations; conversely, in the case of nonlinear spring the system cannot be uncoupled.

The transient dynamics is studied by numerically integrating the dynamical system represented by equations (4-4*a*,*b*), after truncating the series (3-4), see section 3-2 for details; the truncation is suitably chosen by checking the convergence of the expansion.

4.3. Optimization of the dynamic damper

The dynamic damper installed nearby the middle, *d*=0.55*L* for linear and piecewise linear dynamic damper and, *d*=0.53*L* for other kinds of nonlinearities, see Ref. [72]. The maximum deflection occurs at different velocities for the case of the moving load and moving vehicle; in each case, the optimization is carried out for the corresponding critical velocities.3 mode shapes

considered for truncating Galerkin series. Numerical values are the same as section 3-3-2; the damped beam is considered: ξ_p=0.01(p=1,2,...).

4.3.1. Monomial stiffness

Consider a local attachment having a monomial stiffness, $f(u)= c_i u^i$, i=1, 3, 5, 7, 9, see Eq. (4-3*a*). The linear ($f(u)=c_1 u$) and cubic ($f(u)=c_3 u^3$) stiffnesses have been studied in the Ref. [72]; here we use such cases for comparisons.

For each type of monomial, the nonlinear dynamic dampers are optimized, Figures 4-2(a)-(d) show the maximum beam deflection with attachments, having monomial stiffness, versus the coefficient c_i,; the optimal coefficients are readily obtained, it is to note that a unique minimum is present; results are summarized in the Table 4-1. In the Ref. [72], it was found that, cubic stiffness shows better performances with respect to the linear one; the results reported in Table 4-1 show that, using higher power for the nonlinear stiffness leads to a more effective reduction of the beam deflection; for example using a linear dynamic damper we can reduce the beam deflection of 6.159% and using a cubic one, it is possible to reduce the beam deflection of 7.418%; while if the stiffness force is $f(u)=c_9 u^9$ ($c_9=88\times10^{27}$ N/m^9) the optimal dynamic damper is able to reduce the beam deflection of 8.147%.

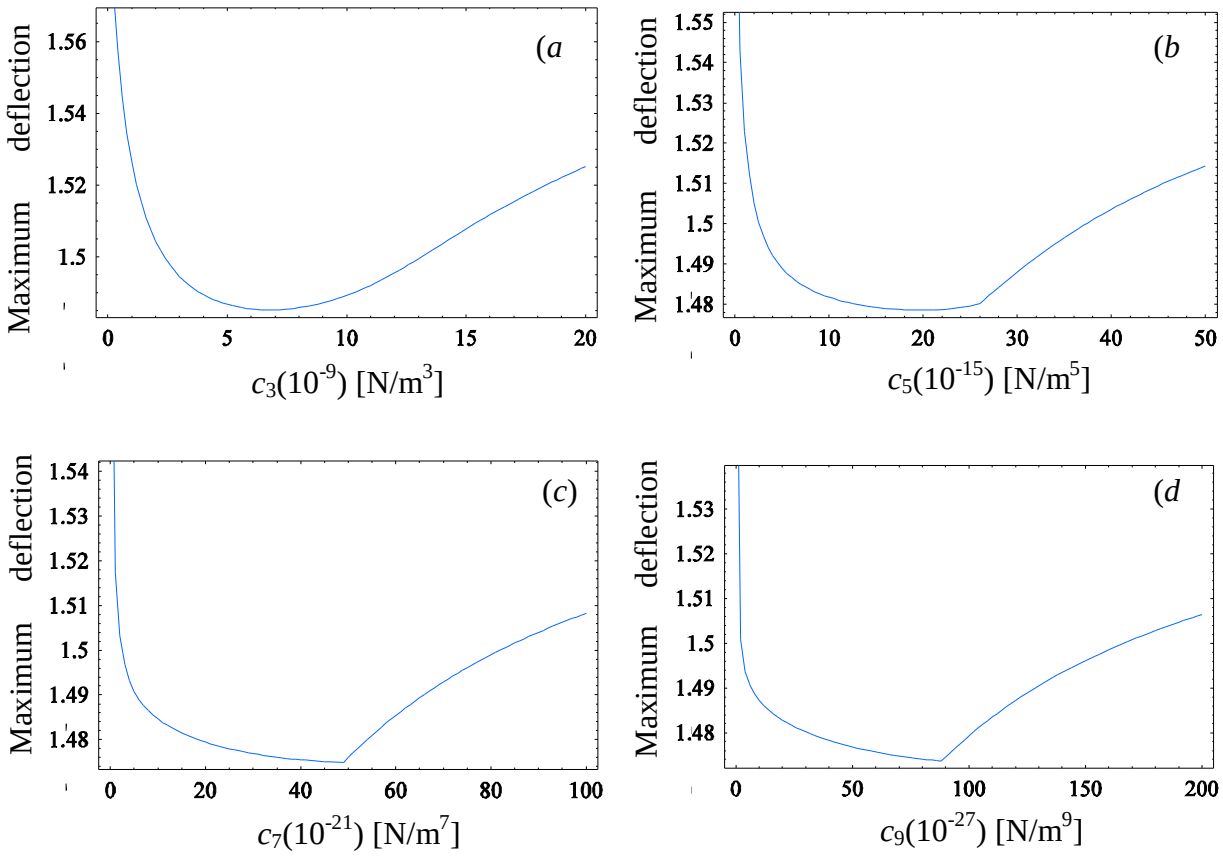

Fig. 4-2. The optimal monomial stiffness, (*a*): $f(u)= c_3u^3$, (*b*): $f(u)= c_5u^5$, (*c*): $f(u)= c_7u^7$, (*d*): $f(u)= c_9u^9$.

4.3.2. Polynomial stiffness

Consider a dynamic damper having a linear viscous damper and a polynomial stiffness, $f(u)=c_1u+c_3u^3+c_5u^5+c_7u^7$.

The optimization is carried out considering a four parameter space: c_1, c_3, c_5 and c_7. Such parameters are randomly sampled and the minimum deflection is found. The total number of random samples (sets of parameters) is 1720000.

After carrying out the random search one obtains a set of values of the objective function (maximum beam deflection) versus four parameters c_i; this set is projected on sections of the parameter space to allow a visualization, see Figures 4-3(a)-(d).

The optimal set is found by means of a suitable code developed for the Mathematica software; however, Figures 4-3(a)-(d) allow a quick finding of the minimum and the corresponding parameters set; such set is presented in Table 4-1, case 6; it gives the maximum beam deflection equal to 1.4757mm (8.01% reduction respect to bare beam). Similarly to the previous cases we used a small dissipation, λ=0.1Ns/m.

It turns out that, the most important part of this compound dynamic damper is the seventh power, (c_7=46.6(10^{21})N/m^7); i.e., the effects of linear (c_1=15.7N/m), cubic (c_3=0.49(10^9)N/m^3) and fifth power terms (c_5=0.56(10^{15})N/m^5) are negligible with respect to the seventh power term; this can be proven by comparing case 6 of Table 4-1 with cases 2-5.

Figures 4-3(a)-(d) display the same minimum, on the abscissa of each figure one can read the corresponding parameter. The optimal values for c_1 (Fig. 4-3(a)), c_3 (Fig. 4-3(b)) and c_5 (Fig. 4-3(c)) are small and c_7 (Fig. 4-3(d)) is the most significant parameter. By comparing case 6 of Table 4-1 with cases 5, 7, it turns out that a high power monomial stiffness performs better than a polynomial one.

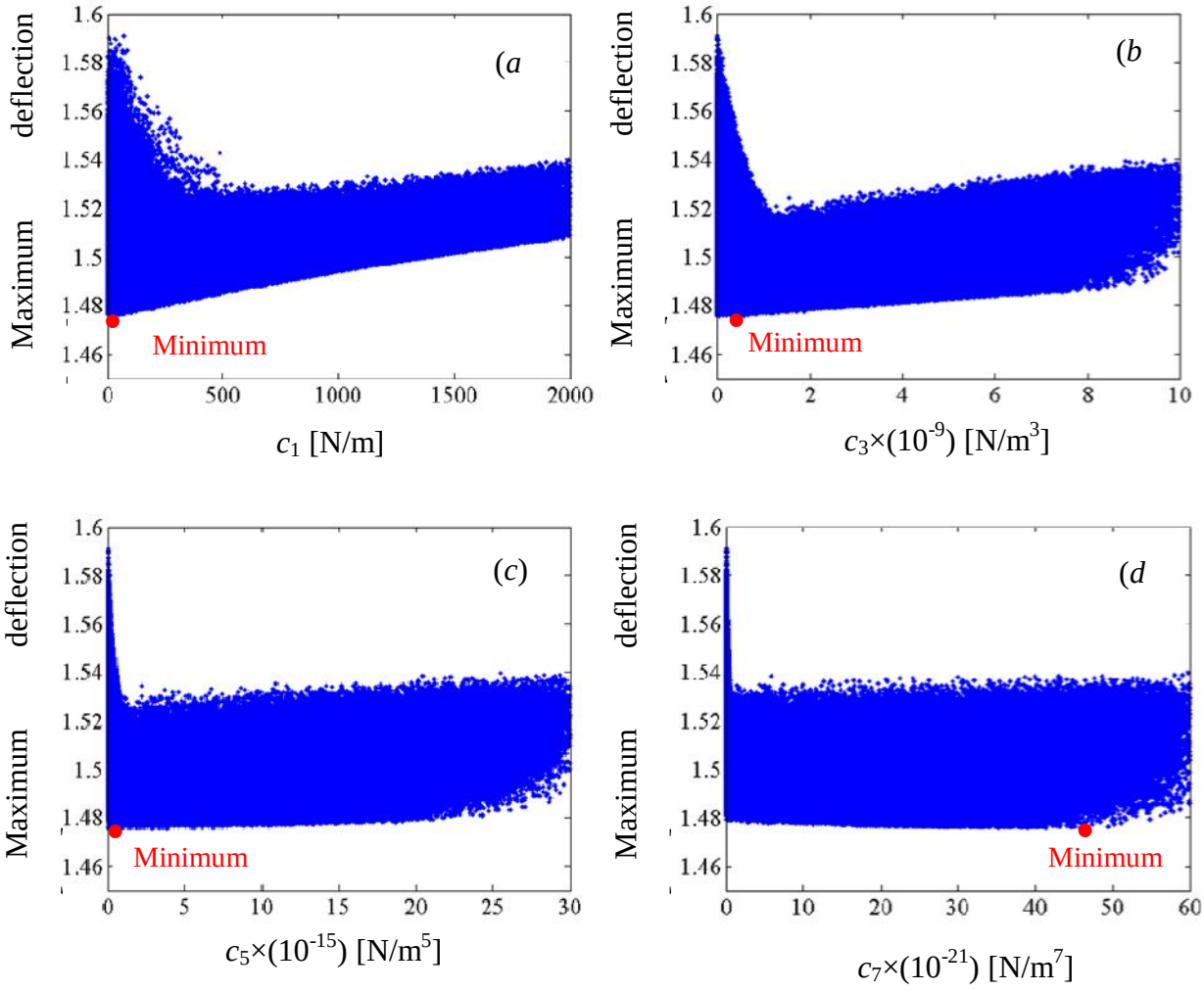

Figure 4-3, the maximum beam deflection versus different coefficients of polynomial stiffness function: random optimization results; *a*: maximum deflection vs. c_1, *b*: maximum deflection vs. c_3, *c*: maximum deflection vs. c_5, *d*: maximum deflection vs. c_7.

4.3.3. Piecewise linear stiffness

Now piecewise linear dynamic dampers are considered. Figure 4-4 shows a schematic graph for the present kind of restoring force versus a generic elongation u. When the elongation $|u|$ is smaller than the gap Δ, the restoring force is zero (2Δ is the dead zone). For $|u|>\Delta$ the restoring force varies linearly with u; the slope is given by k.

The optimization is carried out considering two parameters: Δ and k; such parameters are regularly sampled. Figs. 4-5 and 4-6 depicts the maximum beam deflection versus Δ and k,

finding the optimal parameters is trivial, the optimal pair is k=37000N/m and Δ=0.58mm, corresponding to a maximum beam deflection equal to 1.4735mm (8.147% reduction respect to the bare beam). Table 4-1 shows that the piecewise linear dynamic damper is the most effective for reducing the beam deflection (Case 8).

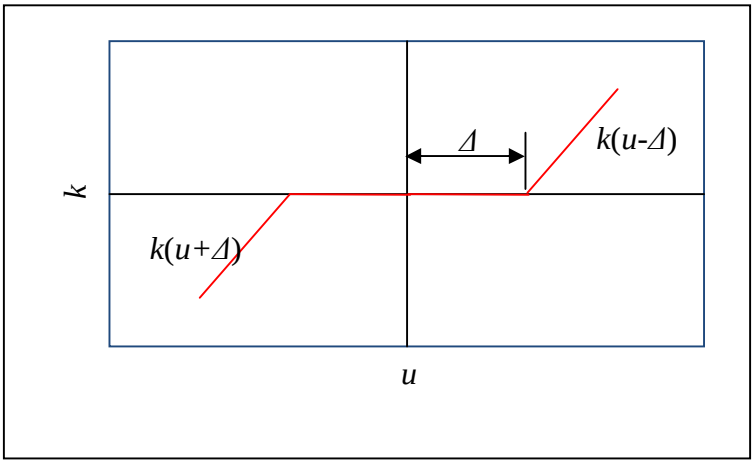

Figure 4-4, the schematic stiffness force versus stiffness deflection for piecewise linear dynamic damper.

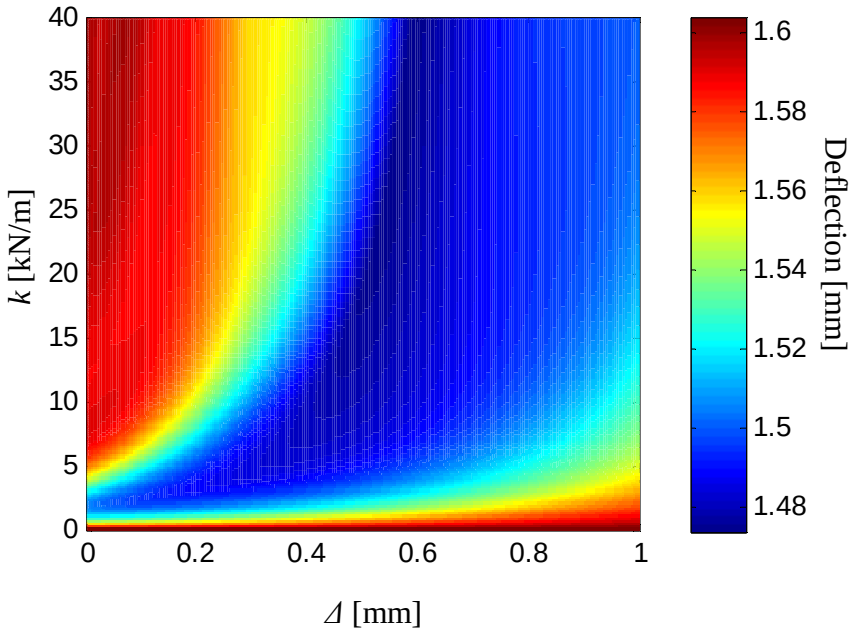

Fig 4-5. Maximum deflection vs. gap Δ and stiffness k of the piecewise linear stiffness; the optimum is k=37000N/m and Δ=0.58mm (1.4735mm max deflection).

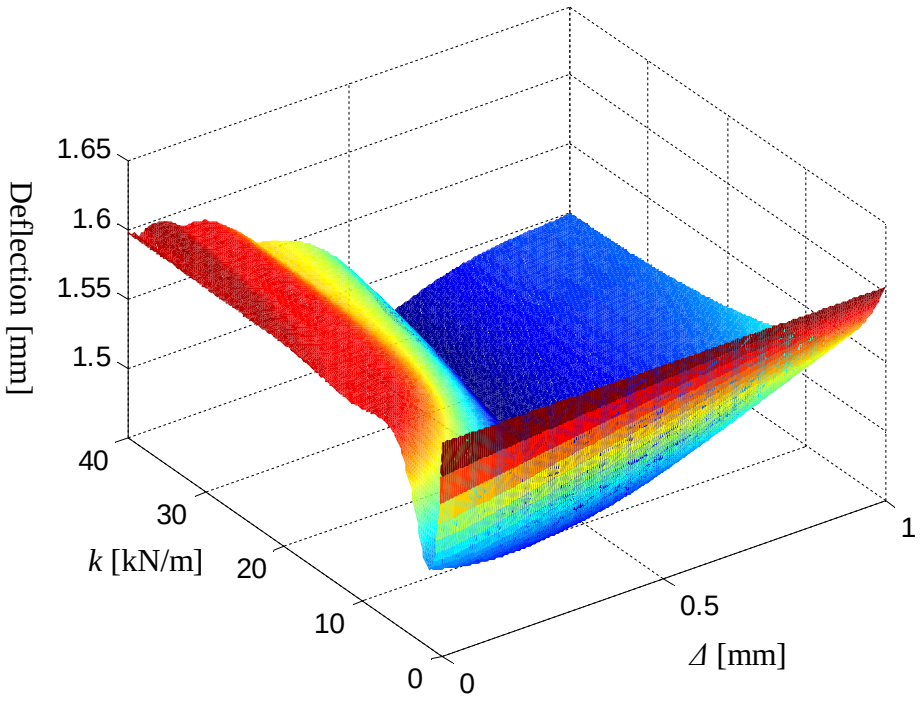

Fig. 4-6. Maximum deflection vs. gap Δ and stiffness k of the piecewise linear stiffness: 3D presentation.

Table 4-1. Comparison of different kinds of dynamic dampers to obtain minimum beam deflection, λ=0.1Ns/m.

Case	Beam and dynamic damper condition	Stiffness	Maximum deflection [mm]	Reduction Percentage
1	Bare beam	0	1.6042	----
2	Linear dynamic damper	c_1=1.79(10^3) N/m	1.5054	6.159%
3	Monomial cubic dynamic damper	c_3=6.7(10^9) N/m^3	1.4852	7.418%
4	Monomial fifth power stiffness	c_5=19.6(10^{15}) N/m^5	1.4786	7.829%
5	Monomial seventh power stiffness	c_7=49(10^{21}) N/m^7	1.4750	8.054%
6	Polynomial seventh power stiffness	c_1=0.0158(10^3) N/m c_3=0.492(10^9) N/m^3 c_5=0.564(10^{15}) N/m^5 c_7=46.58(10^{21}) N/m^7	1.4757	8.010%
7	Monomial ninth power stiffness	c_9=88(10^{27}) N/m^9	1.4737	8.135%
8	Piecewise linear dynamic damper	k=37000 N/m Δ=0.58mm	1.4735	8.147%

CHAPTER 5

Transient Moving Vehicle Excitation

5.1. Introduction

In the previous two chapter we studied the performance of linear and different kinds of nonlinear passive dynamic dampers for the beam subjected to transient traveling load. In this chapter the performance of such vibration absorbers is studied for the case of the Euler-Bernoulli beam under excitation of the moving vehicle.

In the past few decades, the problem of bridge vibration under moving forces or vehicle loads has been studied extensively. The dynamic performance of bridges can be affected by many factors. Different types of vehicles, vehicle speeds, and road surface conditions could all contribute to different bridge dynamic performances [73]. In the literature many vehicle–bridge interaction models have been proposed for the purpose of identifying vehicle parameters. Bridges are usually modeled as simply support beams [74], [75] and [76] or multi-span continuous beams [77] and [78]. For the vehicle model, most researchers used a single-degree-of-freedom (SDOF) system or two-DOF system [79], [80] and [81], while others used a more complex twelve-parameter vehicle model [82]. In the present study, the moving vehicle is modeled as a single DOF mass with linear stiffness and viscous linear damping. One may improve the model and consider more complicated models, while as results show the performance of the different kinds of linear and nonlinear DVAs is almost similar for the case of the moving vehicle and moving load; i.e. when one type of nonlinearity improve the performance of the DVA this type is also effective for the case of the moving vehicle. So we guess that for the different kinds of traveling excitation the effective NESs are similar.

In this chapter the performances of linear, cubic and piecewise linear stiffness for the DVA is considered in order to reduce the deflection of an Euler Bernoulli beam under moving loads or vehicles. From applicable point of view, the use of piecewise linear dynamic absorbers is less expensive with respect to other kinds of nonlinear dampers; therefore, they are more likely suitable for actual applications. The monomial and polynomial nonlinearities did not study for the case of the traveling vehicle, since it demonstrated that piecewise linear stiffness is the most effective nonlinearity when beam is subjected to the traveling excitation.

5.2. Dynamical systems and basic equations

Consider the system of figure 5-1, the simply supported beam is loaded by a moving vehicle (one DOF model) and a dynamic damper is attached to the middle of the beam. The equations of motion for such system are given by

$$EIy_{,xxxx}(x,t) + \rho A y_{,tt}(x,t) + [f(u) + \lambda u_{,t}(t)]\delta(x-d) + [k_v w(t) + c_v w_{,t}(t)]\delta(x-Vt)H\left(\frac{L}{V}-t\right) = 0, \qquad x \in (0,L),\ t > 0 \tag{5-1a}$$

$$y(0,t) = 0, y(L,t) = 0, y_{,xx}(0,t) = 0, y_{,xx}(L,t) = 0 \tag{5-1b}$$

$$y(x,0) = 0, y_{,t}(x,0) = 0 \tag{5-1c}$$

$$m_0 v_{,tt}(t) - f(u) - \lambda u_{,t}(t) = 0\,,\ v(0) = 0,\ v_{,t}(0) = 0\,,\ t > 0 \tag{5-2a}$$

$$u(t) = y(d,t) - v(t) \tag{5-2b}$$

$$m_v(z_{,tt}(t) - g) - k_v w(t) - c_v w_{,t}(t) = 0\,,\ z(0) = 0,\ z_{,t}(0) = 0\,, \qquad 0 < t < \frac{V}{L} \tag{5-3a}$$

$$w(t) = y(Vt,t) - z(t) \tag{5-3b}$$

Where m_v, k_v and c_v are mass, stiffness and viscous damping of the vehicle, respectively; z(t) is the vertical position (down is positive). $f(u)$ is the restoring force of the damper spring; in the present section we consider mainly piecewise linear springs. Note that, due to the nonlinearity of the dynamic damper, this set of partial differential equations cannot be decoupled. After projection of eq. (5-1), similarly to eq. (4-1), one obtains a set of ordinary differential equations:

$$\ddot{a}_p(t) + 2\xi_p\omega_p\dot{a}_p(t) + \omega_p^2 a_p(t) + \left\{D(t) + \lambda\left[\sum_{r=1}^{\infty}\dot{a}_r(t)\,\phi_r(d) - \dot{v}(t)\right]\right\}\phi_p(d) \tag{5-4a}$$

$$-\left\{k_v\left[z(t)-\sum_{r=1}^{\infty}a_r(t)\,\phi_r(Vt)\right]+c_v\left[\dot{z}(t)-\sum_{r=1}^{\infty}\dot{a}_r(t)\,\phi_r(Vt)\right]\right\}H\left(\frac{L}{V}-t\right)\times\phi_p(Vt)=0,\quad p=1,2,\ldots$$

$$m_0\ddot{v}(t)-D(t)+\lambda\left[\dot{v}(t)-\sum_{r=1}^{\infty}\dot{a}_r(t)\,\phi_r(d)\right]=0 \tag{5-4b}$$

$$m_v(\ddot{z}(t)-g)+\left\{k_v\left[z(t)-\sum_{r=1}^{\infty}a_r(t)\,\phi_r(Vt)\right]+c_v\left[\dot{z}(t)-\sum_{r=1}^{\infty}\dot{a}_r(t)\,\phi_r(Vt)\right]\right\}H\left(\frac{L}{V}-t\right)=0 \tag{5-4c}$$

Where $D(t)$ is given by Eqs.(4-5).

The transient response of the ODEs represented by Eqs. (5-4*a*, *b*, *c*) is studied numerically.

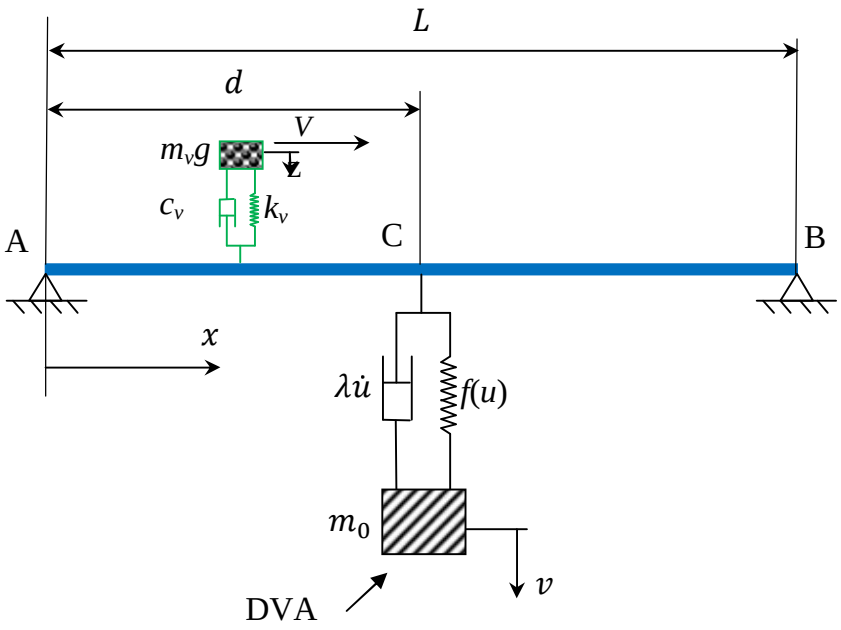

Fig. 5-1. The beam model subjected to moving vehicle.

5.3. Critical loading condition

The physical parameters for the beam are the same as the case of moving load, Chapter 4. Moreover, m_v=1kg, k_v=980N/m and c_v=6.26Ns/m are mass, stiffness and viscous damping of the moving vehicle and g=9.81m/s^2 is the gravitational acceleration. Note that the weight of the present moving vehicle is the same as moving load in the previous chapter.

For the present case, the maximum deflection of the beam, 2.498mm, occurs at V=19.5m/s; this velocity is slightly less than the critical one for the case of the moving load; see table 5-1 for details.

Table 5-1. Critical velocities for the traveling load and traveling vehicle.

	Moving load		Moving vehicle	
	Undampped beam	Dampped beam	Undampped beam	Dampped beam
Critical velocity [m/s]	21.5	21.25	19.5	19.5
Mid-span maximum deflection [mm]	1.6217	1.5981	2.5315	2.4946
Absolute maximum deflection [mm]	1.6279 at x=0.53L	1.6042 at x=0.53L	2.5349 at x=0.5175L	2.4980 at x=0.5175L

5.4. Optimization of the dynamic damper

On the view of the results of the previous chapter the best candidate dynamic damper is the piecewise linear; in order to give a comprehensive view of the performances, such type of damper is compared with linear and cubic types.

5.4.1. Performance of the monomial stiffness (linear and cubic)

The optimal linear and cubic dynamic dampers are found following the procedure outlined in the previous section, details are omitted for the sake of brevity.

5.4.1.1. Maximum dissipated energy approach

The portion of input energy dissipated by the viscous damper of the DVA at time t_1 is computed by the expression (see section 3-3-1 for more details),

$$\eta = \frac{E_{NES}}{E_{in}} = \frac{\int_0^{t_1} \lambda[\dot{v}(t) - \sum_{r=1}^{n} \dot{a}_r(t)\phi_r(d)]^2 dt}{\int_0^{t_0} F_0[\sum_{r=1}^{n} \dot{a}_r(t)\phi_r(Vt)]dt} \tag{5-5}$$

E_{NES} is the energy passively absorbed and locally dissipated by the DVA i.e. TMD or NES; t_1 is assumed large enough in order to assure that the transient dynamics is nearly damped; E_{in} represents the total portion of the input energy of the beam due to the load and $t_0 = L/V$ is the loading duration.

The numerical value for integrating time is considered t_1=150s, this value is large enough to have almost complete damp of free vibration. Fig. 5-2 presents time history response for the case

of the beam with optimal linear DVA; it is observable that this value is suitable to evaluated the portion of input energy absorbed by DVA.

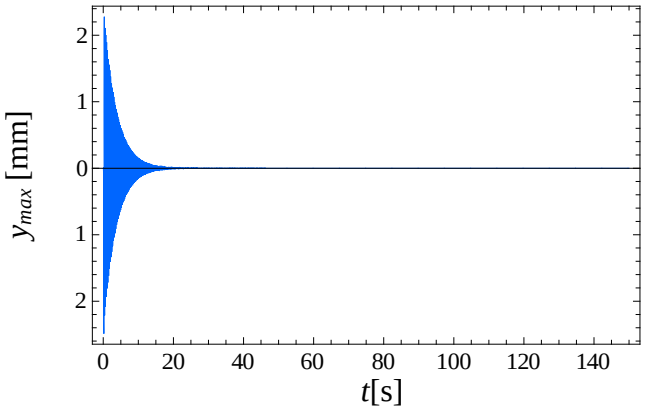

Fig 5-2. Time history response for the case of the beam with optimal TMD; t_1=150.

Table 5-2. Optimal energy dissipation for linear TMD and cubic stiffness nonlinear NES under moving load and moving vehicle excitation.

Case	DVA type	Excitation	Stiffness	λ[Ns/m]	d[m]	η
1	linear TMD	Traveling load	900N/m	10.5	0.55L	88.9%
2	Cubic stiffness NES	Traveling load	0.3×10^9N/m^3	11	0.53L	87.4%
3	linear TMD	Traveling vehcile	925N/m	10.5	0.55L	89.4%
4	Cubic stiffness NES	Traveling vehcile	0.13×10^9N/m^3	11.5	0.53L	87.5%

Table 5-2 presents the optimal portion of input energy that linear and cubic stiffness absorbers are able to absorb. Comparing cases 3 and 4 for the moving vehicle excitation shows that linear absorber behave better in order to absorb more portion of input energy and damp vibration sooner. This behavior is similar to the case of the moving load excitation, compare cases 1 and 2.

5.4.1.2. Minimum dynamic deflection approach

The optimal linear and cubic dynamic dampers are found following the procedure outlined in the section 4-3-1. Fig. 5-2 presents the maximum deflection of the TMD vs. stiffness coefficient and location. The same as moving load excitation the optimal location for the transient loading as not at mid-span while it is moved to the right; it depends on the velocity direction: left to right. The optimal linear dynamic damper (damper location, d=0.55L) corresponds to k=2120N/m, it allows a reduction of the maximum beam deflection of 6.35% with respect to the bare beam, i.e.

2.3393mm max deflection; when the dynamic damper is in the middle of the beam, d=0.50L, the optimum is k=2030N/m, the maximum beam deflection is 2.3427mm (6.22% reduction).

It is to be mentioned that, using a dynamic damper without dissipation results is a better vibration reduction. It verified for the moving vehicle as well; Fig. 5-3 illustrate this verification.

Using a cubic nonlinear stiffness, one is able to reduce the maximum beam deflection from 2.4980mm (bare beam) to 2.3393mm, i.e., 6.35% reduction; the damper is more effective with respect to the case of the beam under moving load. Similar to Fig. 5-2, Fig. 5-4 is illustrative optimal parameters seeking for nonlinear cubic stiffness NES. Table 5-3 summarizes the results, the viscous damping is set as λ=0.1 Ns/m.

It mentioned that for the maximum dissipated energy optimization linear TMD presents better behavior respect to different types of the nonlinear dynamic dampers. Therefore at this stage we do not examine dissipated energy by absorber anymore.

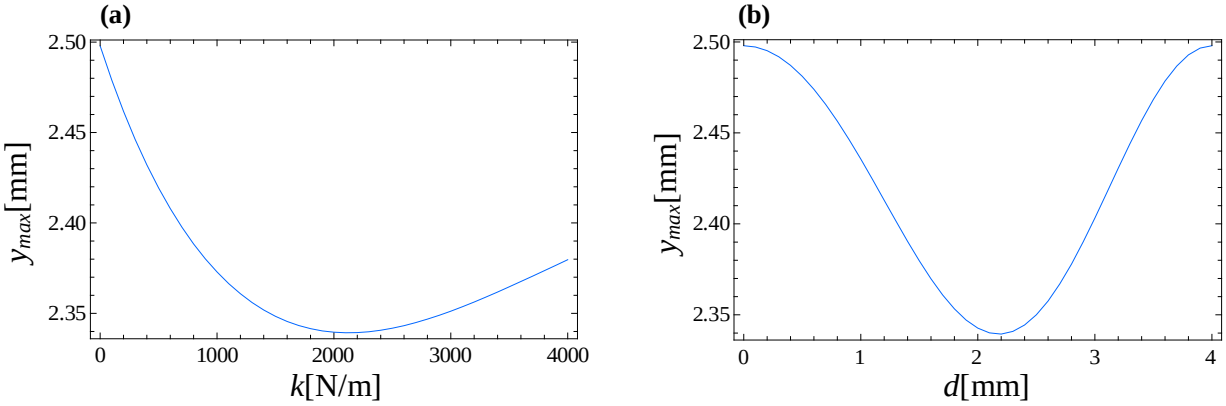

Fig. 5-2. Optimal linear absorber parameters; a)Optimal stiffness, b)Optimal location.

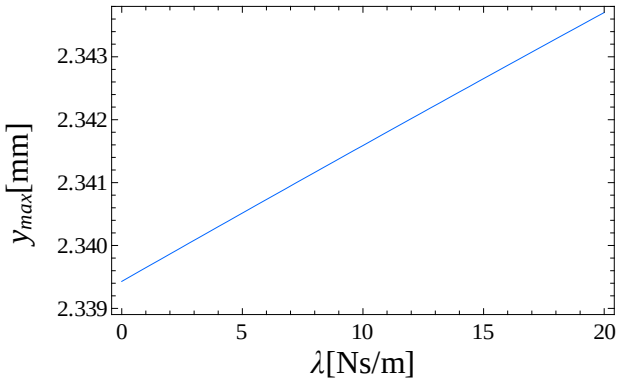

Fig. 5-3. Verification of optimal damping for linear absorber.

(a) **(b)**

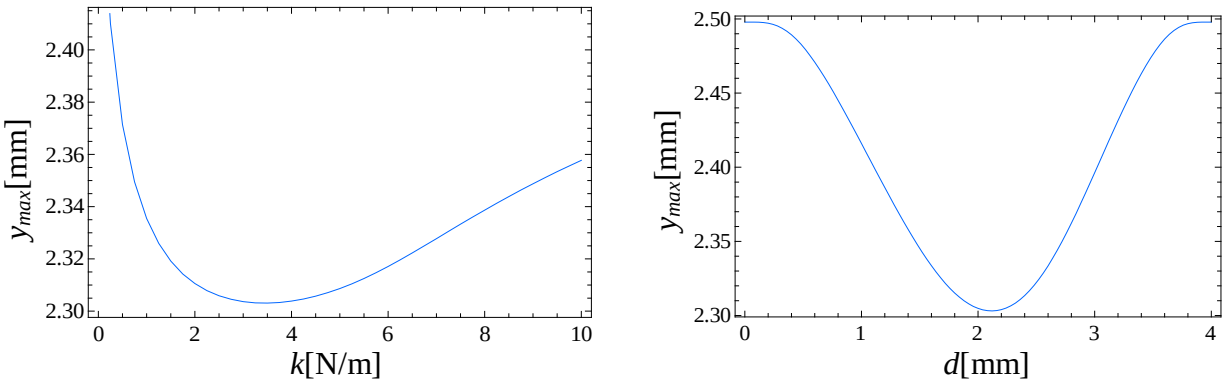

Fig. 5-4. Optimal cubic stiffness nonlinear absorber parameters; a)Optimal stiffness, b)Optimal location.

5.4.2. Performance of the piecewise linear stiffness

The nonlinear attachment having a piecewise linear stiffness is now investigated. In order to find the optimal pair Δ and k, a regular sampling is carried out; the position of the attachment is, d=0.55L.

Figures 5-5 and 5-6 show the maximum beam displacement versus Δ and k; similarly to the case of the beam under moving load, the piecewise linear dynamic damper is the most effective kind of absorber to reduce beam deflection, 8.43% reduction, see table 5-3 (case 4).

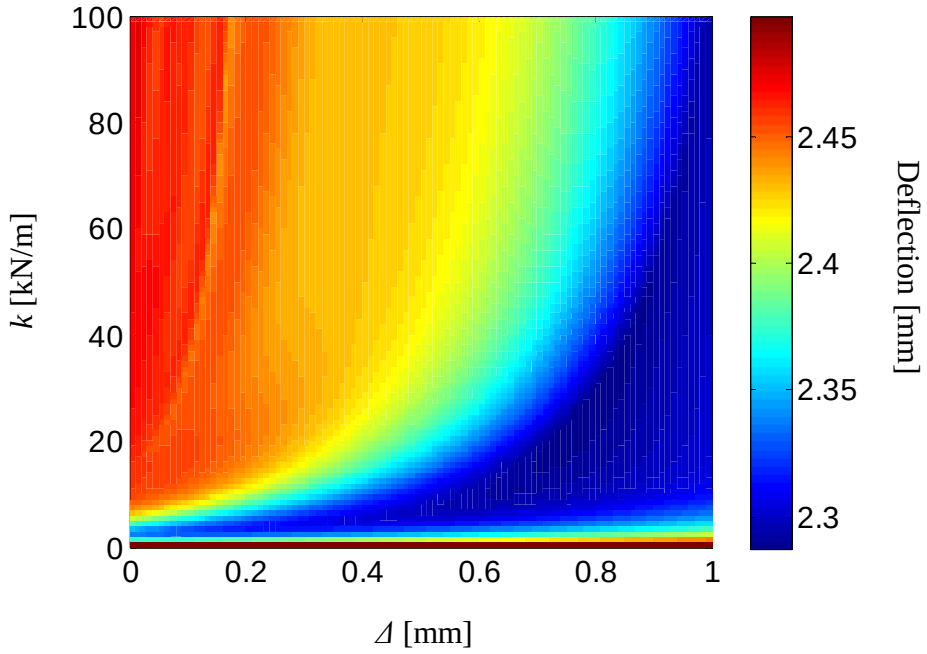

Fig. 5-5. Maximum deflection vs. gap Δ and stiffness k of the piecewise linear stiffness; the optimum is k=28000N/m and Δ=0.79mm (2.2874mm max deflection).

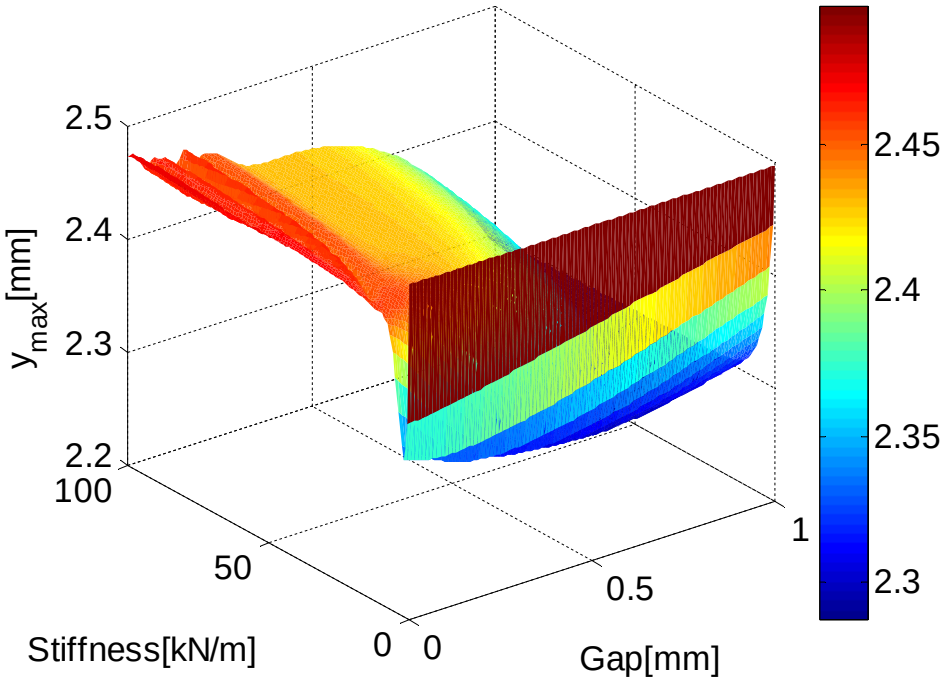

Fig. 5-6. Maximum deflection vs. gap Δ and stiffness k of the piecewise linear stiffness; 3D representation.

Table 5-3. performance of the nonlinear dynamic damper for the beam under moving vehicle, λ=0.1 Ns/m.

Case	Beam and dynamic damper condition	Stiffness	Maximum deflection [mm]	Reduction Percentage
1	Bare beam	0	2.4980	----
2	linear dynamic damper	c_1=2120N/m	2.3393	6.35%
3	Monomial cubic dynamic damper	c_3=3.5×10^{9}N/m^3	2.3031	7.80%
4	Piecewise linear dynamic damper	k=28000 N/m Δ=0.79mm	2.2874	8.43%

CHAPTER 6

Successive Moving Load Excitation

6.1. Introduction

A problem of repetitive moving loads is classified in this chapter as one in which a beam is subject to infinite series of moving loads which repeat at regular time intervals. Such problems are relevant in the transportation industry as well as in the consumer electronics industry. In a video cassette recorder, a system of 2-4 heads repetitively cross the magnetic tape as a signal is read from, or written on to, the video tape. In order to achieve high data density and ensure signal integrity, the heads must be kept very close to the tape and the spacing variation between the tape and head must be minimal. Optimizing these conditions requires a sound understanding of the deflection behavior of the tape under moving loads Ref. [83].

In the present chapter the response of a simply supported beam subjected to infinite sequence of regularly spaced concentrated moving loads, is determined. Moreover, the performance of dynamic dampers possessing linear, cubic, 9^{th} power and piecewise linear stiffnesses as well as linear and cubic nonlinear viscous dampers studied. The critical speed for repetitive loading differs from the critical speeds for a single load, which corresponds to the apparent critical speed. Bolotin [84] studied a beam subjected to an infinite sequence of equal loads with uniform intervals d and constant speed v. In his study, the period d/v of the moving loads has been identified as a key parameter. For the same problem, Fryba [1] concluded that the response of the forced steady-state vibration will attain its maximum when the time intervals between two successive moving loads are equal to some periods of the beam in free vibration or to an integer multiple thereof [85].

The resonance phenomenon relates to the continuous build-up of the free-vibration response on the bridge as there are more loads passing by. In contrast, the cancellation phenomenon implies that the waves associated with the free-vibration responses of the bridge generated by the sequential moving loads cancel out each other. Both the phenomena of resonance and cancellation relate to the free vibrations induced by the moving loads. When a moving load has passed the beam, waves of the sinusoidal form will be induced on the beam. If the time lag of the wave components induced by each moving load equals a multiple of the period $2\pi/\omega$, (ω is the principal natural frequency); then superposition of all the wave components will result in amplified responses. This is the so-called phenomenon of resonance. On the contrary, if the time lag equals an odd multiple of half of the period, the wave components induced by the

sequentially moving loads will just cancel out, indicating that the phenomenon of cancellation has occurred. Whether the phenomena of resonance or cancellation will occur or not depends only on the free vibration part of the motion. The resonance condition in terms of the speed parameter $S = \frac{\pi v}{\omega L}$ (L, beam length) is the same for the beam with both the elastic and simple supports [86].

There is no doubt that, whenever the cancellation speed comes close to or coincides with the resonance speed, the phenomenon of resonance will be suppressed, meaning that the cancellation condition is more decisive than the resonance condition.

Timoshenko [87] determined the response of a finite length Euler-Bernoulli beam due to a single moving load and also found the critical speed of the load. For the periodic travelling load on the undamped beam a steady-state solution does not exist at a critical speed, as the deflections continually increase with time. It is noted that as a load traverses the length of the beam, it undergoes a zero net vertical displacement. Thus it appears that the work of the load should be zero; this is known as the Timoshenko paradox. It was later pointed out by Timoshenko et al. [41] that as a wheel crosses over a beam the orientation of the force must depart slightly from the vertical; the energy acquired by the beam can be related to the work done by the horizontal component of the force. In addition, the monograph by Fryba [1] is an excellent reference for many problems involving moving loads on beams and plates.

In the past several decades, steel truss bridges have often been used in railways for crossing streams or chasms, because of their advantages of light weight, high strength, and relative efficiency in spanning short to medium distances. Compared with girder bridges made of pre-stressed concrete, steel truss bridges are generally more flexible in stiffness. In general, larger dynamic responses will be induced on a steel truss bridge when travelled by trains at high speeds. Partly for this reason, the dynamic responses of truss bridges to moving trains have received considerable attention in the past. For the sake of better riding comfort or maneuverability of passing trains, the dynamic responses of bridges and moving vehicles should be kept within allowable limits, say, through increasing of the structural stiffness or implementation of vibration absorbers on bridges. The tuned mass damper (TMD) devices have often been adopted as an effective means for suppressing the vibrations induced on long-span bridges and high-rise buildings due to wind or seismic excitations, Ref[88,89].

The regular repetitive wheel loads of a moving train imply certain driving frequencies that are not well spaced when passing a railway bridge. Whenever any of the driving frequencies coincides with any of the bridge frequencies, resonance may occur on the bridge. For a continuous bridge with closely spaced frequencies, the first several frequencies of the bridge may be excited to resonance during the passage of a train, resulting in the so-called multiple resonance problem, which is harmful not only for the riding comfort of the train, but also for maintenance of the railway tracks [87].

Nissen et. al. [90] optimized a nonlinear dynamic vibration absorber (DVA) using a softening spring composed of a stack of Belleville washers [91] for the absorber suspension. The effect of a nonlinear energy sink (NES) possessing cubic stiffness and linear viscous damper on the dynamics of a coupled system under periodic forcing is studied by Gendelman et al. [89]. They showed that depend on the system parameters, quasi-periodic response is expected. The quasi-periodic response regime may be interpreted as jump between stable branches. However, they demonstrate that the quasi-periodic response the NES ensure better suppression of oscillations than the best linear absorber with the same mass.

The snap-through truss vibration absorber, Fig. 6-1, was compared with the linear TMD by Avramov and Mikhlin, [92]. The mass and stiffness of the linear absorber are suggested to be equal to the corresponding parameters of the snap-through truss. They showed that the snap-through absorber leads to small oscillation amplitude of the main subsystem in the wide frequency range.

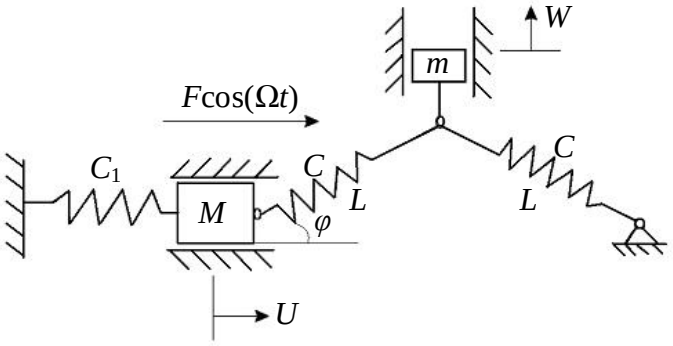

Fig. 6-1. The model of the snap-through truss vibration absorber, Ref. [92].

The performance of a NES possessing nonlinear damping element or nonlinear stiffness element numerically investigated by Zhang et. al. [93]. They presented that a bifurcation might occur in the nonlinear spring designed system. The bifurcation can cause a jump in the system response, which will usually not be acceptable in the engineering design. Moreover, they claimed that damper nonlinearity can be described by an odd-order polynomial function, of which the cubic nonlinearity is the simplest and the most effective, Ref. [94].

In this chapter, we develop the strategy of elimination of the undesired beam deflections subjected to series of the travelling load in steady state regime. This strategy is based on application of nonlinear stiffness or nonlinear damping. General description of the system is presented in section 6-2. Moreover, in this section the analytical formula to evaluate the optimal linear absorber as well as the resonance and cancellation phenomena is studied. In section 6-3, we validate the results for transient and steady state response, separately. Section 6-4 defines the absolute critical loading condition for the present case. The effect of cancellation inside resonance is illustrated. Optimal linear absorber for our case study is defined in section 6-5. In section 6-6 we evaluate five different kinds of NES; for each kind, numerical seek in order to define optimal NES is developed. The behavior of the system response when the response is not periodic illustrated.

6.2. System description

We Considered the mitigation of a simply support Euler-Bernoulli beam subjected to infinite equidistance successive moving loads, Fig. 6-2. The dynamic vibration absorber (DVA) possesses linear or nonlinear spring as well as linear or nonlinear damper. Several kinds of nonlinearity for the spring and the damper are evaluated.

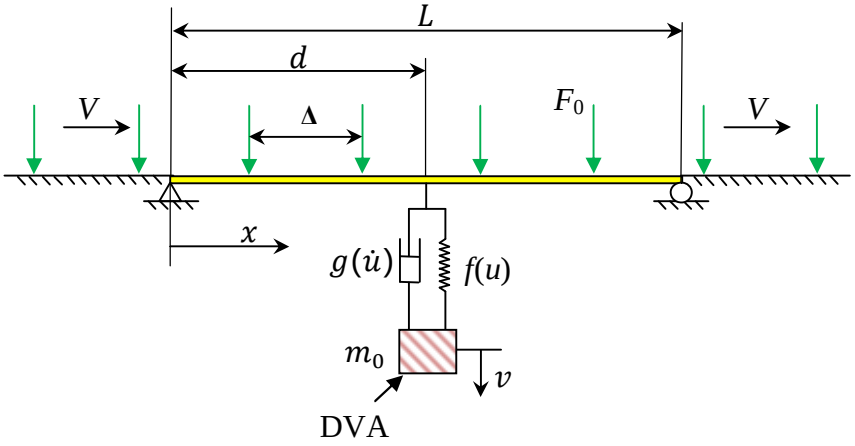

Fig. 6-2. the beam model subjected to sequence of moving loads.

6.2.1. Basic equations

The dynamical system can be described by the following model:

$$EIy_{,xxxx}(x,t) + \rho A y_{,tt}(x,t) + [f(u) + g(u_{,t})]\delta(x-d) = F(x,t), \qquad x \in (0,L),\ \ t > 0 \tag{6-1a}$$

$$y(0,t) = 0, y(L,t) = 0, y_{,xx}(0,t) = 0, y_{,xx}(L,t) = 0 \tag{6-1b}$$

$$y(x,0) = y_{0(x)}, y_{,t}(x,0) = y_{1(x)} \tag{6-1c}$$

$$F(x,t) = \sum_{i=-\infty}^{\infty} F_0 \delta[x - (Vt - i\Delta)] S(i,t), \qquad x \in (0,L),\ \ t > 0 \tag{6-2a}$$

$$S(i,t) = H\left[\left(t - \frac{i\Delta}{V}\right)\left(\frac{L}{V} - \left(t - \frac{i\Delta}{V}\right)\right)\right] \tag{6-2b}$$

$$m_0 v_{,tt}(t) - f(u) - g(u_{,t}) = 0, \ \ v(0) = v_0, \ \ v_{,t}(0) = v_1, \ \ t > 0 \tag{6-3a}$$

$$u(t) = y(d,t) - v(t) \tag{6-3b}$$

The PDE in equation (6-1a) represent the dynamics of the beam with simply supported boundary conditions (6-1b) and initial conditions (6-1c). Initial conditions can be zero or when

there is a variable parameter, these initial conditions can be extract from final conditions of the preceding variable value. $f(u)$ and $g(u_{,t})$ represent spring and damper forces. These functions can be linear or nonlinear functions of the relative displacement or velocity, i.e., $u(t)$ and $\dot{u}(t)$; see equation (6-3*b*) for definition. $\delta(x-d)$ defines the location of the DVA; $F(x,t)$ is the external periodic force, equation (6-2*a*) is excitation force definition. Considering equidistance loads, Δ is the distance between two successive loads. $\delta[x-(Vt-i\Delta)]$ defines the location of the ith load; $S(i,t)$ define whether the ith load at t time lies on the beam or that load is out of beam boundaries, equation (6-2*b*).

Equation (6-3*a*) governs the dynamics of the DVA. $y(x,t)$ is the transverse displacement field of the beam (down is positive), $y_{,x}=\partial y/\partial x$ (similar meaning for the other derivatives), E is the Young's modulus, I is the moment of inertia of the cross section area, $m=\rho A$ is the mass per unit length, ρ is the material density, A is the cross section area, $v(t)$ is the absolute position of the mass m_0, $x=d$ represents the location of the damper on the beam, m_0 is the mass of the DVA.

Moreover, δ is the Dirac function and $H(t)$ is the Heaviside function:

$$H(t)=\begin{Bmatrix}0, & t<0\\ 1, & t>0\end{Bmatrix} \tag{6-4}$$

The dynamics of the system (6-1), (6-2) and (6-3) is analyzed after projecting the partial differential equation (6-1*a*) into a complete and orthonormal basis; for the present problem the eigenfunctions of the linear operator representing the simply supported beam with no attachments can be used,

$$\phi_r(x)=(2/mL)^{1/2}\sin(r\pi x/L),\qquad \omega_r=(r\pi)^2(EI/mL^4)^{1/2},\qquad r=1,2,\dots \tag{6-5a}$$

Where ω_r is the natural frequency of the rth mode.

The eigenfunctions satisfy the following orthonormality conditions,

$$\int_0^L m\phi_i(x)\phi_j(x)dx=\delta_{ij};\quad \int_0^L \phi_i(x)\left(EI\phi_j{}''(x)\right)''dx=\omega_j^2\delta_{ij},\qquad i,j=1,2,\dots \tag{6-5b}$$

Where δ_{ij} is Kronecker's delta and $(\cdot)'=d(\cdot)/dx$.

It can be assumed that the transverse vibration of the beam is expressed in the form

$$y(x,t) = \sum_{r=1}^{\infty} a_r(t)\,\phi_r(x) \tag{6-6}$$

Where $a_r(t)$ are unknown functions of time (modal coordinates) and $\phi_r(x)$ are the normalized eigenfunctions.

By substituting equation (6-6) into equation (6-1) and (6-3), projecting on the p^{th} eigenfunction and using the orthonormality conditions, one obtains

$$\ddot{a}_p(t) + 2\xi_p\omega_p\dot{a}_p(t) + \omega_p^2 a_p(t) + \{\bar{f}(t) + \bar{g}(t)\}\phi_p(d) = \bar{F}_p(t),\ \ p = 1,2,\dots \tag{6-7a}$$

$$m_0\ddot{v}(t) - \{\bar{f}(t) + \bar{g}(t)\} = 0 \tag{6-7b}$$

Where $\dot{a}_p(t) = da_p/dt$ and $\bar{f}(t)$ and $\bar{g}(t)$ due to stiffness and damper of the DVA which will define later. A viscous damping term is added to the generic modal equation (6-7a) after projection. The periodic forcing function expanded using Fourier series expansion:

$$\bar{F}_p(t) = \alpha_p^0 + \sum_{j=1}^{\infty} \alpha_p^j Cos\left(\frac{2j\pi t}{T}\right) + \beta_p^j Sin\left(\frac{2j\pi t}{T}\right),\ \ p = 1,2,\dots \tag{6-8a}$$

$$\alpha_p^0 = \frac{2}{T}\sum_{i=-n_L}^{0}\int_0^T F_0 S(i,t)\phi_p(Vt - i\Delta)dt,\ \ p = 1,2,\dots \tag{6-8b}$$

$$\alpha_p^j = \frac{2}{T}\sum_{i=-n_L}^{0}\int_0^T F_0 S(i,t)\phi_p(Vt - i\Delta)Cos\left(\frac{2j\pi t}{T}\right)dt,\ \ p = 1,2,\dots\ ,\ j = 1,2,\dots \tag{6-8c}$$

$$\beta_p^j = \frac{2}{T}\sum_{i=-n_L}^{0}\int_0^T F_0 S(i,t)\phi_p(Vt - i\Delta)Sin\left(\frac{2j\pi t}{T}\right)dt,\ \ p = 1,2,\dots\ ,\ j = 1,2,\dots \tag{6-8d}$$

$T = \Delta/V$ is the excitation period; n_L is the minimum number of loads lying on the beam, i.e. the integer part of the L/Δ.

6.2.2. Optimal linear DVA

In order to suppress the first resonance of a beam subjected to periodic load, one need to evaluate the equivalent mass of the beam, which depends on the position of the DVA, Ref. [95]. Considering the principal mode shape of the undamped beam the optimal values for the stiffness and damper of the linear DVA is as follow:

$$k = m_0 \left(\frac{\omega_1}{1+\mu}\right)^2 \tag{6-9a}$$

$$\lambda = 2m_0\omega_1\sqrt{\frac{3\mu}{8(1+\mu)^3}} \tag{6-9b}$$

Where ω_1 is the principal natural frequency of the beam, $\mu = \frac{m_0}{m_e}$ is the mass ratio, m_e is the beam equivalent mass, equation (6-10).

$$m_e = \frac{mL}{2Sin^2\left(\frac{\pi d}{L}\right)} \tag{6-10}$$

Bigger mass ratio cause better vibration suppression; so minimum beam equivalent mass is desirable. Clearly, as expected, the optimal position to attach a DVA to a simply supported beam to suppress the first mode, is the middle of the beam. On the other hand, it should be kept in mind that a large DVA mass may not be desirable from a practical point of view, due to the increase of mass of the total system.

6.2.3. Resonance and Cancellation

The resonance phenomenon relates to the continuous build-up of the free-vibration response on the bridge as there are more loads passing by. In contrast, the cancellation phenomenon implies that the waves associated with the free-vibration responses of the bridge generated by the sequential moving loads cancel out each other. Both the phenomena of resonance and cancellation relate to the free vibrations induced by the moving loads.

When a moving load has passed the beam, waves of the sinusoidal form will be induced on the beam. If the time lag of the wave components induced by each moving load equals a multiple of the period $2\pi/\omega$; then superposition of all the wave components will result in amplified responses. This is the so-called phenomenon of resonance. On the contrary, if the time lag equals an odd multiple of half of the period, the wave components induced by the sequentially moving loads will just cancel out, indicating that the phenomenon of cancellation has occurred. Whether the phenomena of resonance or cancellation will occur or not depends only on the free vibration part of the motion.

To evaluate the resonance and cancellation phenomena, only the first mode of vibration of the beam need to be considered, Ref. [86]. With Ω_r denoting the exciting frequencies of the moving

loads, $\Omega_r = r\pi V/L$. The speed parameter S_r is defined as the ratio of the exciting frequency to the frequency of the beam:

$$S_r = \frac{\Omega_r}{\omega_r} = \frac{r\pi V}{\omega_r L} \tag{6-11}$$

For undamped beam the condition of resonance occur when $\mathrm{Sin}(\omega_1 \Delta/2V) = 0$, i.e. $\frac{\omega_1 \Delta}{2V} = i\pi$, with *i*=1,2,3,… , Ref. [85]. The resonant speed parameter can be found as:

$$S_1 = \frac{\Delta}{2iL}, \quad i = 1,2,3,\dots \tag{6-12}$$

Which implies that in the principal resonance condition, the speed, loads distance ratio is:

$$\frac{V}{\Delta} = \frac{\omega_1}{2i\pi}, \quad i = 1,2,3,\dots \tag{6-13}$$

Note that the *i* indicator is differ from indicator for the mode shapes and the present formula is for the principal mode function.

By letting *i*=1,2,3..., the equation (6-12) indicates that resonance may occur at the following speeds: S_1=0.50Δ/*L*, 0.25Δ/*L*, 0.167Δ/*L*, 0.125Δ/*L*...,with diminishing values. Since a train is accelerated from zero to its full speed, it becomes obvious that resonance of certain levels will always be encountered by trains during their motion.

The condition of cancellation is met whenever $\mathrm{Cos}(\omega_1 L/2V) = 0$; by definition of $S_1 = \pi V/(\omega_1 L)$, the speed parameter can be determined from the condition of cancellation as follow:

$$S_1 = \frac{1}{2i-1}, \quad i = 1,2,3,\dots \tag{6-14}$$

Since the effect of cancellation remains always valid, regardless of occurrence of resonance. Whenever the cancellation speed comes close to or coincides with the resonance speed, the phenomenon of resonance will be suppressed, meaning that the cancellation condition is more decisive than the resonance condition, Ref. [85].

From applicable point of view, the resonant response induced by high speed trains will reach its maximum, when S_1 equals the first equals the first resonant speed, i.e. 0.5Δ/*L*. In practice, the first resonance can be circumvented through the selection of car length or span length for the beam such that the condition of cancellation is enforced. Moreover, in the case of constant load distances, the principal natural frequency of the beam (bridge) can be manipulate to have the

condition of cancellation, Eq. (6-14), in the velocity of resonance, Eq. (6-12). For instance, be letting the first resonant speed, S_1=0.5Δ/L, equal to the speeds for cancellation, one obtains:

$$\frac{L}{\Delta} = i - 0.5, \quad i = 1,2,3,\ldots \tag{6-15}$$

This is the condition cancellation when the resonant response occurs, which is irrespective of the speed parameter S_1. For instance consider i=2 or $\Delta = 2/3L$; means when the loads distance is equal to 0.667L the condition of cancellation occurs and the beam without attachment does not vibrate due to the sequence of travelling loads.

6.3. Validations

For the case of the beam subjected to transient travelling single load with linear and cubic nonlinear attachments, some comparisons have been done in Ref.[72] .To model the beam without attachment (bare beam) subjected to successive loading, consider $\bar{f}(t) = 0$ and $\bar{g}(t) = 0$ in equation (6-7a).

6.3.1. Transient response comparisons

In order to evaluate the accuracy of the present model possessing bare beam, the transient response evaluated with those from Ref. [96]. Consider the model of figure 6-3: the beam subjected to two series of sequential traveling loads with the same magnitude, F_0. The following series enter the beam with the delay, $t_d = L_c/V$. The basic equations remain unchanged, while Eq. (6-8a) should change to Eq. (6-16).

$$\bar{F}_p(t) = \left[\alpha_p^0 + \sum_{j=1}^{\infty} \alpha_p^j Cos\left(\frac{2j\pi t}{T}\right) + \beta_p^j Sin\left(\frac{2j\pi t}{T}\right)\right] + \left[\alpha_p^0 + \sum_{j=1}^{\infty} \alpha_p^j Cos\left(\frac{2j\pi (t-t_d)}{T}\right) + \beta_p^j Sin\left(\frac{2j\pi (t-t_d)}{T}\right)\right] H[t-t_d], \quad p = 1,2,\ldots \tag{6-16}$$

Savin, Ref. [96], compared his results with measured accelerations on an existing railway bridge in France. In his study the number of loads is finite, 5 wagons, while in the present study the infinite number of loads is considered, i.e. the results for the transient time till 6th load enter the beam are comparable. The following numerical parameters are considered; EI=1.12(10^{11}), ρA=34088kg/m, L=20m, ξ_p=0.025 (p=1, 2, ...), Δ=24m and L_c=18m. As Savin, pointed out, the

force magnitude calculated $F_0 = (215.6 + 22 \times 9.806)/2 = 215.6\text{kN}$ from Ref. [85]. For all computations, 3 mode shapes are considered, Ref. [72].

Figure 6-4 shows the comparison for the transient response between the present results and the results of Ref. [96]. The velocity is 589.7km/h, which is a critical speed. In the present model with the input data mentioned above, at t=0.733s the 6th load enter the beam; the comparison until this time gives accurate agreement.

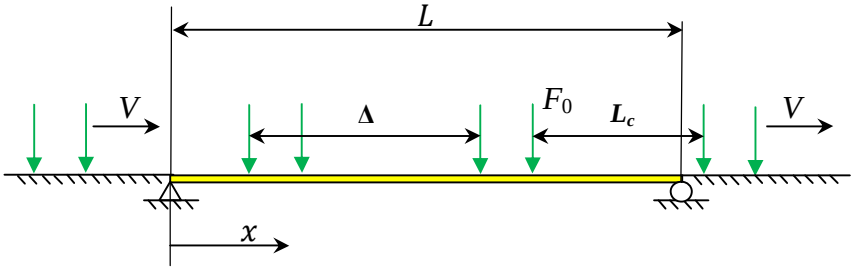

Fig. 6-3. the beam model subjected to two series of sequential moving loads.

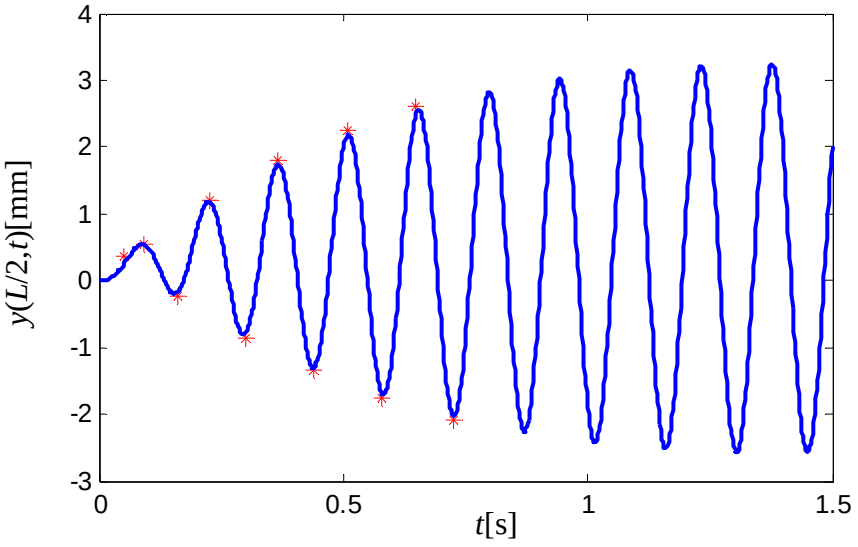

Fig. 6-4. time history of the mid-span deflection, ___:present results, *:Ref. [96].

6.3.2. Performance of Fourier series expansion

Consider figure 6-2 without attachment and single sequence of moving loads. Two method for load applying is presented: i) Periodic loading taking advantage of Fourier series; ii) Applying huge repetitive moving loads following each other (direct integrating). For the computations, the second approach takes much more time respect to the first one. In this method the superposition of passing several travelling single loads evaluated. The following numerical parameters are considered: EI=13959, ρA=7.038kg/m, L=4m, ξ_p=0.01 (p=1, 2, ...), Δ=1.33m and V=6.12m/s. These parameters is used for all numerical computations.

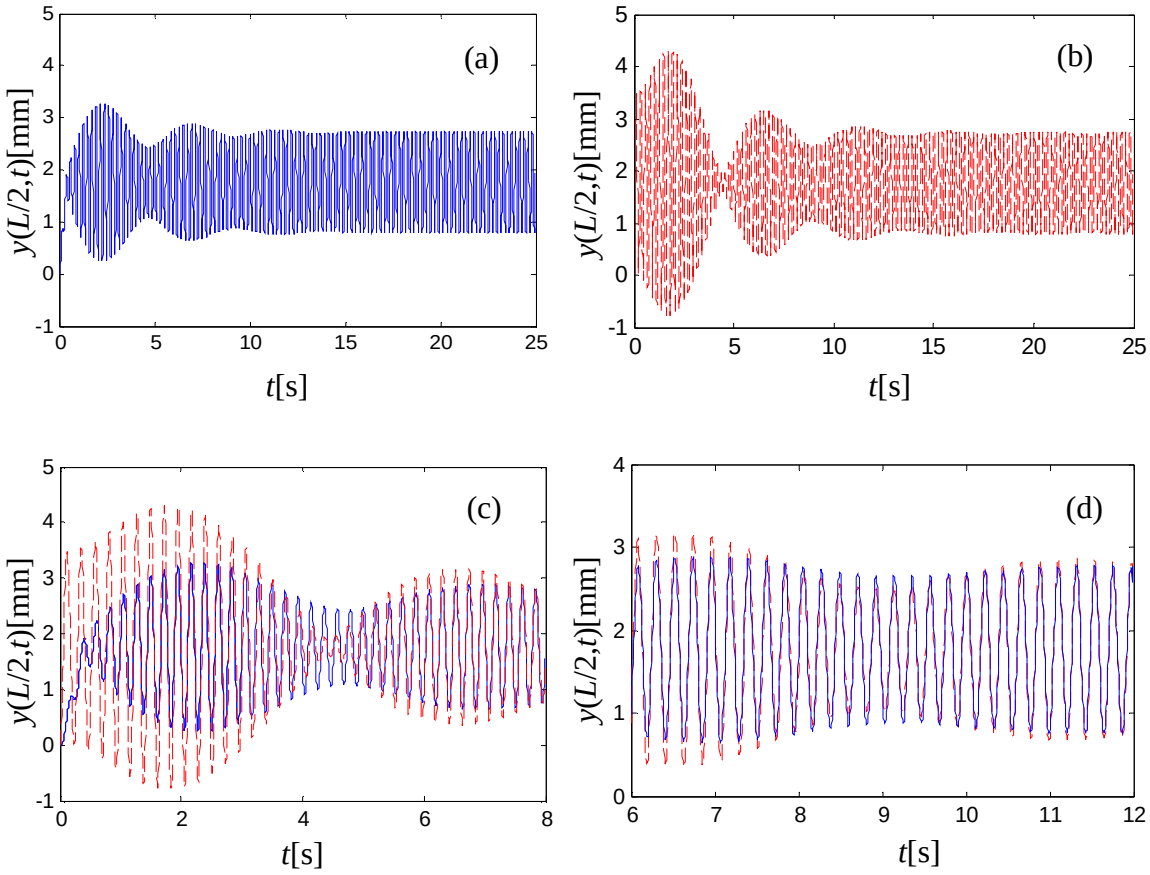

Fig. 6-5. Time history comparison between direct integrating (——) and using Fourier series expansion(-----); a: direct integrating, b: Fourier series expansion, c: time history comparison, transient response, d: time history comparison, steady state response.

Figure 6-5a shows the mid-span deflection time history with direct integrating loading; the number of loads that should travel on the beam during the integrating time (25 seconds) is 118; this is why this method is time consuming. The mid-span deflection time history, taking advantage of Fourier series expansion, is presented in figure 6-5b. In this method at initial time there are several loads on the beam while in previous method at t=0 the first load enter the beam.

Figures 6-5c and 6-5d show the initial transient and passing from transient to steady state response. Moreover, table 1 shows the mid-span maximum deflections vs. time for the two present methods. The differences in steady state response is vanished. From present comparisons, for the steady state response the accuracy of the Fourier series load expansion is Free of ambiguity. For different velocities and load distances the convergence of Fourier series evaluated, 3 terms of this series found accurate enough for our purpose; for the sake of brevity details are omitted.

Table 6-1. The comparison between direct loading and Fourier series expansion.

Time [sec]	y(L/2,t) [mm] direct integrating	y(L/2,t) [mm] Fourier series	Error percentage
3.4307	**2.8956**	**1.7823**	**38.448**
6.8614	**2.9168**	**2.4833**	**14.861**
10.292	**2.9266**	**2.7578**	**5.766**
13.722	**2.9309**	**2.8652**	**2.241**
17.153	**2.9329**	**2.9073**	**0.872**
20.584	**2.9337**	**2.9238**	**0.339**
24.015	**2.9341**	**2.9302**	**0.132**
27.445	**2.9342**	**2.9327**	**0.051**
30.876	**2.9343**	**2.9337**	**0.019**
34.307	**2.9343**	**2.9341**	**0.007**

6.4. Critical loading condition

Equation (6-13) give the critical velocity in resonance condition as a function of principal beam natural frequency, ω_1 and load distance, Δ. For a define beam structure, i.e. defined ω_1, the lowest critical velocity is correspond to i=1:

$$V_{cr} = (\omega_1/2\pi)\Delta \tag{6-17}$$

Equation (6-17) is found considering the first mode shape and it is equivalent to the first term in Fourier series. In order to evaluate the effect of other mode shapes and Fourier series terms, consider equation (6-7a) for the bare beam, i.e. $\bar{f}(t) = 0$ and $\bar{g}(t) = 0$. The loading function can expand as follow:

$$\bar{F}_p(t) = \sum_{i_f=1}^{n_f} F_{i_f,p} e^{j i_f \omega_0 t} \tag{6-18a}$$

$$F_{i_f,p} = \frac{1}{T}\int_0^T \bar{F}_p(t)\, e^{j i_f \omega_0 t} dt \tag{6-18b}$$

Where, n_f is the number of considered terms for Fourier series, $\omega_0 = 2\pi/T$ is the excitation frequency. For the case of beam without attachment, the coefficients matrixes are orthogonal so the modal coordinates can obtain as follow

$$a_p(t) = \sum_{i_f=1}^{n_f} \left[-{i_f}^2{\omega_0}^2 + 2ji_f\omega_0\xi_p\omega_p + {\omega_p}^2\right]^{-1} F_{i_f,p}e^{ji_f\omega_0 t} \tag{6-19}$$

The maximum amplitude of the modal coordinates creates the maximum value of dynamic displacement; so for the case of the small damping, $\xi_p \cong 0$, resonance condition obtain as follow:

$$-{i_f}^2{\omega_0}^2 + {\omega_p}^2 = 0 \Rightarrow \omega_0 = \frac{\omega_p}{i_f} \Rightarrow V_{cr} = \left(\omega_p/2\pi i_f\right)\Delta \tag{6-20}$$

Figure 6-6 shows the seeking among velocities and load distances in order to define the maximum absolute deflection during steady state response. Numerical values are those in section 3.2. In figure 6-6a absolute maximum mid-span deflection is presented; when Δ is small, i.e. there are many successive loads on the beam, simultaneously and so the static deflection increase. Figure 6-6b shows the mid-span dynamic deflection (deflection amplitude) in one period: $y_a = (y_{max} - y_{min})/2$. Equation (6-20) define straight lines for different mode shapes and Fourier series terms. Comparison between this theoretical lines and numerical seeks is available in figure 6-6c; for red line: p=1, i_f =1, green line: p=1, i_f =2, white line: p=1, i_f =3 and yellow line: p=2, i_f =1. The effect of second and even the third Fourier series is not negligible, while the second mode shape does not produce big deflections. Note that the effect of second and third mode shapes can be effective when the vibration of the first mode damp out using a dynamic vibration absorber. Figure 6-6d shows the mid-span dynamic deflection in 3D map.

Resonance condition is evaluated in figure 6-7. Maximum absolute deflection and dynamic deflection in the steady state response presented. Resonance condition for the principal mode shape and first Fourier series is convinced, i.e. $V = (\omega_1/2\pi)\Delta$. Regardless of the occurrence of the resonance, effect of cancellation remains valid; it can be observe from this figure, see Eq. (6-14). Critical load distance and corresponding critical velocity can evaluate from this graph: Δ=5.84m and V=25.53m/s; y_{max}=25.27mm. For the present numerical parameters, ω_1=27.47Rad/s and T_1=0.2287s.

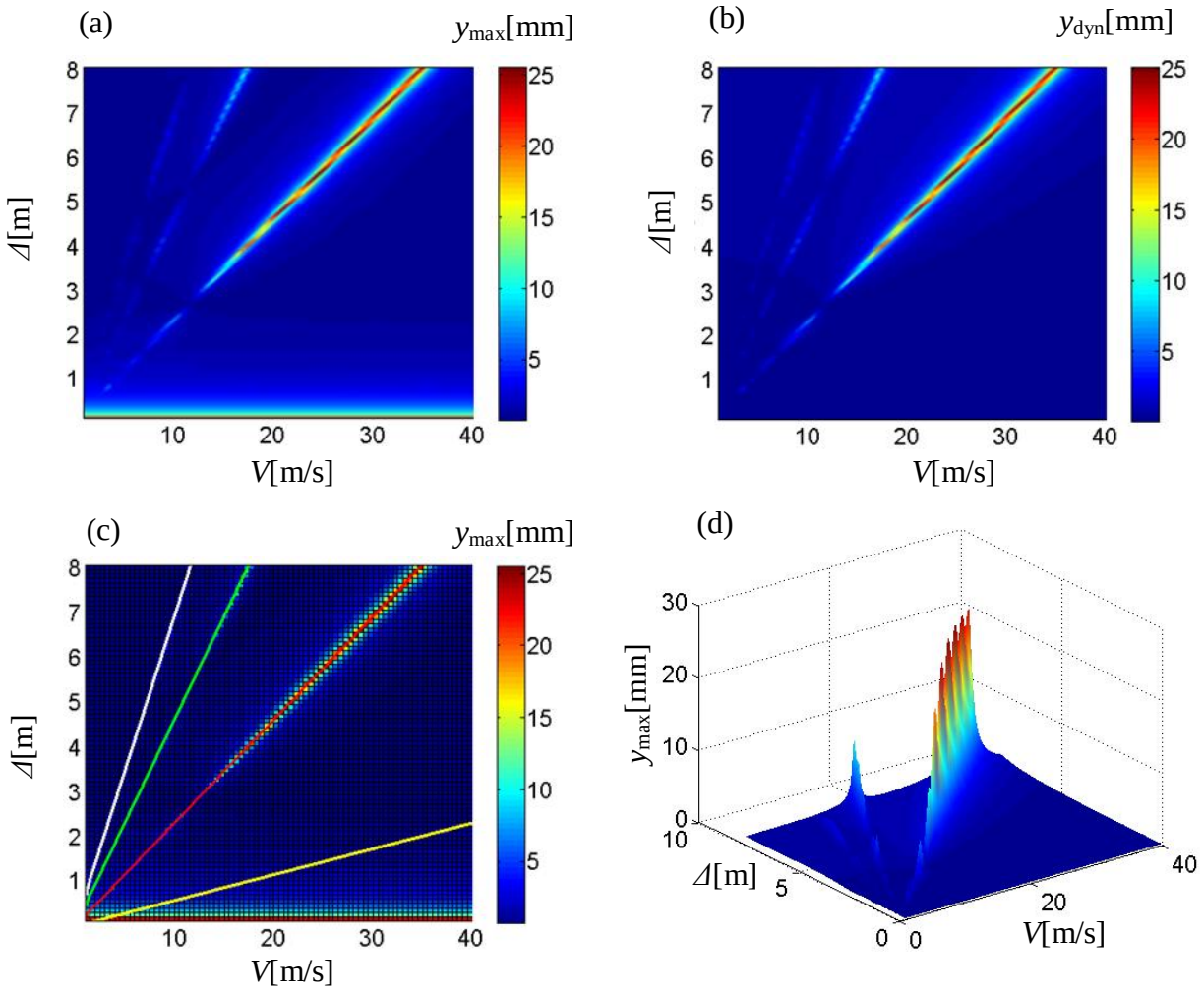

Fig. 6-6. Maximum deflection vs. velocity and load distance; a: Maximum mid-span deflection, b: Dynamic mid-span deflection, c: Resonant condition lines on maximum mid-span deflection, d: 3D representation of dynamic mid-span deflection.

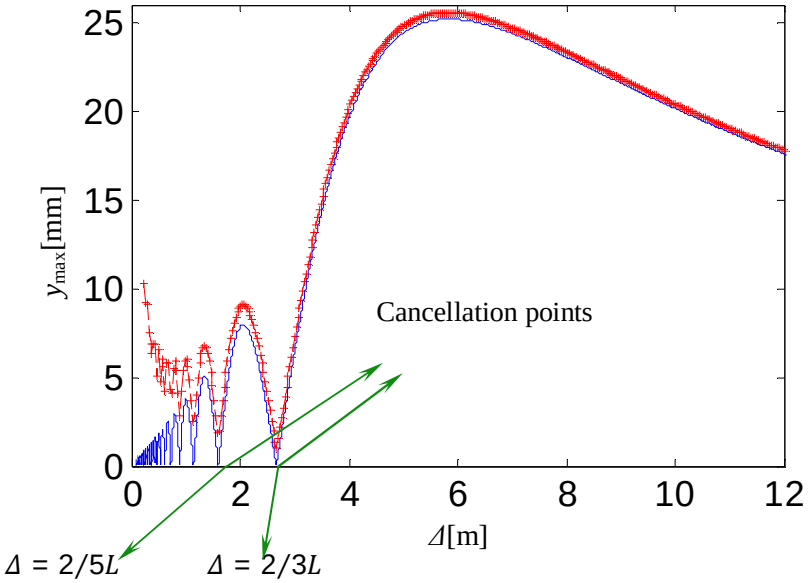

Fig. 6-7. Deflection vs. load distance in resonant velocity; -----:Dynamic deflection, --*--:Maximum deflection.

6.5. Performance of linear DVA

To suppress the oscillation of the beam subjected to sequence of travelling loads, one can take advantage from Frahm linear DVA, Ref. [15]. Den Hartog [42] presented formulation to obtain optimal linear DVA. Suppose that the absorber is designed to reduce the amplitude of the beam when it is at resonance. In this case the damping value is zero, λ=0 in equation (6-21b). The natural frequency of the DVA should be equal to the frequency of the periodically varying force. In equation (6-7) for the linear stiffness, and linear damping the forcing functions are:

$$\bar{f}(t) = k\left[\sum_{r=1}^{\infty} a_r(t)\,\phi_r(d) - v(t)\right] \tag{6-21a}$$

$$\bar{g}(t) = \lambda\left[\sum_{r=1}^{\infty} \dot{a}_r(t)\,\phi_r(d) - \dot{v}(t)\right] \tag{6-21b}$$

Suppose numerical parameters which create maximum deflection, Δ=5.84m and V=25.53m/s. $k/m_0 = \omega_0 = 27.47\,rad/s \Longrightarrow k = 1062.2N/m$. The optimal location for the DVA is at the mid-span, d=L/2; while for the case of the transient loading, optimal locations near mid-span has been found, Ref. [72]. Figure 6-8 shows the mid-span time history deflection for the resonance condition.

It is well known that linear DVA which optimized for resonance condition cannot remain effective for other excitation frequencies. Figure 6-9 shows the performance of this DVA for other excitation frequency, i.e. travelling load speeds. Two new peaks appear where the undamped linear TMD behave worse than bare beam. To overcome this drawback, Den Hartog proffered the damped TMD. Equation (6-9) gives the optimal values for damped linear TMD; equation (6-10) calculates the beam equivalent mass considering the only first mode shape. For optimal DVA location, $d=L/2$, Simple computations presents m_e=14.078kg, k=877.9N/m and λ=12.98Ns/m, y_{max}=2.58mm. Moreover, to assess the effectiveness of higher mode shapes and to include the natural structural damping ,ξ_p, seeking has been done by solving numerically equations (6-7) and (6-8). Fig. 6-10. presents the maximum absolute mid-span deflection for different velocities. The optimal set is defined as k=870.0N/m and λ=14.0Ns/m, y_{max}=2.56mm,V_{cr}=26.6m/s. The performance of this optimal TMD is evident in figure 6-9 (black thick line).

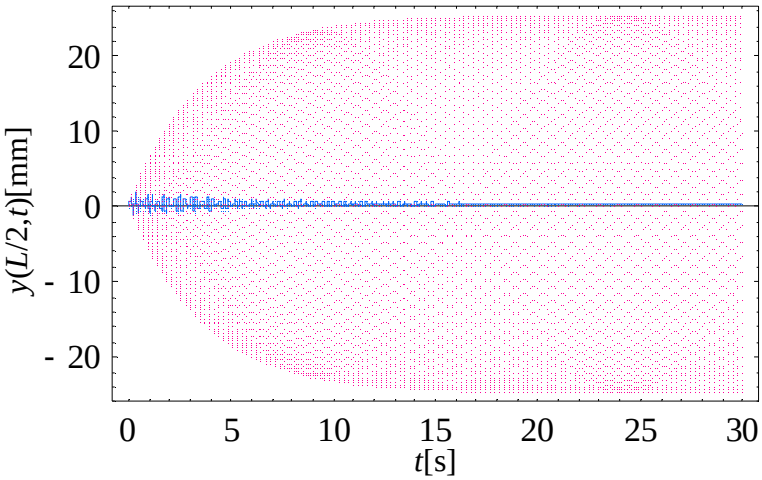

Fig. 6-8. Mid-span time history deflection; ……: Without DVA, ____: With DVA.

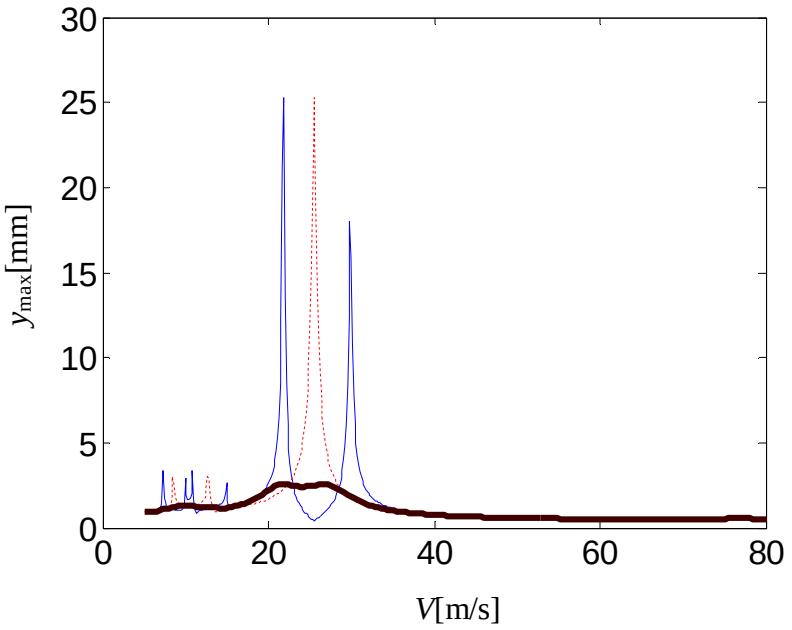

Fig. 6-9. Maximum mid-span beam deflection; .....: Bare beam, ____ with undamped TMD (optimized for resonance condition), ——: with damped TMD (overall optimized).

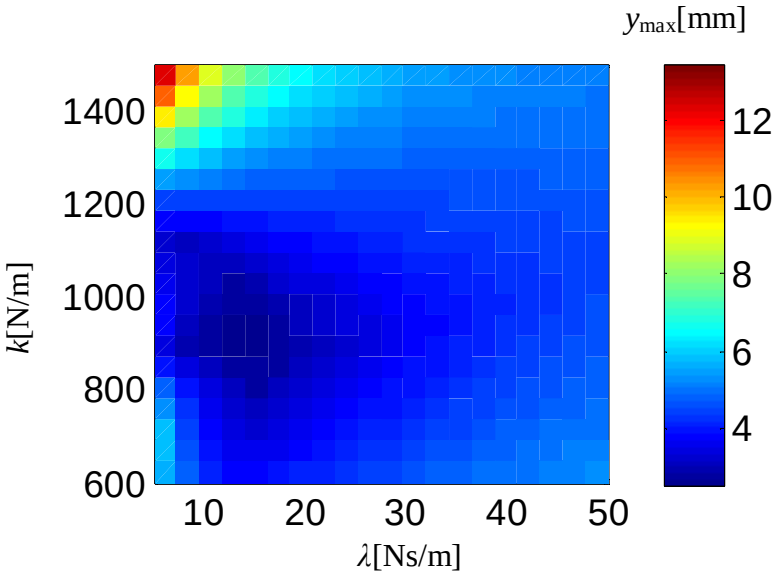

Fig. 6-10. Overall seek to define optimal linear TMD.

6.6. Nonlinear dynamic absorbers

In this section we evaluate the performance of the different kinds of nonlinearity in order to reduce the beam deflection in steady state regime. The optimal coefficients are found by

numerical seeking among DVA parameters. To define the boundary values for the numerical search, we took advantage from the point that the order of the stiffness force and damping force for a nonlinear NES is the same as linear one. By evaluating maximum deflection and velocity of the linear absorber, i.e. u_{max} and $\dot{u}_{max}$ (see Eq. (6-3*b*)) we are able to determine the minimum and maximum NES parameters values.

6.6.1. Cubic stiffness NES

Nonlinear energy sinks (NESs) possessing nonlinear cubic stiffness and linear damping for the systems under periodic excitation has been studied by several researchers; e.g. find Refs. [97-100]. In equation (6-7) for the linear stiffness, and linear damping the forcing functions are:

$$\bar{f}(t) = k_3 \left[\sum_{r=1}^{\infty} a_r(t)\,\phi_r(d) - v(t)\right]^3 \tag{6-22a}$$

$$\bar{g}(t) = \lambda \left[\sum_{r=1}^{\infty} \dot{a}_r(t)\,\phi_r(d) - \dot{v}(t)\right] \tag{6-22b}$$

The optimal NES parameters is found by seeking for different velocities. By linear absorber the response to the periodic excitation is periodic, while, in some cases, cubic stiffness NES with small damping present quasiperiodic responses, see Ref. [100]. Figure 6-11 present the maximum deflection vs. cubic stiffness deflection for damping coefficient λ=11.2Ns/m. This graph is correspond to Δ=5.84m and V=25.53m/s. Forward and backward are due to initial conditions which is the last response of previous stiffness. In figure 6-12 steady state responses for a candidate stiffness in periodic response region, k_3=80(10^6)N/m^3 and another one in quasiperiodic region, k_3=30(10^6)N/m^3 are presented. Note that, while figure 6-11 shows minimum stiffness less than 2mm for critical velocity, the absolute maximum velocity is 3.59mm for V=24.34m/s with the optimal set: k_3=45(10^6)N/m^3 and λ=23.25Ns/m. By increasing damping coefficient quasiperiodic response change to periodic response; while with high damping minimum deflection increase.

Poincare map (first recurrence map) is the intersection of a periodic orbit in the state space of a continuous dynamical system with a certain lower dimensional subspace, called the Poincare section, transversal to the flow of the system. More precisely, one considers a periodic orbit with

initial conditions on the Poincare section and observes the point at which this orbits first returns to the section, thus the name first recurrence map. The transversality of the Poincare section basically means that periodic orbits starting on the subspace flow through it and not parallel to it.

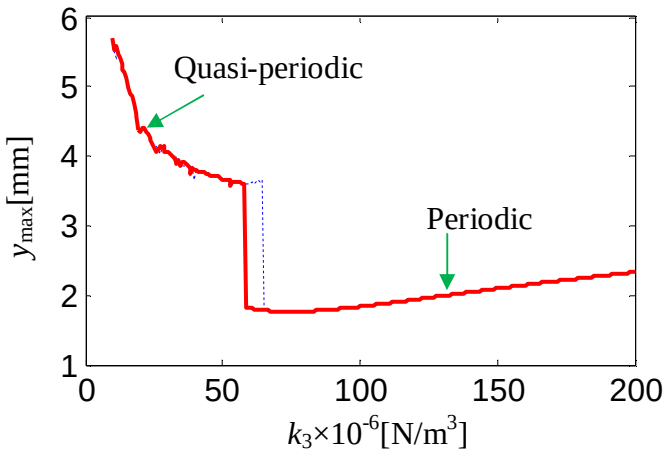

Fig. 6-11. Maximum overall deflection for wide range velocities, ——: Forward, -----: Backward.

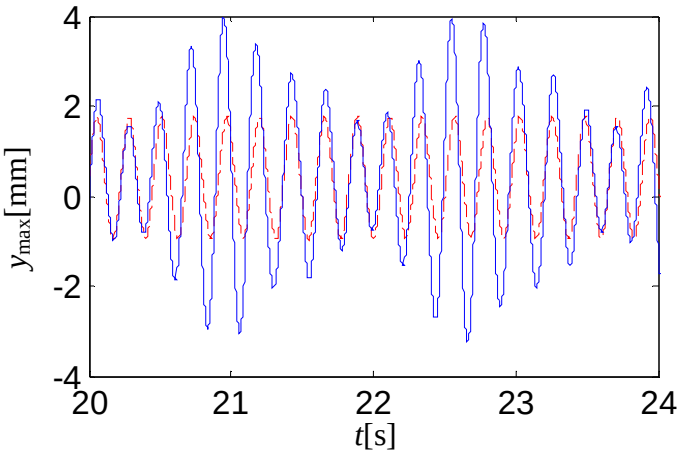

Fig. 6-12. Steady state responses, ____: k_3=30(10^6)N/m^3, -----: k_3=80(10^6)N/m^3.

Table 6-2, presents the behavior of the system with cubic stiffness NES. The characteristics of each case is defined in table 6-3, separately. t_0 is the time big enough to convince the initial of the steady state response; i is an integer. Case 1 give a periodic steady state response; phase portrait is a single close orbit ;Poincare map is a unique point, {0.585,-12.742}, the small area distribution is due to numerical errors. See appendix C for description of phase portrait and

appendix D for description of Poincare map. alike first case, the second one also presents periodic response, while the Poincare map illustrate that the response converge to the unique point. Case 3 presents quasiperiodic response; phase portrait is a close curve after several periods and Poincare section is a close orbit instead of single point for periodic response. Case 4 illustrate chaotic solution; phase portrait is open curve and Poincare section shows a cloud of points. This orbit is a aperiodic or chaotic attractor. In this case response is sensitive to initial condition. Cases 5 to 8 present chaotically modulated motion, see Ref. [101]. In these cases special shape for the Poincare map is visible. comparing case 7 and 8 shows that by increasing NES damping the response pass from chaotically modulated motion to quasi periodic motion.

Table 6-2. Illustration of the NES behavior with different stiffness and damping coefficients, V=40m/s.

Case	Steady state response x axis: t [s] y axis: $y(L/2,t)$ [mm]	Phase portrait x axis: $y(L/2,t)$ [mm] y axis: $dy(L/2,t)/dt$ [mm]	Poincare map x axis: $y(L/2,t_0+iT)$ [mm] y axis: $dy(L/2, t_0+iT)/dt$ [mm]
I	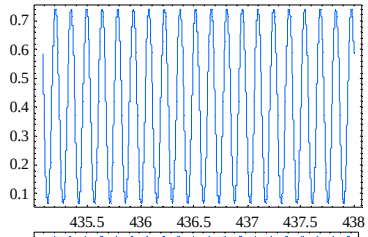	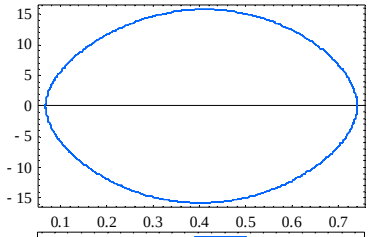	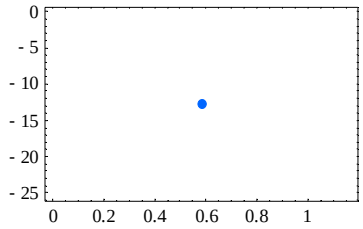
II	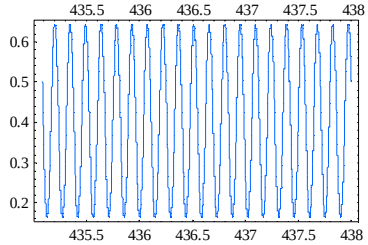	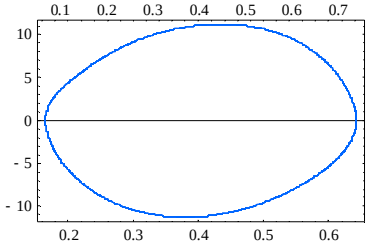	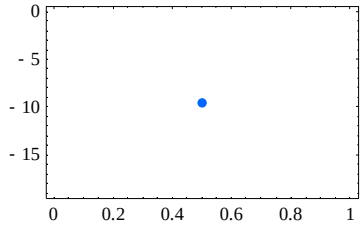
III	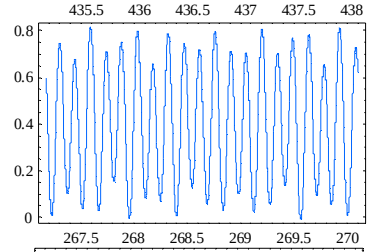	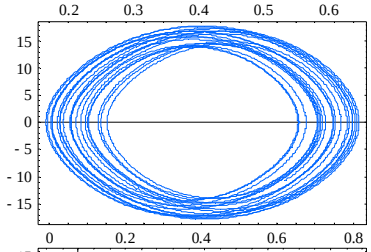	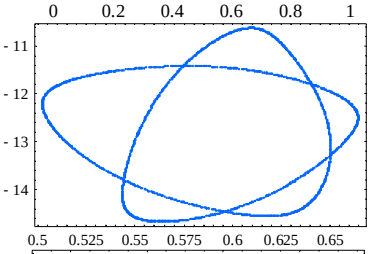
IV	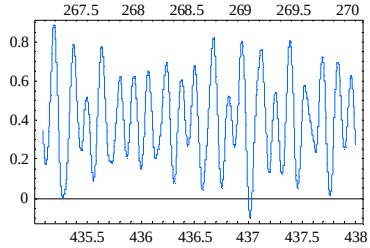	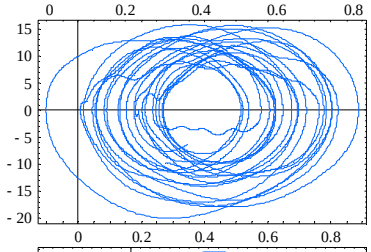	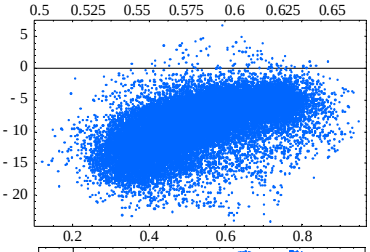
V	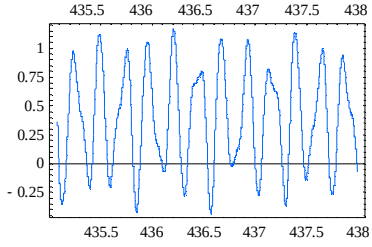	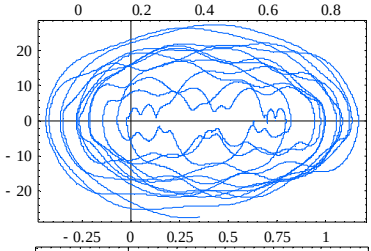	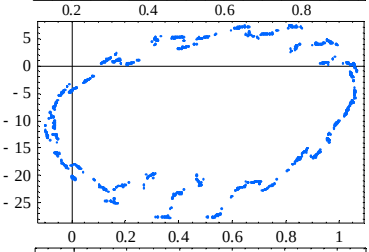
VI	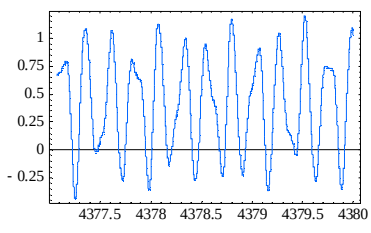	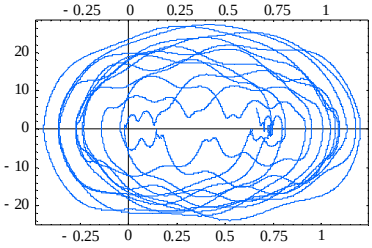	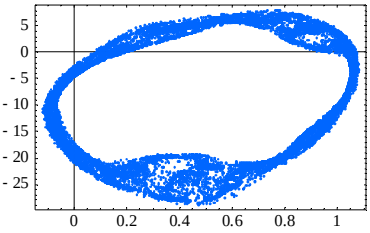

Case	Steady state response x axis: t [s] y axis: $y(L/2,t)$ [mm]	Phase portrait x axis: $y(L/2,t)$ [mm] y axis: $dy(L/2,t)/dt$ [mm]	Poincare map x axis: $y(L/2,t_0+iT)$ [mm] y axis: $dy(L/2, t_0+iT)/dt$ [mm]
VII	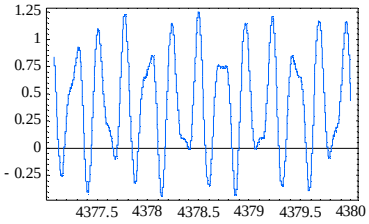	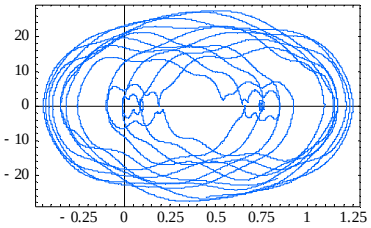	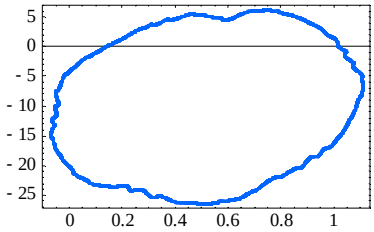

Table 6-3. NES characteristics for the cases in table 6-2.

Case number	$k_3(10^6)$[N/m^3]	λ[Ns/m]
I	50	5
II	20000	20
III	50	0.1
IV	5000	0.1
V	5000	5
VI	5000	5
VII	1000	10

6.6.2. High odd-order polynomial stiffness NES

In order to investigate the way in which an higher odd-order monomial stiffness modifies energy distribution fifth power monomial stiffness is studied. However the seventh power stiffness is studied as well, but no improvement has been found; so, for the sake of brevity those results are omitted. By fifth power stiffness, stiffness force in equation (7) is:

$$\bar{f}(t) = k_5 \left[\sum_{r=1}^{\infty} a_r(t)\,\phi_r(d) - v(t)\right]^5 \tag{6-23a}$$

$$\bar{g}(t) = \lambda \left[\sum_{r=1}^{\infty} \dot{a}_r(t)\,\phi_r(d) - \dot{v}(t)\right] \tag{6-23b}$$

Damping force remain linear, Eq. (6-23b). Figure 6-13 shows an overall seek to define the optimal fifth power monomial stiffness coefficient. Several damping examined; just two damping close to optimum presented in this figure. In optimal set, k_5=2.16(10^{12})N/m^5 and λ=30Ns/m, maximum deflection is 4.48mm for V=24m/s.

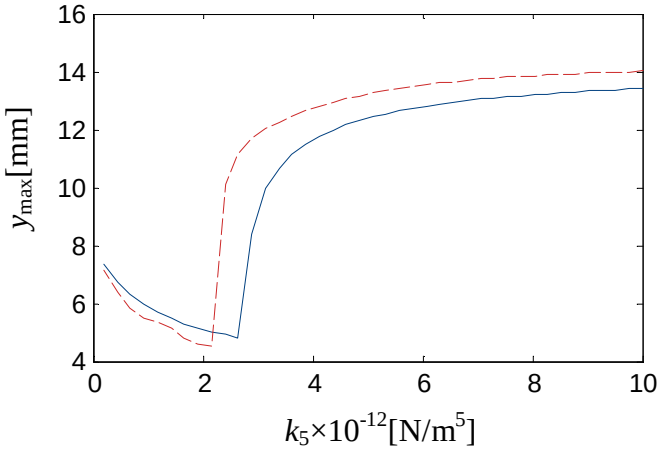

Fig. 6-13. Maximum deflection vs. fifth power monomial stiffness, – –:λ=30Ns/m, ——: λ=35Ns/m.

6.6.3. Piecewise linear stiffness

Consider the model of figure 6-2 with a piecewise linear stiffness NES. Fig. 6-14 shows the schematic stiffness force of the piecewise linear NES and Eq. (6-24*a*) present its governing equation.

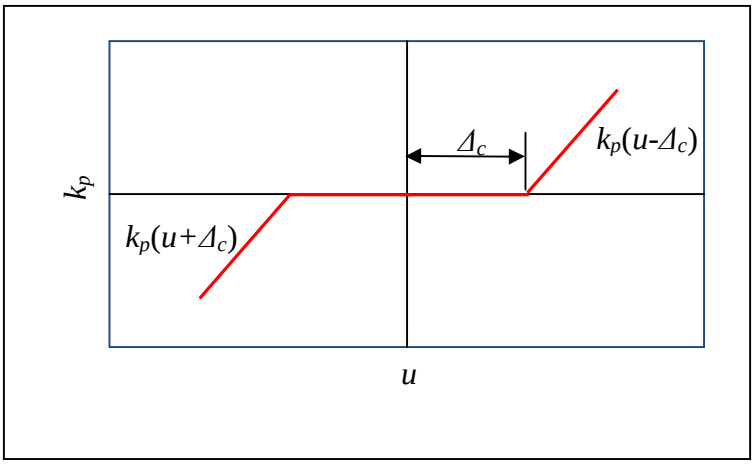

Fig. 6-14. the schematic stiffness force versus stiffness deflection for piecewise linear dynamic damper.

$$\bar{f}(t) = k_p \times \left[\left(\sum_{r=1}^{\infty} a_r(t)\,\phi_r(d) - v(t)\right) - \Delta_c\right] \times H\left[\left(\sum_{r=1}^{\infty} a_r(t)\,\phi_r(d) - v(t)\right) - \Delta_c\right]$$
$$+k_p \times \left[\left(\sum_{r=1}^{\infty} a_r(t)\,\phi_r(d) - v(t)\right) + \Delta_c\right] \times H\left[-\left(\sum_{r=1}^{\infty} a_r(t)\,\phi_r(d) - v(t)\right) - \Delta_c\right] \quad (6\text{-}24a)$$

$$\bar{g}(t) = \lambda\left[\sum_{r=1}^{\infty} \dot{a}_r(t)\,\phi_r(d) - \dot{v}(t)\right] \quad (6\text{-}24b)$$

The piecewise stiffness effect when the clearance amplitude, Δ_c is exceeded. This represents a sudden change in the system properties which accounts for the inherent hard nonlinearity of the piecewise linear system.

Figure 6-15 shows the overall seek in order to define the optimal stiffness and clearance set for the optimal NES. minimum deflection 2.58mm obtained by k_p=1024N/m, Δ_c=0.61mm and λ=14Ns/m. The variation of the maximum deflection vs. velocity around critical velocity zone is presented in figure 6-16. With the present NES, new critical velocity, which maximum deflection occurs, is 24.13m/s.

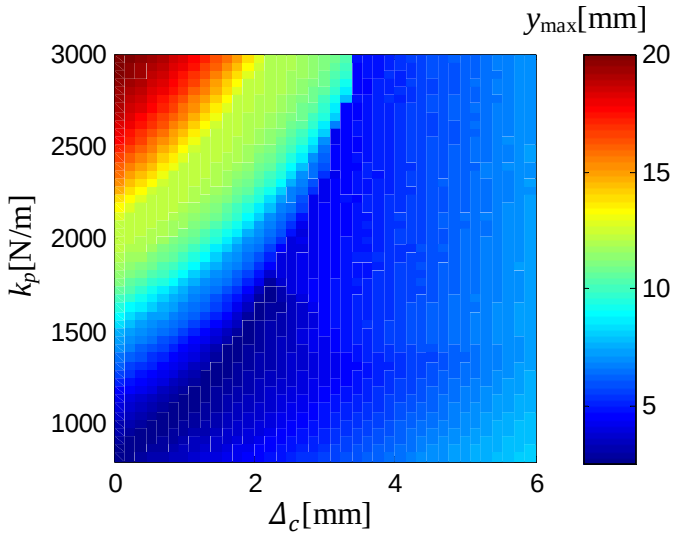

Fig. 6-15. Overall search to determine the optimum NES with piecewise linear stiffness.

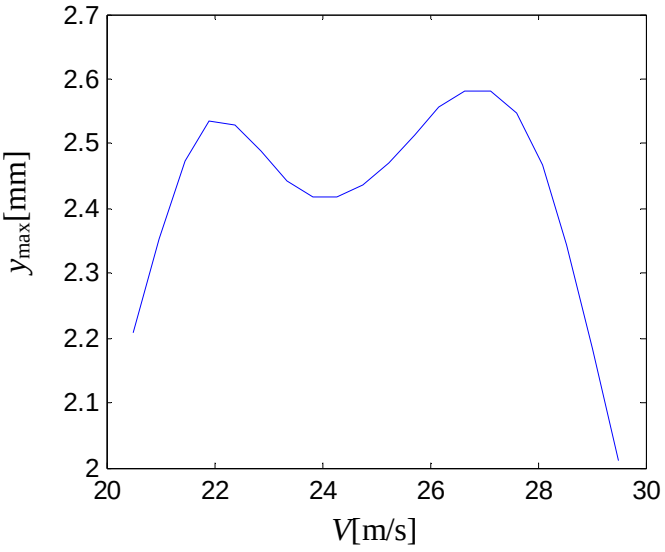

Fig. 6-16. Beam mid-span maximum deflection vs. velocity.

Suppose that the desire is to obtain minimum beam deflection at critical condition, i.e. V=25.53m/s and Δ=5.84m. Figure 6-17 present maximum deflection for this loading condition and different NES characteristics parameters, NES linear low damping remains constant, λ=0.1Ns/m. In table 6-4 the illustration of the steady state response, phase portrait and corresponding Poincare map is presented for different NES parameters; see table 6-5 for the parameter values. Case 1 is the case with periodic response; this point lie on blue area in figure 16. All points which lie on the areas with regular behavior present periodic steady state response. Cases 2 and 3 lie on the area 'A'; parameters in this area present a unique Poincare section shape. It is true even for the area 'B'; cases 4,5 and 6 correspond to this area. 7^{th} case is for the one of the point which gave irregular behavior in area 'C'; Poincare map is 10 separate points which presents super harmonic modulation.

Figures 6-18 shows the bifurcation diagram of the Poincaré map for the λ=0.1Ns/m. The control parameter is the piecewise linear stiffness coefficient. $y_i=y(L/2,t_0+iT)$, i=1,2,3,…,N; N is an integer big enough to illustrate the system behavior, here N=2000. In figure 6-18(a), Δ_c=0.47mm and in figure 6-18(b) Δ_c=0.99mm. Figures 6-18(a) and 6-18(b) are correlated to the lines EF and GH of figure 6-17 with λ=0.1Ns/m.

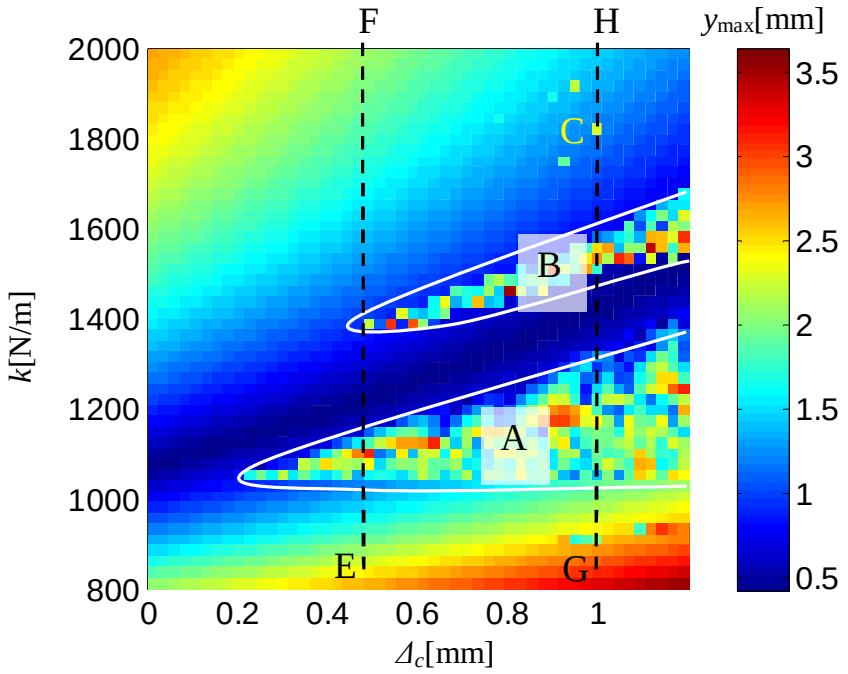

Fig. 6-17. Beam mid-span maximum deflection; V=25.53m/s and Δ=5.84m.

Table 6-4. Illustration of the NES behavior with different stiffness and damping coefficients, V=25.53m/s, Δ=5.84m and λ=0.1Ns/m.

Case	Steady state response x axis: t [s] y axis: $y(L/2,t)$ [mm]	Phase portrait x axis: $y(L/2,t)$ [mm] y axis: $dy(L/2,t)/dt$ [mm]	Poincare map x axis: $y(L/2,t_0+iT)$ [mm] y axis: $dy(L/2,t_0+iT)/dt$ [mm]
I	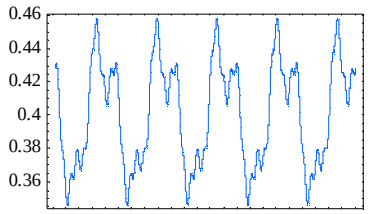	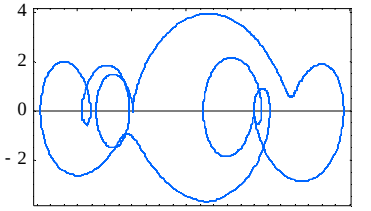	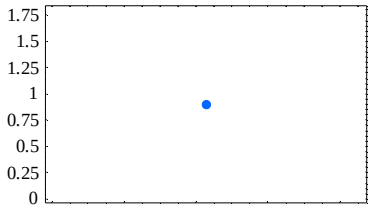
II	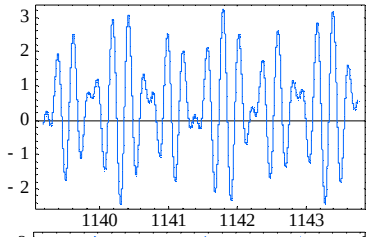	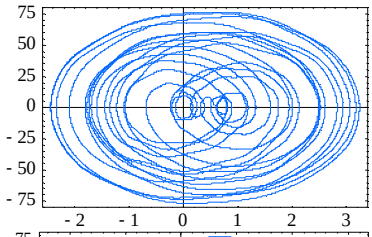	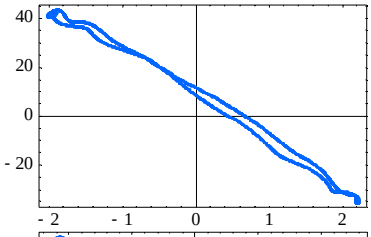
III	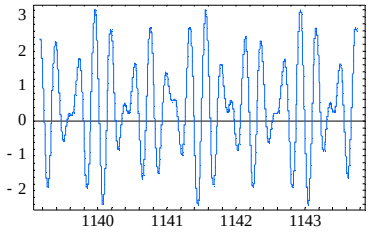	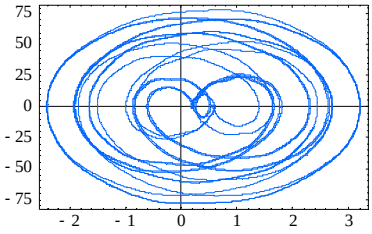	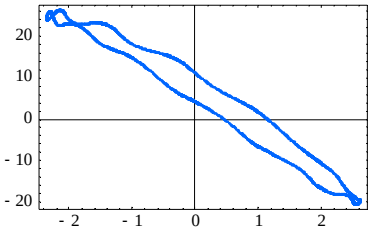

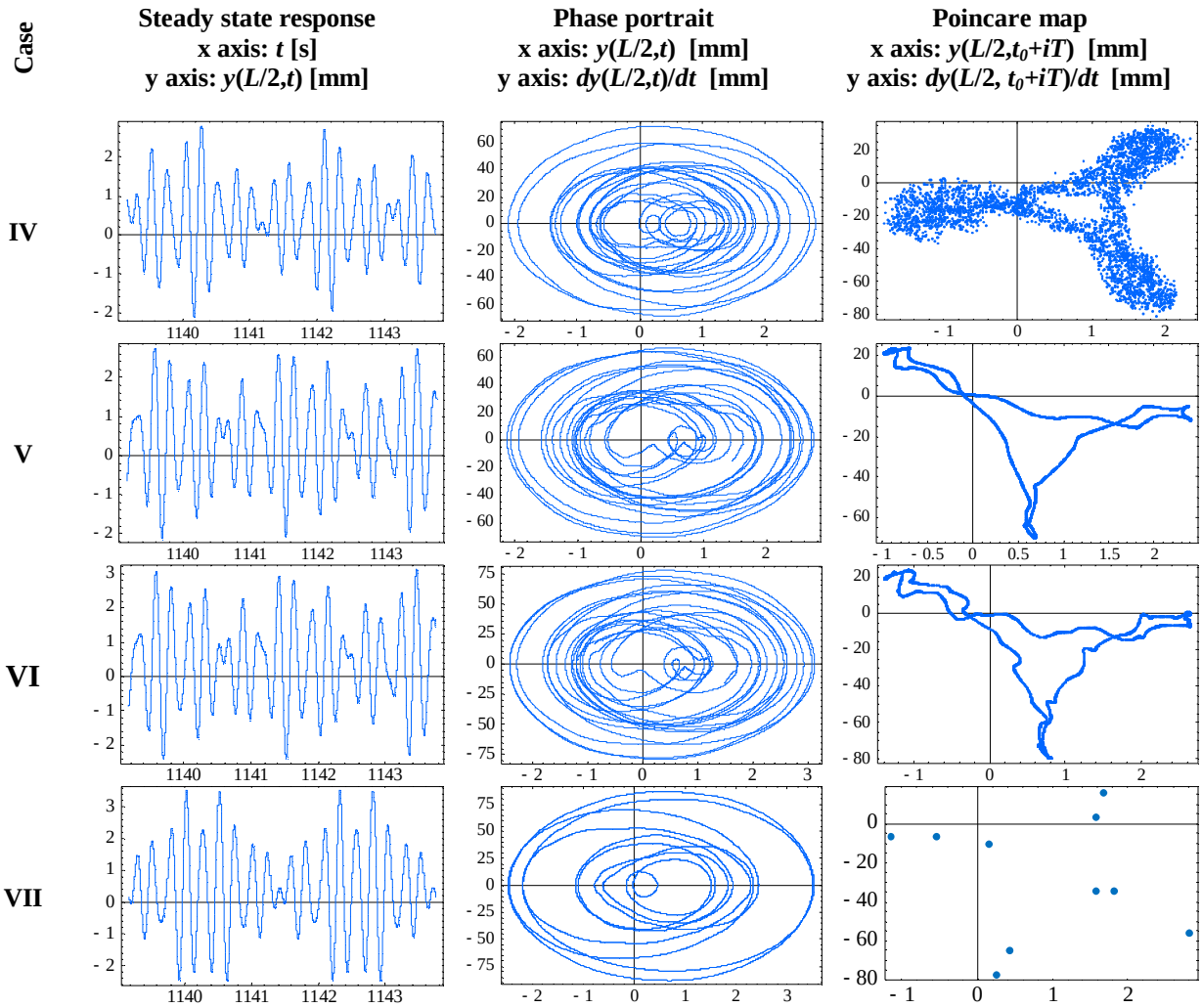

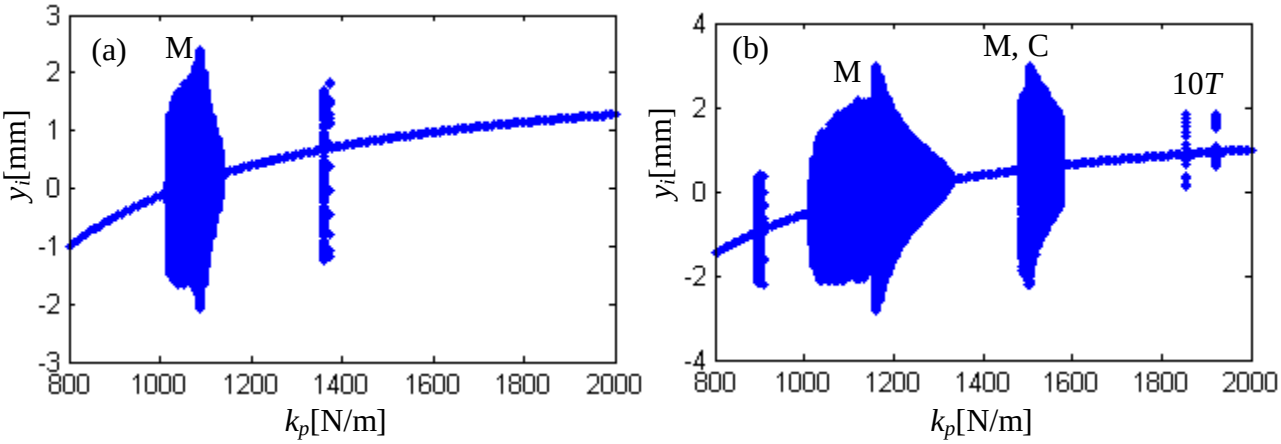

Fig. 6-18. Bifurcation diagram; V=25.53m/s and Δ=5.84m, λ=0.1Ns/m; a:Δ_c=0.47mm, b: Δ_c=0.99mm.

Table 6-5. NES characteristics for the cases in table 4.

Case number	k_p[N/m]	Δ_c [mm]
I	**1424**	**0.984**
II	**1184**	**0.984**
III	**1112**	**0.624**
IV	**1424**	**0.672**
V	**1544**	**1.008**
VI	**1520**	**0.984**
VII	**1736**	**0.912**

6.6.4. Cubic damping NES

Suppose NES containing linear stiffness and cubic viscous damping. In this case the stiffness and damping force functions in equation (6-7) are:

$$\bar{f}(t) = k\left[\sum_{r=1}^{\infty} a_r(t)\,\phi_r(d) - v(t)\right] \tag{6-25a}$$

$$\bar{g}(t) = \lambda_3\left[\sum_{r=1}^{\infty} \dot{a}_r(t)\,\phi_r(d) - \dot{v}(t)\right]^3 \tag{6-25b}$$

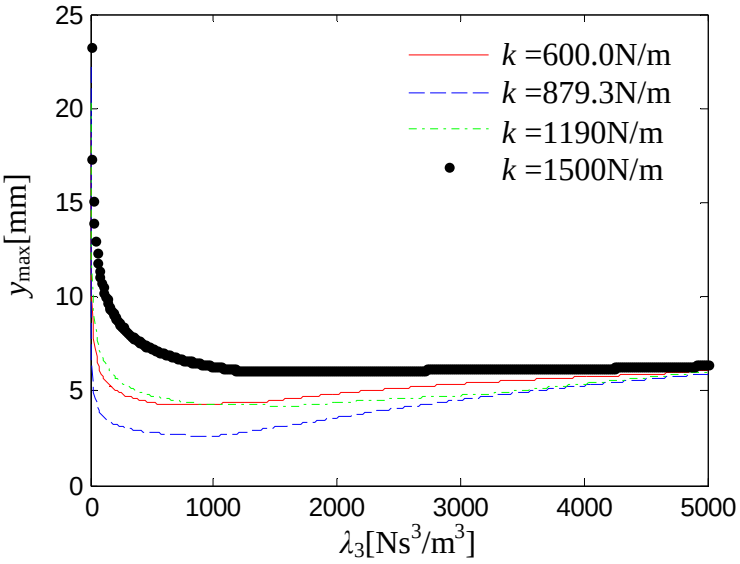

Fig. 6-19. Seeking between stiffness and cubic damping coefficients.

In order to determine the optimal parameter set for the present NES, we sought between different linear stiffness and cubic damping coefficients and for each case the maximum deflection in steady state response is determined for different velocity values. Figure 6-19 shows the maximum deflection among different velocities and each stiffness-damping parameter set.

The behavior is regular and responses for this parameters ranges are periodic. optimal set is defined as k=885N/m and λ_3=997.5Ns^3/m^3. Using this optimal cubic damping NES critical velocity is at V=20.82m/s and y_{max}=2.603mm.

6.6.5. Linear-quadratic damping NES

In order to reduce system deflection at critical loading conditions, some researchers suggested the nonsymmetrical damping, e.g. Starosvetsky and Gendelman [102] applied piecewise quadratic damping to a system subject to harmonic excitation. Consider linear stiffness force function and linear-quadratic nonlinear damping:

$$\bar{f}(t) = k\left[\sum_{r=1}^{\infty} a_r(t)\,\phi_r(d) - v(t)\right] \tag{6-26a}$$

$$\bar{g}(t) = \lambda_1\left[\sum_{r=1}^{\infty} \dot{a}_r(t)\,\phi_r(d) - \dot{v}(t)\right] + \lambda_2\left[\sum_{r=1}^{\infty} \dot{a}_r(t)\,\phi_r(d) - \dot{v}(t)\right]^2 \tag{6-26b}$$

Numerical seek shows that maximum deflection, y_{max}=2.42mm, can get with optimal set: k=870N/m, λ_1=14Ns/m and λ_2=132.8Ns^2/m^2; it shows 5.8% deflection reduction respect to the system with optimal linear DVA. With linear-quadratic optimal damper, the critical velocity is 27.10m/s, see figure (6-20a). Figure (6-20b) presents the absorber mass maximum displacement for linear TMD and linear-quadratic damping NES.

Figure 6-21 shows the DVA damper force for linear and linear-quadratic dampers. Note that if the damping force exceed zero when elongation speed is positive, instability occurs. From applicable point of view, in order to conquest this lack one can add the cubic term with adjust coefficient to the quadratic damping; this cubic term will be effective when the DVA elongation speed is too high.

The performance of the linear TMD and different types of nonlinearities for NESs are listed in table 6-6. Deflections are absolute maximum deflections for different load velocities. Critical load distances, Δ=5.84m, is considered. Results show that NES possessing linear stiffness and linear-quadratic damping is more effective respect to linear TMD. Using this type of nonlinearity we are able to decrease beam deflection 5.8% more than pure linear DVA. The quadratic part of the present damping does not effect when the load velocity is far from critical one; i.e. the behavior of this NES is similar to the linear TMD. Around critical velocity, where the deflection

and velocity amplitudes increase the quadratic term presents its performance and restrain the main structure, beam, from high deflection.

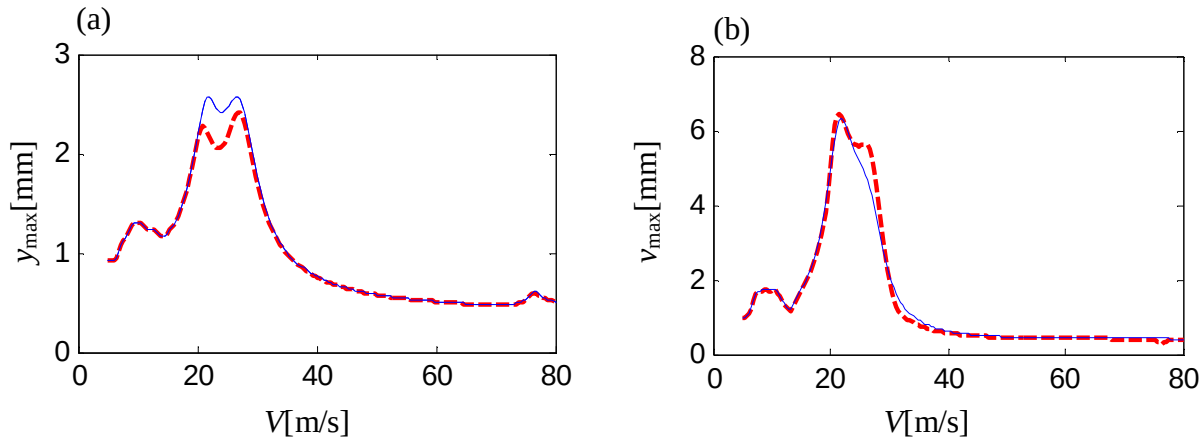

Fig. 6-20. a: Maximum mid-span beam deflection, b: Maximum DVA displacement vs. velocity variation; ——:linear DVA, — —:Quadratic NES.

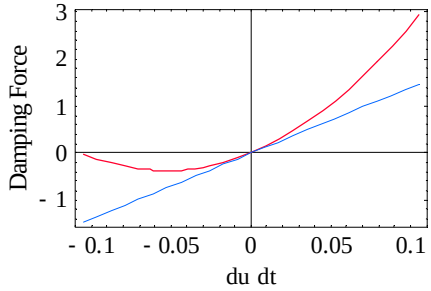

Fig. 6-21. Damping force vs. DVA elongation speed; ——:linear-quadratic damping, ____linear damping.

Table 6-6. The performance of the different types of the TMD and NESs.

Type of DVA	y_{opt}[mm]	V_{cr}[m/s]	Optimal parameter set
Bare beam	25.27	25.5	Without attachment
Linear TMD	2.56	26.6	k=870.0N/m, λ=14.0Ns/m
Cubic stiffness NES	3.59	24.3	k_3=45(10^6)N/m^3, λ=23.25Ns/m
5th order monomial stiffness	4.48	24.0	k_5=2.16(10^{12})N/m^5, λ=30Ns/m
Piecewise linear stiffness	2.58	24.1	k_p=1024N/m, Δ_c=0.61mm, λ=14Ns/m
Cubic damper NES	2.60	20.8	k=885N/m, λ_3=997.5Ns^3/m^3
Linear-quadratic damper NES	2.42	27.1	k=870N/m, λ_1=14Ns/m, λ_2=132.8Ns^2/m^2

CHAPTER 7

Conclusion Remarks

In this dissertation the performance of the linear and several types of nonlinear dynamic absorbers under moving load excitation is investigated. Types of nonlinearities that considered for nonlinear energy sinks are: cubic stiffness, high odd order monomial stiffness (5^{th}, 7^{th} and 9^{th} power), polynomial and piecewise linear stiffness as well as linear, cubic and combination of linear quadratic damping. Excitations which are applied on simply supported Euler Bernoulli beam are i) transient single traveling load without inertia, ii)transient traveling vehicle considering the effects of inertia and the effects of stiffness and damping of the traveling vehicle, iii) the infinite series of sequential traveling loads; this excitation presents nonzero steady state response under periodic excitation. For the first two types of excitations, the analysis has been focused on the transient structural response. Several optimization strategies are considered in order to obtain the best set of parameters considering the beam maximum dynamic amplitude or the energy absorbed by dynamic damper.

From present dissertation we can conclude the results as follow:

1. Under transient traveling load excitation, either load or vehicle, piecewise linear stiffness and linear damping is the best type of dynamic damper in order to reduce maximum beam deflection.
2. Under transient traveling load excitation, either load or vehicle, linear stiffness and linear damping (classical TMD) is the most effective type of dynamic damper in order to dissipate maximum portion of energy.
3. Under successive traveling loads excitation the dynamic damper possessing linear stiffness and combination of linear-quadratic nonlinear presents the best performance for different velocities values.

It is confirmed that dynamic dampers are capable to reduce the vibration amplitude also in the case of excitation due to moving loads: essentially nonlinear (cubic) dynamic dampers are more suitable for reducing the maximum amplitude of vibration respect to linear TMD. Linear dynamic dampers behave better when the goal is to maximize the vibration energy pumped out from the structure.

Under transient excitations the location of the absolute maximum deflection of beam is close to the mid-span (x=0.53L) for the transient excitation problems; the optimal location for the cubic stiffness nonlinear damper is at the same location (d=0.53L), for linear damper it is at d=0.55L. The maximum portion of input energy absorbed by nonlinear dynamic damper is about

87% regardless of kind of loading or beam geometry. Under periodic excitation optimal location is at the mid-span.

Using these dynamic dampers can improve fatigue life of structures. Firstly, the dynamic absorber causes a faster vibration damping, this implies that the number of cycles decreases; secondly, a moderate reduction of the maximum deflection greatly increases the fatigue life.

Using cubic stiffness nonlinearity and under transient excitation interesting conservation laws are found in terms of optimal parameters and beam geometry: i) the optimal stiffness C_{opt} for reducing the maximum beam vibration and absorbing the vibration energy is related to the beam length: $C_{opt}L^9 = \text{constant}$; ii) the optimal damping for maximizing the energy pumped out from the structure is related to the beam length: $\lambda_{opt}L = \text{constant}$; iii) the optimal damping for reducing the maximum beam vibration is zero. It is worthwhile to stress that such simple conserved quantities are extremely useful for designers as they allow the generalization of the results to a class of problems.

Moreover, results show that under transient excitations the dynamic dampers with monomial stiffness with higher exponents are more effective in reducing the maximum beam deflection. Moreover, optimal dynamic damper having piecewise linear stiffness is the most powerful passive dynamic damper, when the goal is to reduce the maximum beam deflection for both transient moving loads and moving vehicles excitations. When the goal of optimization is the maximum portion of input energy dissipated by dynamic damper, the optimum classical tuned mass damper is the most effective absorber.

Under successive traveling loads depend on velocity and distance between loads, the resonance and cancellation phenomena can come off. For transient excitation when one defines optimal set parameters for a special type of dynamic damper under critical loading condition, the defined absorber is also effective for other velocities, i.e. the maximum structure deflection with that optimal absorber is always less than structure deflection without absorber. Under periodic excitation, optimizing the absorber for critical loading (resonance condition) cause two separate new critical condition which constitute two new deflection peaks. For periodic excitation overall seek is needed in order to verify each optimal parameters set for different loading conditions.

We found that the vibration absorber possessing piecewise linear stiffness and linear damping which is the most effective type for reducing beam deflection under transient loading has the same performance as optimal linear absorber, not more. While, under successive moving load for

some parameter sets of nonlinear stiffness absorbers quasi periodic, super harmonic and chaotic responses appear; these responses are not desire because of high amplitude of deflection that usually appears in this responses. Nonlinear damping absorbers present periodic responses for both two nonlinear damping types which have been studied in this dissertation. NES possessing linear stiffness and linear-quadratic damper is the most effective dynamic damper for reducing beam vibration. Using this type of nonlinearity we are able to decrease beam deflection up to 90% respect to the beam without attachment. This performance is 5.8% more than pure linear DVA. The quadratic part of the present damper does not effect when the load velocity is far from critical one; i.e. the behavior of this NES is similar to the linear TMD. Around critical velocity, where the deflection and velocity amplitudes increase the quadratic term presents its performance and restrain the main structure, beam, from high deflection.

Some suggestions for improving present research depends on application is sited bellow:

1. Considering nonlinear beam deflection, i.e. large beam deflections.
2. Model of beam with variable cross section of area.
3. Simulating more complex loading (one or two degree of freedom car, with stiffness).

APPENDIXES

A. Dirac delta function

The Dirac delta or Dirac's delta is a mathematical construct introduced by theoretical physicist Paul Dirac. Informally, it is a generalized function representing an infinitely sharp peak bounding unit area: a 'function' $\delta(x)$ that has the value zero everywhere except at $x = 0$ where its value is infinitely large in such a way that its total integral is 1. In the context of signal processing it is often referred to as the unit impulse function.

The Dirac delta is not strictly a function, because any function that is equal to zero everywhere but a single point must have total integral zero. While for many purposes it can be manipulated as a function, formally it can be defined as a distribution that is also a measure. In many applications, the Dirac delta is regarded as a kind of limit (a weak limit) of a sequence of functions having a tall spike at the origin. The approximating functions of the sequence are thus *approximate* or *nascent* delta functions.

The Dirac delta is used to model a tall narrow spike function (an impulse), and other similar abstractions such as a point charge, point mass or electron point. For example, to calculate the dynamics of a baseball being hit by a bat, one can approximate the force of the bat hitting the baseball by a delta function. In doing so, one not only simplifies the equations, but one also is able to calculate the motion of the baseball by only considering the total impulse of the bat against the ball rather than requiring knowledge of the details of how the bat transferred energy to the ball.

In applied mathematics, the delta function is often manipulated as a kind of limit (a weak limit) of a sequence of functions, each member of which has a tall spike at the origin: for example, a sequence of Gaussian distributions centered at the origin with variance tending to zero.

An infinitesimal formula for an infinitely tall, unit impulse delta function (infinitesimal version of Cauchy distribution) explicitly appears in an 1827 text of Augustin Louis Cauchy, [103]. Siméon Denis Poisson considered the issue in connection with the study of wave propagation as did Gustav Kirchhoff somewhat later. Kirchhoff and Hermann von Helmholtz also introduced the unit impulse as a limit of Gaussians, which also corresponded to Lord Kelvin's notion of a point heat source. At the end of the 19th century, Oliver Heaviside used formal Fourier series to manipulate the unit impulse, [104]. The Dirac delta function as such was

introduced as a convenient notation by Paul Dirac in his influential 1927 book Principles of Quantum Mechanics, [105]. He called it the "delta function" since he used it as a continuous analogue of the discrete Kronecker delta.

A-1. Definition

The Dirac delta can be loosely thought of as a function on the real line which is zero everywhere except at the origin, where it is infinite,

$$\delta(x) = \begin{cases} +\infty, & x = 0 \\ 0, & x \neq 0 \end{cases}$$

and which is also constrained to satisfy the identity

$$\int_{-\infty}^{+\infty} \delta(x)dx = 1$$

This is merely a heuristic definition. The Dirac delta is not a true function, as no function has the above properties. Moreover there exist descriptions of the delta function which differ from the above conceptualization. Figure A-1 shows a schematic representation of the Dirac delta function by a line surmounted by an arrow. The height of the arrow is usually used to specify the value of any multiplicative constant, which will give the area under the function. The other convention is to write the area next to the arrowhead.

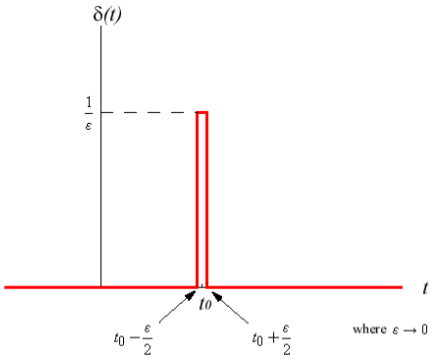

Fig. A-1. Schematic representation of the Dirac delta function, $\delta(t - t_0)$

A-2. Properties

1. *Integral*: One of the most important properties of the delta function has already been mentioned: it integrates to 1.

2. *Sifting property*: When a delta function $\delta(x - x_0)$ multiplies another function $f(x)$, the product must be zero everywhere except at the location of the infinite peak, x_0. At that location, the product is infinite like the delta function, but it might be a larger or smaller infinity, depending on whether the value of $f(x)$ at that point is larger or smaller than 1. In other words, the area of the product function is not necessarily 1 anymore, it is modified by the value of $f(x)$ at the infinite peak. This is called the *sifting property* of the delta function:

$$\int_{-\infty}^{+\infty} \delta(x - x_0) f(x) dx = f(x_0)$$

3. *Symmetry*: A few other properties can be readily seen from the definition of the delta function:

a. $\delta(-x) = \delta(x)$

b. $\delta(x - x_0) = \delta(-x + x_0)$

4. *Linear systems*: If a physical system has linear responses and if its response to delta functions (impulses) is known, then in theory the output of this system can be determined for almost *any* input, no matter how complex. This rather amazing property of linear systems is a result of the following: almost any arbitrary function can be decomposed into (or “sampled by”) a linear combination of delta functions, each weighted appropriately, and each of which produces its own impulse response. Thus, by application of the superposition principle, the overall response to the arbitrary input can be found by adding up all of the individual impulse responses.

B. Heaviside step function

The Heaviside step function, *H*, also called the unit step function, is a discontinuous function whose value is zero for negative argument and one for positive argument. The function is used in the mathematics of control theory and signal processing to represent a signal that switches on at a specified time and stays switched on indefinitely. It was named after the English polymath Oliver Heaviside.

The Heaviside function is the integral of the Dirac delta function: $H' = \delta$. This is sometimes written as

$$H(x) = \int_{-\infty}^{x} \delta(t)dt$$

B-1. Definition

Heaviside step function when defined as a piecewise constant function, is given by

$$H(x) = \begin{cases} 0, & x < 0 \\ 1, & x > 0 \end{cases}$$

Figure A-2 presents schematic representation of Heaviside step function; figure A-3 presents 7 different types of the smooth approximations of the step function.

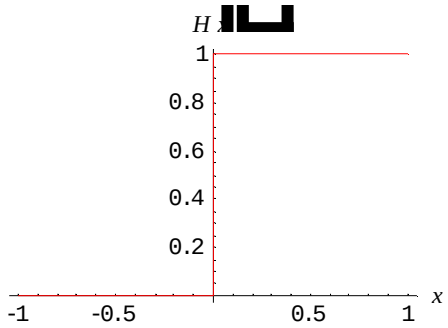

Fig. A-1. Schematic representation of the Heaviside step function, $H(x)$

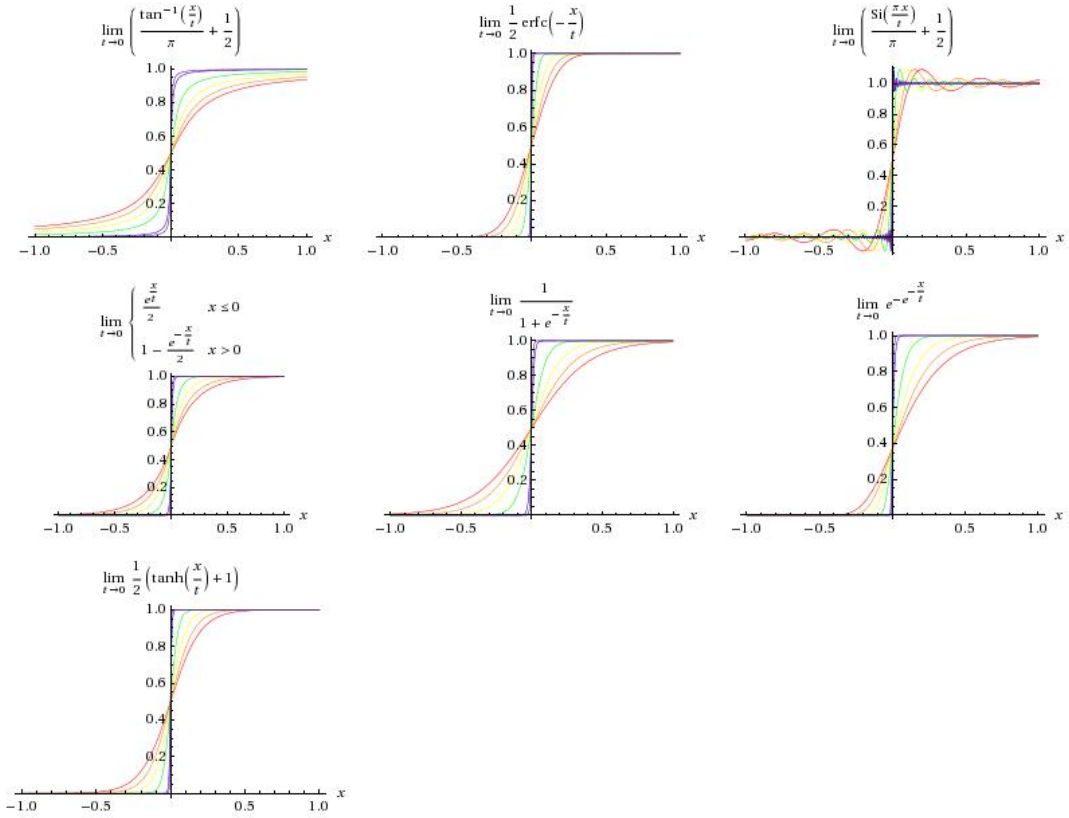

Fig. A-3. Smooth approximations of the step function

C. Phase portrait

A phase portrait is a geometric representation of the trajectories of a dynamical system in the phase plane. Each set of initial conditions is representated by a different curve, or point. Phase portraits are an invaluable tool in studying dynamical systems. They consist of a plot of typical trajectories in the state space. This reveals information such as whether an attractor, a repellor or limit cycle is present for the chosen parameter value. The concept of topological equivalence is important in classifying the behavior of systems by specifying when two different phase portraits represent the same qualitative dynamic behavior. A phase portrait graph of a dynamical system depicts the system's trajectories and stable steady states and unstable steady states in a state space. The axes are of state variables.

In the single differential equation case we are able to sketch the solution, y(t) in the *y*-*t* plane and see actual solutions. However, this would somewhat difficult in some case when the solutions are vectors. In this cases one may have the solutions to the system as points in the x_1-x_2 plane and plot these points. Equilibrium solution will correspond to the origin of x_1-x_2 plane and the x_1-x_2 plane is called the phase plane.

To sketch a solution in the phase plane we can pick values of *t* and plug these into the solution. This gives us a point in the x_1-x_2 or phase plane that we can plot. Doing this for many values of t will then give us a sketch of what the solution will be doing in the phase plane. A sketch of a particular solution in the phase plane is called the trajectory of the solution. Once we have the trajectory of a solution sketched we can then ask whether or not the solution will approach the equilibrium solution as *t* increases. Usually phase portraits only include the trajectories of the solutions and not any vectors. Fig. A-4 presents an exampleof potential energy (top) and phase portrait (bottom) of a simple pendulum. Note that the *x*-axis, being angular, wraps onto itself after every 2π radians.

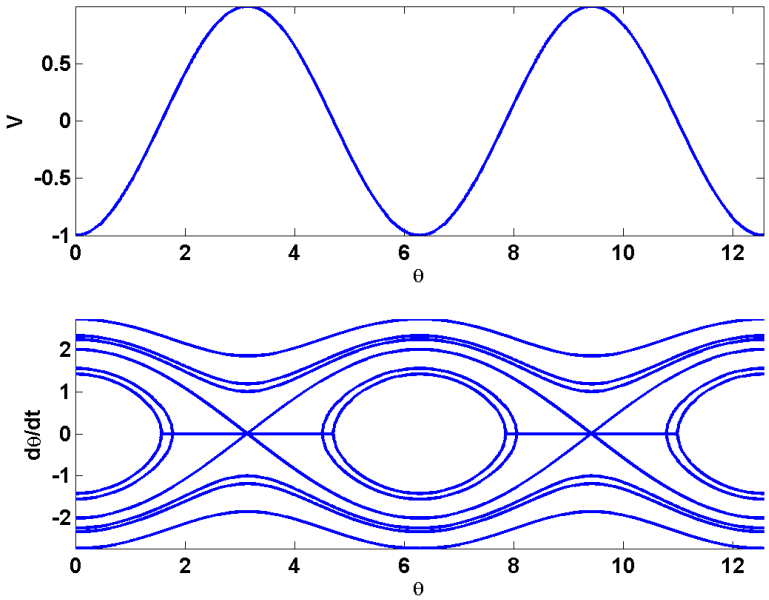

Fig. A4. Potential energy (top) and phase portrait (bottom) of a simple pendulum.

D. Poincare map

In mathematics, particularly in dynamical systems, a first recurrence map or Poincare map, named after Henri Poincare, is the intersection of a periodic orbit in the state space of a continuous dynamical system with a certain lower dimensional subspace, called the Poincare section, transversal to the flow of the system. More precisely, one considers a periodic orbit with initial conditions on the Poincare section and observes the point at which this orbits first returns to the section, thus the name first recurrence map. The transversality of the Poincare section basically means that periodic orbits starting on the subspace flow through it and not parallel to it.

A Poincare map can be interpreted as a discrete dynamical system with a state space that is one dimension smaller than the original continuous dynamical system. Because it preserves many properties of periodic and quasi periodic orbits of the original system and has a lower dimensional state space it is often used for analyzing the original system. In practice this is not always possible as there is no general method to construct a Poincare map.

A Poincare map differs from a recurrence plot in that space, not time, determines when to plot a point. For instance, the locus of the moon when the earth is at perihelion is a recurrence plot; the locus of the moon when it passes through the plane perpendicular to the earth's orbit and passing through the sun and the earth at perihelion is a Poincare map. It was used by Michel Henon to study the motion of stars in a galaxy, because the path of a star projected onto a plane looks like a tangled mess, while the Poincare map shows the structure more clearly.

Poincare maps are used to investigate periodic or quasi-periodic dynamical systems. Often these systems exhibit a periodic cycle or a chaotic attractor. A Poincare section S is now assumed to be a part of a plane, which is placed within the 3D phase space of the continuous dynamical system such that either the periodic orbit or the chaotic attractor intersects the Poincare section. The Poincare map is now defined as a discrete function $P:S\rightarrow S$, which associates consecutive intersections of a trajectory of the 3D flow. Fig. A5 shows an illustration of Poincare map, in this figure S is Poincare section, P shows the Poincare map which projects point x onto point $P(x)$.

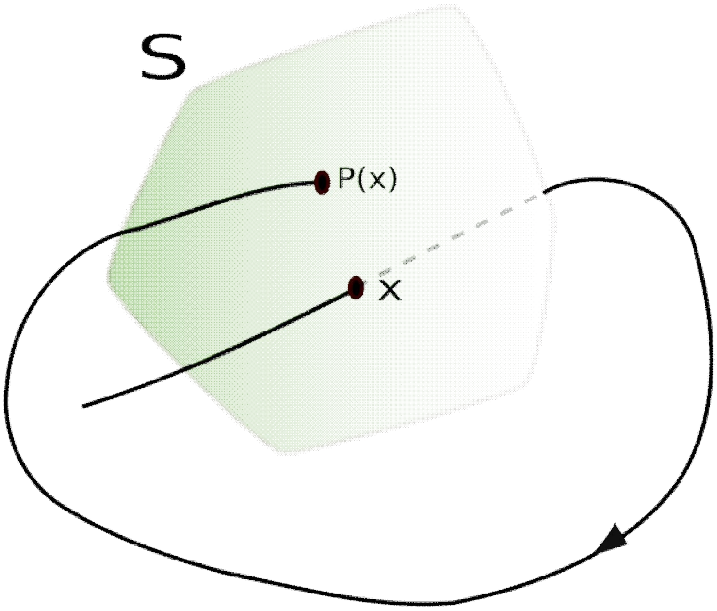

Fig. A5. Poincare map illustration.

E. Bifurcation diagram

In dynamical systems, a bifurcation diagram shows the possible long-term values (equilibria/fixed points or periodic orbits) of a system as a function of a bifurcation parameter in the system. It is usual to represent stable solutions with a solid line and unstable solutions with a dotted line.

Fig. A6 presents a well-known bifurcation diagram of the Logistic map nonlinear difference equation. The logistic map is a polynomial mapping of degree 2, often cited as an archetypal example of how complex, chaotic behavior can arise from very simple nonlinear dynamical equations; see Eq. (A-1). x_n is a number between zero and one, and represents the population at year n, and hence x_0 represents the initial population (at year 0). r is a positive number, and represents a combined rate for reproduction and starvation. Bifurcation parameter (control parameter) is r.

$$x_{n+1} = r x_n (1 - x_n) \tag{A-1}$$

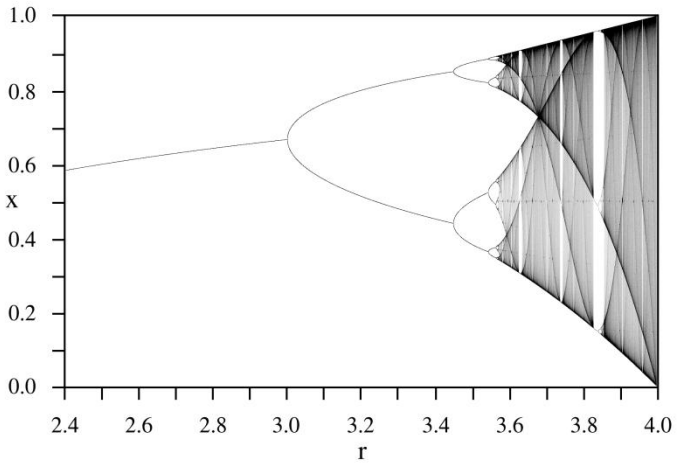

Fig. A6. Bifurcation diagram of the logistic map.

References

[1] L. Frýba, Vibration of Solids and Structures under Moving Loads, Telford, London (1999).

[2] S.P. Timoshenko, On the forced vibrations of bridges. Philosophical Magazine Series 6 43 (257) (1922), pp. 1018-1019.

[3] E. Esmailzadeh, M. Ghorashi, Vibration analysis of beams traversed by uniform partially distributed moving mass, Journal of Sound and Vibration, 184 (1) (1995), pp. 9-17.

[4] J.D. Yau and L. Fryba, Response of suspended beams due to moving loads and vertical seismic ground excitations, Engineering Structures 29 (2007), pp. 3255-3262.

[5] L. Fryba, A rough assessment of railway bridges for high speed trains, Engineering Structures 23 (2001), pp. 548-556.

[6] L. Yu, T.H.T. Chan, Recent research on identification of moving loads on bridges, Journal of Sound and Vibration 305 (1-2) (2007), pp. 3-21.

[7] C. O'CONNOR and T.H.T. CHAN, Dynamic wheel loads from bridge strains, Journal of Structural Engineering ASCE 114 (1988), pp. 1703-1723.

[8] L. Yu, Accounting for Bridge Dynamic Loads Using Moving Force Identification System (MFIS), Ph.D. Thesis, The Hong Kong Polytechnic University, Hong Kong, (2002).

[9] E.A. Sekhniashvili, I.E. Byus and Y.S. Sarkisov, Work of girder bridge structures under dynamic loads, Beton zhelezobeton 11 (1961), pp. 491-494.

[10] S. Sadiku and H.H.E. Leipholz, On the dynamics of elastic systems with moving concentrated masses, Ingenieur-Archiv 57 (1987), pp. 223-342.

[11] H.P. Lee, Transverse vibration of a Timoshenko beam acted on by an accelerating mass, Applied Acoustics 47 (4) (1996), pp. 319-330.

[12] A.V. Pesterev and L.A. Bergman, Response of elastic continuous carrying moving linear oscillator, Journal of Engineering Mechanics ASCE 123 (8) (1997), pp. 878-884.

[13] K.B. Todd, B.T. Kulakowski, Simple computer models for predicting ride quality and loading for heavy trucks, Transportation Research Record, 1215 TRB, National Research Council Washington DC (1989).

[14] P. Watts, On a method of reducing the rolling of ships at sea, Transactions of the Institution of Naval Architects 24 (1883), pp. 165-190.

[15] H. Frahm, Device for damping vibrations of bodies, US Patent No. 989958 (1911).

[16] J. Ormondroyd, J.P. Den Hartog, The theory of the dynamic vibration absorber, Transaction of the American Society of Mechanical Engineers 50 (1928), pp. 9-22.

[17] B. Matt, The Long Interview: Flavio Briatore, F1 Racing (2006), pp. 66-76.

[18] C. Bergin, Ares I Thrust Oscillation meetings conclude with encouraging data, changes, NASAspaceflight.com (2008).

[19] X. Shi, C.S. Cai, Suppression of Vehicle-Induced Bridge Vibration Using Tuned Mass Damper, Journal of Vibration and Control 14 (7) (2008), pp. 1037-1054.

[20] J.J. Wu, Study on the inertia effect of helical spring of the absorber on suppressing the dynamic responses of a beam subjected to a moving load, Journal of Sound and Vibration 297 (2006), pp. 981-999.

[21] Ataei, Agha Koochak, Zahrai, M.S. Marefat, Controlling the vibrations of Tale Zang Railway Bridge with tuned mass damper, The 6th international conference on Civil Engineering (In Persian) (1382), pp. 473-480.

[22] B. F. Spencer Jr., S. Nagarajaiah, State of the Art of Structural Control, Journal of Structural Engineering 129(7) (2003), pp. 845-856.

[23] Y.Y. Lin,C.M. Cheng, C.H. Lee, A tuned mass damper for suppressing the coupled flexural and torsional buffeting response of long-span bridges, Engineering Structures 22 (9) (2000), pp. 1195-1204.

[24] E.O. Ayorinde, G.B. Warburton, Minimizing structural vibration with absorbers, Earthquake Engineering and Structural Dynamics 8 (1980), pp. 219-236.

[25] G.B. Warburton, Optimum absorber parameters for minimizing vibration response, Earthquake Engineering and Structural Dynamics 9 (1981), pp. 251-262.

[26] G.B. Warburton, Optimum absorber parameters for various combinations of response and excitation parameters, Earthquake Engineering and Structural Dynamics 10 (1982), pp. 381-401.

[27] H.C. Tsai, G.C. Lin, Optimum tuned mass dampers for minimizing steady-state response of support excited and damped system, Earthquake Engineering and Structural Dynamics 22 (1993), pp. 957-973.

[28] H.C. Tsai, G.C. Lin, Explicit formulae for optimum absorber parameters for force excited and viscously damped systems, Journal of Sound and Vibration 89 (1993), pp. 385-396.

[29] A.G. Thompson, Optimum tuning and damping of a dynamic vibration absorber applied to a force excited and damped primary system, Journal of Sound and Vibration 77 (1981), pp. 403-415.

[30] Y. Fujino, M. Abe, Design formulas for tuned mass dampers based on a perturbation technique, Earthquake Engineering and Structural Dynamics 22 (1993), pp. 833-854.

[31] J.A. Macinante, Seismic mountings for vibration isolation, John Wiley and Sons, Inc., New York (1984).

[32] M. Gu, S.R. Chen, C.C. Chang, Parametric study on multiple tuned mass dampers for buffeting control of Yangpu Bridge, Journal of Wind Engineering and Industrial Aerodynamics 89 (11-12) (2001), pp. 987-1000.

[33] M.D. Martínez-Rodrigoa, J. Lavadob, P. Museros, Dynamic performance of existing high-speed railway bridges under resonant conditions retrofitted with fluid viscous dampers, Engineering Structures 32(3) (2010), pp. 808-828.

[34] R.A. Ibrahim, Recent advances in nonlinear passive vibration isolators, Journal of Sound and Vibration 314 (3-5) (2008), pp. 371-452.

[35] M.Z. Kolovsky, Nonlinear Dynamics of Active and Passive Systems of Vibration Protection, Springer-Verlag, New York, (1999).

[36] J.P. Den Hartog, Forced vibrations with constrained coulomb damping and viscous friction, Transactions of the ASME Advance Papers, New York, USA (1931), pp. 107-115.

[37] J.E. Ruzicka, T.F. Derby, Influence of Damping in Vibration Isolation, The Shock and Vibration Information Center, Washington DC (1971).

[38] S.M. Metwalli, Optimum nonlinear suspension system, ASME Design Engineering Technical Conference A4, Cincinnati, OH, USA (1985).

[39] T.A. Nayfeh, E. Emaci, A.F. Vakakis, Application of nonlinear localization to the optimization of a vibration isolation system, American Institute of Aeronautics and Astronautics Journal 35 (1997), pp. 1378-1386.

[40] X. Yu, S.J. Zhu, S.Y. Liu, Nonlinear normal modes for multi-degree-of-freedom nonlinear vibration isolation system, Proceedings of the ASME Dynamic Systems and Control Division DSC, IMECE2006, Chicago, IL, USA (2006).

[41] S. Timoshenko, D.H. Young, W. Weaver, Vibration Problems in Engineering, New York, John Wiley, fourth edition (1974).

[42] J.P. Den Hartog, Mechanical Vibrations, McGraw-Hill, New York (1985).

[43] A. Greco, A. Santini, Dynamic response of a flexural non-classically damped continuous beam under moving loadings, Computers & Structures 80 (2002), pp. 1945-1953.

[44] Y.S. Lee, G. Kerschen, A.F. Vakakis, P.N. Panagopoulos, L.A. Bergman, D.M. McFarland, Complicated dynamics of a linear oscillator with a light, essentially nonlinear attachment, Physica D: Nonlinear Phenomena 204 (2005), pp. 41-69.

[45] H. Kwon, M. Kim, I. Lee, Vibration control of bridges under moving loads, Computers & Structures 66 (1998), pp. 473-480.

[46] P. Muserosa, M.D. Martinez-Rodrigo, Vibration control of simply supported beams under moving loads using fluid viscous dampers, Journal of Sound and Vibration, 300 (2007), pp. 292-315.

[47] J.F. Wang, C.C. Lin, B.L. Chen, Vibration suppression for high-speed railway bridges using tuned mass dampers, International Journal of Solids and Structures 40 (2003), pp. 465-491.

[48] J.D. Yau, Y.B. Yang, Vibration reduction for cable-stayed bridges travelled by high-speed trains, Finite Elements in Analysis and Design 40 (2004), pp. 341-359.

[49] A.K. Das, S.S. Dey, Effects of tuned mass dampers on random response of bridges, Computers & Structures 43 (1992), pp. 745-750.

[50] J. Lin, F.L. Lewis, T. Huang, Passive control of the flexible structures subjected to moving vibratory systems, ASME Special Publication on Active and Passive Control of Mechanical Vibrations PVP 289 (1994), pp. 11-18.

[51] J. Lin, Multi-timescale fuzzy controller for a continuum with a moving oscillator, IEE Proceedings - Control Theory and Applications 151 (3) (2004), pp. 310-318.

[52] F.Georgiades, A.F.Vakakis, Dynamics of a linear beam with an attached local nonlinear energy sink, Communications in Nonlinear Science and Numerical Simulation 12 (2005), pp. 643-651.

[53] A.F. Vakakis, L.I. Manevitch, O. Gendelman, L. Bergman, Dynamics of linear discrete systems connected to local essentially nonlinear attachments, Journal of Sound and Vibration 264 (2003), pp. 559-577.

[54] O.V. Gendelman, Targeted energy transfer in systems with non-polynomial nonlinearity, Journal of Sound and Vibration 315 (2008), pp. 732-745.

[55] S. Wolfram, The Mathematica Book, Wolfram Media, Cambridge University Press, New York (1996).

[56] I. Christie, J.M. Sanz-Serna, A Galerkin method for a nonlinear integro-differential wave system 44 (1984), pp. 229-237.

[57] T. Yoshimura, J. Hino, Vibration analysis of a nonlinear beam subjected to moving loads by using Galerkin method, Journal of Sound and Vibration 104(2) (1986), pp. 179-186.

[58] O.A. Ladyzhenskaja, V.A. Solonnikov, N.N. Uraltseva, Linear and Quasilinear Equations of Parabolic Type (Translations of Mathematical Monographs), American Mathematical Society, (1968).

[59] B.A. Finlayson, Convergence of the Galerkin Method for Nonlinear Problems Involving Chemical Reaction, SIAM Journal on Numerical Analysis 8(2) (1971), pp. 316-324.

[60] G.R. Bhashyam, G. Prathap, Galerkin finite element method for nonlinear beam vibration, Journal of sound and vibration 72 (2) (1980), pp. 191-203.

[61] J.H. Argyrisa, J.S. Doltsinisa, W.C. Knudsona, L.E. Vaza, K.J. Willam, Numerical solution of transient nonlinear problems, Computer Methods in Applied Mechanics and Engineering 17 (2) (1979), pp. 341-409.

[62] A.K. Noor, Recent advances in reduction methods for nonlinear problems, Computers & Structures 13 (1) (1981), pp. 31-44.

[63] N. Metropolis, S. Ulam, The Monte Carlo Method, Journal of the American Statistical Association 44 (247) (1949), pp. 335-341.

[64] N. Metropolis, A.W. Rosenbluth, M. Rosenbluth, A.H. Teller, E. Teller, Equation of State Calculations by Fast Computing Machines, Journal of Chemical Physics 21 (6) (1953), pp. 1087-1093.

[65] J.C. Snowdon, Vibration and Shock in Damped Mechanical Systems, John Wiley and Sons, New York (1978).

[66] J.C. Snowdon, Isolation from mechanical shock with a mounting system having nonlinear dual-phase damping, The Shock and Vibration Bulletin 41 (1970), pp. 21-45.

[67] K. Cornelius, A study of the performance of an optimum shock mount, The Shock and Vibration Bulletin 38 (1968), pp. 213-218.

[68] R.R. Guntura and S. Sankar, Performance of different kinds of dual phase damping shock mounts, Journal of Sound and Vibration 84(2) (1982), pp. 253-267.

[69] Y.S. Lee, F. Nucera, A.F. Vakakis, D.M. McFarland, L.A. Bergman, Periodic orbits, damped transitions and targeted energy transfers in oscillators with vibro-impact attachments, Physica D: Nonlinear Phenomena 238 (2009), pp. 1868-1896.

[70] S. Deshpande, S. Mehta, G.N. Jazar, Optimization of secondary suspension of piecewise linear vibration isolation systems, International Journal of Mechanical Sciences 48 (2006), pp. 341-377.

[71] F. Rüdinger, Tuned mass damper with nonlinear viscous damping, Journal of Sound and Vibration 300 (2007), pp. 932-948.

[72] F.S. Samani, F. Pellicano, Vibration reduction on beams subjected to moving loads using linear and nonlinear dynamic absorbers, Journal of Sound and Vibration, 325 (2009), pp. 742-754.

[73] L. Denga, C.S. Cai, Identification of parameters of vehicles moving on bridges, Engineering Structures 31 (10) (2009), pp. 2474-2485.

[74] S.S. Law, T.H.T. Chan, Q.H. Zeng, Moving force identification: A time domains method, Journal of Sound and Vibration 201 (1) (1997), pp. 1-22.

[75] S.S. Law, T.H.T. Chan, Q.H. Zeng, Moving force identification: A frequency and time domains analysis, Journal of Dynamic Systems, Measurement, and Control 12 (3) (1999), pp. 394-401.

[76] S.S. Law, T.H.T. Chan, X.Q. Zhu, Q.H. Zeng, Regularization in moving force identification, Journal of Engineering Mechanics 127 (2) (2001), pp. 136-148.

[77] X.Q. Zhu, S.S. Law, Practical aspects in moving load identification, Journal of Sound and Vibration 258 (1) (2002), pp. 123-146.

[78] T.H.T. Chan, D.B. Ashebo, Theoretical study of moving force identification on continuous bridges, Journal of Sound and Vibration 295 (2006), pp. 870-883.

[79] F.T.K. Au, R.J. Jiang, Y.K. Cheung, Parameter identification of vehicles moving on continuous bridges, Journal of Sound and Vibration 269 (2004), pp. 91-111.

[80] R.J. Jiang, F.T.K. Au, Y.K. Cheung, Identification of vehicles moving on continuous bridges with rough surface, Journal of Sound and Vibration 274 (2004), pp. 1045-1063.

[81] J.Q. Bu, S.S. Law, X.Q. Zhu, Innovative bridge condition assessment from dynamic response of a passing vehicle, Journal of Engineering Mechanics 132 (12) (2006), pp. 1372-1379.

[82] S.S. Law, J.Q. Bu, X.Q. Zhu and S.L. Chan, Vehicle condition surveillance on continuous bridges on response sensitivity, Journal of Engineering Mechanics 132 (1) (2006), pp. 78-86.

[83] G.G. Adams, Critical speeds and the response of a tensioned beam on an elastic foundation to repetitive moving loads, International Journal of Mechanical Sciences 37 (1995), pp. 773-781.

[84] V.V. Bolotin, The Dynamic Stability of Elastic Systems, Holden-Day, San Francisco, CA (1964).

[85] Y.B. Yang, J.D. Yau, L.C. Hsu, Vibration of simple beams due to trains moving at high speeds, Engineering Structures 19 (11) (1997), pp. 936-944.

[86] Y.B. Yang, C.L. Lin, J.D. Yau, D.W. Chang, Mechanism of resonance and cancellation for train-induced vibrations on bridges with elastic bearings, Journal of Sound and Vibration 269 (2004), pp. 345-360.

[87] S.P. Timoshenko, Method of analysis of static and dynamic stresses in rails. In: Proc. Second International Congress for Applied Mechanics (1926), p. 407.

[88] J.D. Yau, Y.B. Yang, A wideband MTMD system for reducing the dynamic response of continuous truss bridges to moving train loads, Engineering Structures 26 (12) (2004), pp. 1795-1807.

[89] O.V. Gendelman, E. Gourdon, C.H. Lamarque, Quasiperiodic energy pumping in coupled oscillators under periodic forcing, Journal of Sound and Vibration 294 (4) (2006), pp. 651-662.

[90] J.C. Nissen, K. Popp, B. Schmalhorst, Optimization of a nonlinear dynamic vibration absorber, Journal of Sound and Vibration 99 (1985), pp. 149-154.

[91] J.B. Hunt, J.C. Nissen, The broadband dynamic vibration absorber, Journal of Sound and Vibration, 83 (1982), pp. 573-578.

[92] K.V. Avramov, Yu.V. Mikhlin, Snap-through truss as a vibration absorber, Journal of Vibration and Control 10 (2004), pp. 291-308.

[93] B. Zhang, S.A. Billings, Z.Q. Lang, G.R. Tomlinson, Suppressing resonant vibrations using nonlinear spring and dampers, Journal of Vibration and Control 1 (2009), pp. 1-14.

[94] B. Zhang, S.A. Billings, Z.Q. Lang, G.R. Tomlinson, A novel nonlinear approach to suppress resonant vibrations, Journal of Sound and Vibration 317 (2008), pp. 918-936.

[95] J.H. Bonsel, Application of a dynamic vibration absorber to a piecewise linear beam system, Master's thesis, Eindhoven university of technology (2003).

[96] E. Savin, Dynamic amplification factor and response spectrum for the evaluation of vibrations of beams under successive moving loads, Journal of Sound and Vibration 248 (2001), pp. 267-288.

[97] K.V. Avramov, O.V. Gendelman, On interaction of vibrating beam with essentially nonlinear absorber, Meccanica 45 (3) (2009), pp. 355-365.

[98] E. Gourdon, C.H. Lamarque, S. Pernot, Contribution to efficiency of irreversible passive energy pumping with a strong nonlinear attachment, Nonlinear Dynamics. 50 (4) (2007), pp. 793-808.

[99] V.M. Rothos, A.F. Vakakis, Dynamic interaction of traveling waves propagating in an infinite linear chain with a local essentially nonlinear attachment. Wave Motion 46 (2009), pp. 174-188.

[100] Y. Starosvetsky, O.V. Gendelman, Attractors of harmonically forced linear oscillator with attached nonlinear energy sink II: Optimization of a nonlinear vibration absorber, Nonlinear Dynamics 51 (2008), pp. 47-57.

[101] A.H. Nayfeh, B. Balachandran. Applied Nonlinear Dynamics: Analytical, Computational, and Experimental Methods, Wiley, New York (1995).

[102] Y. Starosvetsky, O.V. Gendelman, Vibration absorption in systems with a nonlinear energy sink: nonlinear damping. Journal of Sound and Vibration 324 (2009), pp. 916-939.

[103] R. Bracewell, The Fourier Transform and Its Applications (2nd edition), McGraw-Hill (1986).

[104] R. Courant, D. Hilbert, Methods of Mathematical Physics, Volume II, Wiley-Interscience (1962).

[105] J. Dieudonné, Treatise on analysis. Vol. II, New York: Academic Press, Harcourt Brace Jovanovich Publishers (1976).

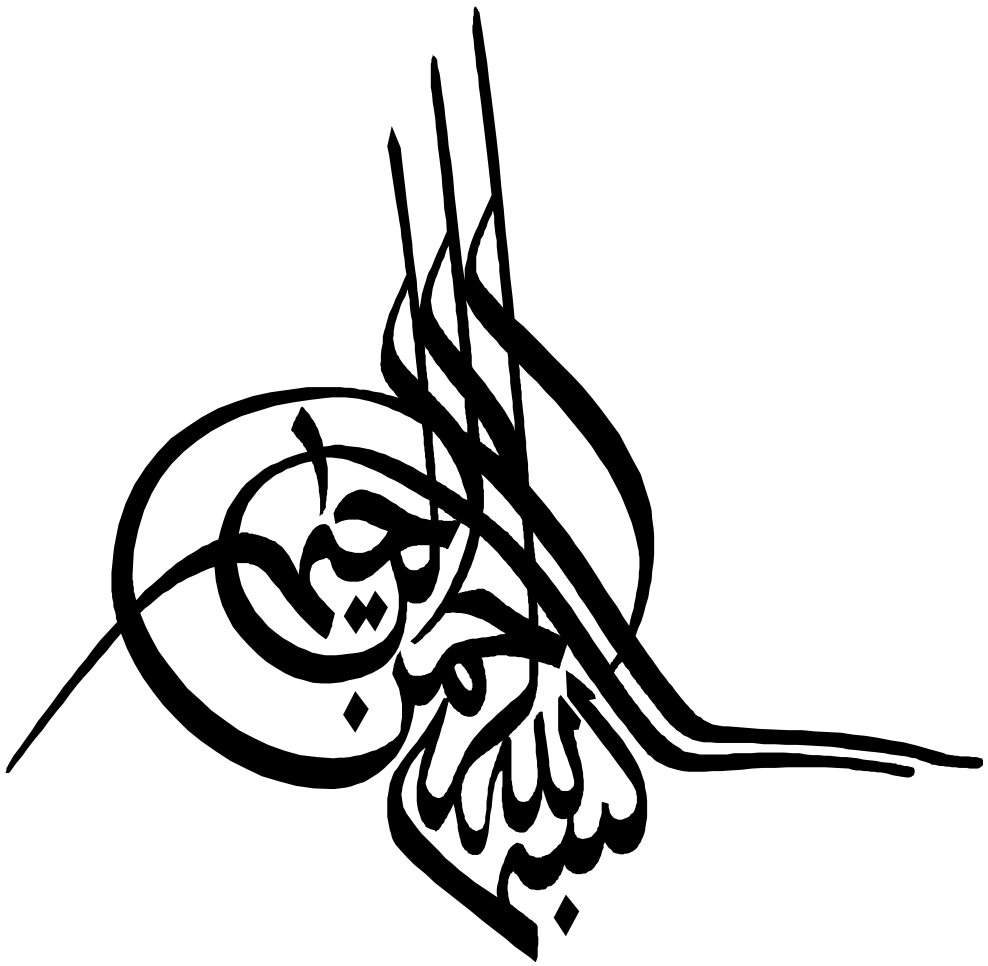
بسم الله الرحمن الرحيم

دانشکده فنی و مهندسی

گروه مهندسی مکانیک

رساله تحصیلی برای دریافت درجه دکتری رشته مهندسی مکانیک گرایش طراحی کاربردی

کاهش ارتعاشات تیر تحت بار متحرک بوسیله جاذبهای ارتعاشی خطی و غیر خطی

استاد راهنما :

پروفسور فرانچسکو پلیکانو

مؤلف :

فرهاد شیخ سامانی

تیرماه 1389

این رساله به عنوان یکی ازشرایط احراز درجه دکتری تخصصی به

گروه مکانیک

دانشکده فنی و مهندسی

دانشگاه شهید باهنر کرمان

تسلیم شده و هیچ گونه مدرکی به عنوان فراغت از تحصیل دوره مزبور شناخته نمی شود.

دانشجو: آقای فرهاد شیخ سامانی

حامی:

استاد راهنما: آقای دکتر سید حسین منصوری

داور۱: آقای دکتر علیرضا سعیدی

داور۲: آقای دکتر محمدعلی حاج عباسی

داور۳: آقای دکتر منصور نیکخواه بهرامی (استاد دانشگاه تهران)

معاون پژوهشی و تحصیلات تکمیلی دانشکده فنی: آقای دکتر پور ابراهیم

نماینده تحصیلات تکمیلی دکتر علی دشتی

تقدیم به روح جاودانه پدر گرانقدرم

تقدیم به استاد فقید و دانشمند

دکتر فرزاد آریانا

تقدیم به مادرم

به شکوه تنفس اول

به ولادت

آنکه امپراطور قصر محبت است

تقدیم به همسرم

سنبل عشق و فداکاری و پشتکار

چکیده

سازه‌های انعطاف‌پذیر، مانند پلهای معلق، تحت بارهای متحرک رفتار دینامیکی پیچیده‌ای از خود نشان می‌دهند. با توجه به هزینهٔ بالای افزایش مقاومت اینگونه سازه‌ها، به همراه پیشرفتهای تکنولوژی اخیر، توجه زیادی به روشهای ابتکاری و نوین در راستای افزایش کارآیی و ایمنی این سازه‌ها در برابر بارهای دینامیکی شده است. در کنار روشهای مختلف برای کاهش ارتعاشات ناخواسته، جاذبهای ارتعاشی عملکرد مناسبی را از خود نشان می‌دهند.

در این پایان‌نامه ارزیابی جامعی بر کارآیی جاذبهای ارتعاشی غیرخطی برای تیرهای تحت بارگذاری متحرک صورت گرفته است. پایان‌نامهٔ حاضر با توصیف و بررسی روشهای مختلف مدلسازی بارهای متحرک آغاز شده است و با معرفی اصول اولیهٔ عملکرد جاذبهای ارتعاشی خطی و غیرخطی ادامه یافته است. سپس تاثیر جاذبهای ارتعاشی خطی و غیرخطی برای سه نوع بارگذاری: بار متحرک گذرا بدون تاثیر اینرسی، خودروی متحرک گذرا دارای اینرسی و بارگذاری متناوب ناشی از بارهای متحرک متوالی بررسی شده است. در آخر به کمک بهینه‌سازی جاذبهای ارتعاشی، مناسبترین پارامترهای جاذب تعیین شده‌اند. همچنین مقایسه بین کارآیی هر نوع جاذب ارتعاشی خطی و غیرخطی برای بارگذاری‌های مختلف انجام شده است.

نتایج تحقیقات نشان داد که برای هر دو نوع از سیستم بار متحرک گذرا: نیرو بدون اینرسی و مدل یک درجه آزادی خودرو، جاذبهای ارتعاشی غیرخطی دارای عملکرد یکسان هستند. جاذب ارتعاشی با فنریت تکه‌ای خطی، برای کاهش دامنهٔ ارتعاشات تیر تحت بار یا خودروی متحرک، بهترین عملکرد را دارد. فنر کلاسیک خطی بهترین رفتار را برای جذب بیشتر انرژی و میرا نمودن سریعتر ارتعاشات دارد.

جاذبهای ارتعاشی با فنریت غیرخطی برای تیر تحت بارگذاری متناوب (سری متوالی از بارهای متحرک) لزوماً پاسخ پریودیک نشان نمی‌دهند، بلکه برای ضرایب میرایی پایین متناسب با نوع غیرخطی بودن فنریت، پاسخهای شبه‌پریودیک یا اغتشاش ارائه می‌دهند. با افزایش میرایی، پاسخ سیستم به پاسخ پریودیک نزدیک می‌شود، از طرفی جاذبهای غیرخطی با میرایی بالا شرایط بهتری از عملکرد جاذب ارتعاشی خطی کلاسیک ارائه نمی‌دهند. برخلاف فنریت غیرخطی، استفاده از میرایی غیرخطی، در این نوع بارگذاری، پاسخهای پریودیک نشان می‌دهد. نتایج نشان داد جاذب ارتعاشی غیرخطی با فنریت خطی و میرایی بصورت خطی و مرتبهٔ دوم، کارآیی بهتری را نسبت به سایر جاذبهای ارتعاشی برای تیر مورد بررسی دارد.